Site U1312[1]

Expedition 306 Scientists[2]

Chapter contents

Background and objectives 1
Operations 2
Lithostratigraphy 3
Biostratigraphy 5
Paleomagnetism 10
Stratigraphic correlation 11
Geochemistry 12
Physical properties 15
References 15
Figures 18
Tables 54

Background and objectives

Site U1312 (proposed Site IRD4A) constitutes a reoccupation of Deep Sea Drilling Project (DSDP) Site 608 located northeast of the Azores on the southern flank of the King's Trough tectonic complex in a water depth of 3554 m (Fig. F1). During DSDP Leg 94, two principal holes (Hole 608 and Hole 608A) were drilled (Ruddiman, Kidd, Thomas, et al., 1987). Hole 608 was continuously cored with the variable-length hydraulic piston coring (VLHPC) system and the extended core barrel system down to the basement at 515.4 meters below seafloor (mbsf) (42 Ma) (Fig. F2), and Hole 608A was continuously cored with the VLHPC to refusal at 146.4 mbsf (3.4 Ma). At this site, a nearly continuous bio- and magnetostratigraphic section of Quaternary to middle upper Oligocene sediments was recovered to 455 mbsf (Baldauf et al., 1987). Below this depth, some coring gaps and the presence of a major hiatus representing at least 7.5 m.y. (late Eocene–early Oligocene) cause the record to be less complete through the Oligocene and into the Eocene. Upper middle Eocene (Zone NP16) sediments lie upon the basaltic basement at 515.4 mbsf. Mean sedimentation rates at Site 608 are 2–3 cm/k.y., with the higher values generally occurring in the late Neogene–Quaternary time intervals.

Together with Sites 607 and 609, Site 608 was part of a north–south paleoceanographic transect from 53° to 37°N in the carbonate-rich sediments along the middle and upper flanks of the Mid-Atlantic Ridge. The objectives of this transect were to study the response of the North Atlantic to (1) increases in volume of Antarctic ice sheet at 14 and 6.5 Ma, (2) the closure and reopening of Atlantic/Mediterranean connections at the end of the Miocene (6–5 Ma), and (3) the closing of the Isthmus of Panama (4.5–3 Ma), as well as to document the magnitude and spectral character of the surface response to high-latitude climate change in the northern hemisphere during times of major northern hemisphere glaciation (i.e., the last at ~2.5 m.y. [Ruddiman et al., 1987]). Sites 607 and 609 especially constitute benchmark sites for generating deep-ocean climate records from the North Atlantic for the Pleistocene (Ruddiman et al., 1989) and late Pliocene (Ruddiman et al., 1986; Raymo et al., 1989, 2004) and interpreting these records in terms of ice sheet variability and oceanic circulation changes and for generating orbitally tuned timescales.

[1] Expedition 306 Scientists, 2006. Site U1312. *In* Channell, J.E.T., Kanamatsu, T., Sato, T., Stein, R., Alvarez Zarikian, C.A., Malone, M.J., and the Expedition 303/306 Scientists. *Proc. IODP,* 303/306: College Station TX (Integrated Ocean Drilling Program Management International, Inc.). doi:10.2204/iodp.proc.303306.111.2006
[2] Expedition 306 Scientists' addresses.

doi:10.2204/iodp.proc.303306.111.2006

The surface North Atlantic between 40° and 50°N was the most thermally reactive ocean area in the world during the Quaternary, undergoing glacial–interglacial oscillations of sea-surface temperatures (SST) of >10°C (Ruddiman, Kidd, Thomas, et al., 1987; Pflaumann et al., 2003). Sites 607, 608, and 609 are located in the area of maximum glacial–interglacial differences in SST as shown for the Last Glacial Maximum (LGM)/modern North Atlantic Ocean (Fig. F3) (Pflaumann et al., 2003).

Partly incomplete recovery and the present condition of the existing DSDP cores collected in 1983 do not permit the high-resolution studies proposed here. The main objective at Site U1312 was to obtain detailed records of surface and deepwater characteristics and their interactions with ice sheet instabilities during Neogene–Quaternary times using gamma ray attenuation (GRA) density, natural gamma radiation (NGR), and other parameters measured using the archive multisensor track and multisensor track (MST) for complete composite section construction as well as high-resolution magnetic, sedimentological, and geochemical techniques both for shipboard and postcruise studies which were not available during Leg 94. Furthermore, an excellent upper Miocene section composed of nannofossil ooze and foraminifer nannofosssil ooze has been recovered at Site 608 at 140–260 mbsf. Thus, an important target at this site is the recovery of a complete undisturbed upper Miocene section using the advanced piston coring (APC) system that will allow the study of climate variability and ocean-atmosphere interactions under very different boundary conditions (see above).

Operations

Expedition 306 officially began with the first line ashore on Ponta Delgada, Azores (Portugal), at 1805 h on 2 March 2005. The third Ponta Delgada port call in a row for the *JOIDES Resolution*, which included refueling and restocking bentonite and attapulgite bulk drilling mud, was concluded at 0806 h on 9 March, ~1.8 days behind schedule because of problems with the passive heave compensator (PHC) seal replacement and severe weather that significantly hampered (and slowed) the PHC repair work. Jeff Fox, Director, Science Services, Integrated Ocean Drilling Program (IODP)-Texas A&M University (TAMU), attended the port call accompanied by the new TAMU Dean of Geosciences, Dr. Bjorn Kjerfve.

Hole U1312A

We completed the 344 nmi transit from Ponta Delgada to Site U1312, averaging 10.3 kt, at 1730 h on 10 March 2005 and spudded Hole U1312A at 0830 h on 11 March. Core 1H was fully recovered (10.08 m), suggesting a seafloor depth of 3533.0 mbrf (Table T2). Because of excessive heave (>5 m), initial coring conditions were not optimal and a more realistic seafloor depth estimate was obtained later in Hole U1312B. APC coring utilizing nonmagnetic core barrels continued to a depth of 237.5 mbsf. The first several cores (1H through 10H; to 95.0 mbsf) had questionable shear pressures, and Core 1H required two wireline runs to recover because of a sheared overshot pin. The swell height decreased after Core 10H, and coring system performance improved accordingly. Coring in Hole U1312A was terminated after recovering Core 25H. Drillover was required for recovery of Cores 23H through 25H, and all core barrels fully stroked. Drillover for the last core required 2 h in the semi-indurated white ooze, and Core 23H was recovered bent. Coring may have continued further; however, risk to the equipment was significant, time required for further advancement was reaching a diminishing return, and the Co-Chief Scientists were concerned about initiating Hole U1312B while heave conditions remained low (~1.5 m). In Hole U1312A, we cored 237.5 m, recovering 248.07 m (recovery = 104.45%) (Table T1).

Hole U1312B

After the seafloor was cleared, the vessel was offset 25 m to the northwest of Hole U1312A. Hole U1312B was spudded at 2115 h on 12 March 2005, with the bit positioned at a depth of 3528.0 mbrf, 5.0 m higher than at Hole U1312A. Core barrel 1H advanced 9.5 m and recovered 3.92 m of sediment, placing the seafloor depth for Hole U1312B at 3533.6 mbrf. After successfully achieving a good mudline core, piston coring advanced to 231.9 mbsf. The core line failed at the rope socket while attempting to recover Core 18H, necessitating a wireline fishing trip for the core barrel and sinker bar assembly. Coring continued through Core 25H (231.9 mbsf) as weather conditions progressively deteriorated, leading to another damaged core line at the rope socket and twisted piston rods. Before repairs were completed, weather conditions deteriorated to a point that precluded additional coring. A wind shift and increased velocity forced a heading change to maintain position over the hole. This caused excessive roll, as the ship was exposed to multiple large swells coming from different directions. Because the electrical supervisor expressed concern about the ability to keep the ship on location, the drill string was pulled out of the hole, clearing the seafloor at 0245 h on 14 March. The ship was allowed to drift

off location to minimize vessel motion during the remainder of the pipe trip. By 1700 h on 14 March, the ship was secured and began the slow dynamic positioning move into the prevailing seas back over the drill site. At 0430 h on 15 March, positioning beacon SN 2199 (15 kHz, 211 dB) was recovered, officially ending operations for Hole U1312B and Site U1312. In Hole U1312B, we cored 231.9 m, recovering 236.84 m (recovery = 102.08%) (Table T1).

Lithostratigraphy

Site U1312 consists of two holes, both cored with the APC system. Hole U1312A reached 238 mbsf and Hole U1312B reached 232 mbsf. Sediments at Site U1312 are composed of varying mixtures of biogenic and detrital components, primarily nannofossils, foraminifers, and clay minerals (Fig. F4). Lithologies include nannofossil ooze, foraminifer nannofossil ooze, foraminifer nannofossil ooze with clay, nannofossil ooze with foraminifers, nannofossil ooze with clay, nannofossil ooze with clay and foraminifers, silty clay nannofossil ooze with foraminifers, silty clay nannofossil ooze, nannofossil silty clay, and silty clay calcareous ooze. Most contacts between these lithologies are bioturbated or gradational.

Typical estimates from smear slides of the most abundant detrital components are clay (5%–30%), calcite (<10%), quartz (<10%), and opaques (<5%). Other detrital components only occur in trace amounts (see **"Site U1312 smear slides"** in "Core descriptions"). No discrete ash layers were observed. Dropstones are rare at Site U1312, with the majority occurring in the upper 23 m (Fig. F5; Table T2).

Common smear slide estimates of biogenic components include nannofossils (30%–90%), foraminifers (5%–30%), diatoms (<5%), radiolarians (trace), silicoflagellates (trace), and sponge spicules (trace) (see **"Site U1312 smear slides"** in "Core descriptions"). Total carbonate contents range from 59 to 98 wt% in these cores and show a clear pattern of higher content and lower variability in the lowermost part of the sequence (Fig. F5; Table T24).

Sediments at Site U1312 are divided into two lithologic units (Fig. F5). Unit I represents deposition during the Holocene to late Pliocene and is dominated by biogenic sediments with major to minor detrital components that produce alternating diffuse color bands through much of the unit. Unit II is composed of upper Pliocene–upper Miocene sediments, dominated by nannofossil ooze that exhibits little color change due to a decreased abundance of both detrital content and diffuse color bands downhole.

Description of units

Unit I

Intervals: Sections 306-U1312A-1H-1, 0 cm, through 9H-2, 145 cm, and 306-U1312B-1H-1, 0 cm, through 9H-7, 30 cm

Depths: Hole U1312A: 0–78.95 mbsf and Hole U1312B: 0–79.70 mbsf

Age: Holocene–late Pliocene

Lithologic Unit I is a Holocene–upper Pliocene sequence of sediment composed of nannofossil ooze, nannofossil ooze with clay, foraminifer nannofossil ooze, nannofossil ooze with foraminifers, clay nannofossil ooze with foraminifers, nannofossil ooze with clay and foraminifers, silty clay nannofossil ooze, and nannofossil silty clay. Sediment from the upper 1.50 m of Unit I in Hole U1312B varies in color from light gray (10YR 7/2), light yellowish brown (10YR 6/4), yellowish brown (10YR 5/4), very pale brown (10YR 7/4), to pale brown (10YR 6/3). At the very top of the section, the brownish colors reflect the surface oxidized equivalents of the underlying lithologies. The top of the section also has increased detrital clay content and, in places, a lower carbonate content relative to the remainder of Unit I (Figs. F5, F26; Table T24).

Changes in color can be seen downhole from 1.50 mbsf to the bottom of Unit I (Fig. F6). The sediment is dominantly white (N9, 10YR 8/1, and 5Y 8/1) and very light gray (N8) and contains striking alternating bands of light gray (10YR 7/1, 10YR 7/2, 5Y 7/1, 5Y 7/2, 2.5Y 7/2, and N7), medium light gray (N6), gray (10YR 6/1 and 10YR 5/1), very dark gray (10YR 3/1), grayish brown (10YR 5/2), light brownish gray (10YR 6/2 and 2.5Y 6/2), very pale brown (10YR 8/3, 10YR 8/2, and 10YR 7/3), pale brown (10YR 6/3), and grayish brown (10YR 5/2 and 2.5Y 5/2). The presence of these decimeter-scale alternating color bands is one of the dominant lithologic characteristics of Unit I, suggesting fluctuating amounts of detrital input. Contacts between these color changes are often gradational and bioturbated. Through much of Unit I, bioturbation varies from rare to abundant. In darker lithologies, bioturbation is most evident by the presence of diffuse millimeter- to centimeter-scale burrows and the mottled appearance of the sediment. In the lighter lithologies, bioturbation is most easily defined by flecks of pyrite near the burrows. Unit I also shows millimeter- to centimeter-scale olive (5Y 5/3), bluish white (5B 9/1), light greenish gray (5G 7/1), and pale green (5G 7/2) bands. The origin of these thinner color bands is unclear, possibly related to either primary or postdepositional processes (Figs. F7, F8; Table T3). The range of carbonate contents varies from 59 to 96 wt% through the entire unit. Accord-

ing to smear slide estimates, biogenic components include nannofossils (40%–90%), foraminifers (0%–30%), diatoms (<5%), radiolarians (0%–trace), silicoflagellates (0%–trace), and sponge spicules (0%–trace). Detrital components include clay (5%–30%), calcite (<10%), quartz (<10%), opaques (<5%), and not more than trace amounts of volcanic glass, feldspar, chlorite, and glauconite (see **"Site U1312 smear slides"** in "Core descriptions"). Two distinct layers containing as much as 20% detrital calcite and 20% quartz were identified by smear slide analyses at 6.38 and 13.76 mbsf in Hole U1312B (Fig. **F9**). X-ray diffraction (XRD) data from the same levels (Sample 306-U1312B-2H-CC, 13–14 cm) illustrate the presence of detrital calcite, dolomite, and quartz (Fig. **F10A**). Both results suggest these levels may represent layers of ice-rafted debris (IRD). Sediment components >2 mm present in Unit I are inferred to be dropstones, and their occurrence is generally rare, except for the upper part (Table **T2**).

Unit I is divided into two subunits: Subunits IA and IB. This division is mainly based on changes in the magnetic susceptibility record and total carbonate content.

Subunit IA

Intervals: Sections 306-U1312A-1H-1, 0 cm, through 5H-1, 125 cm, and 306-U1312B-1H-1, 0 cm, through 5H-4, 140 cm

Depths: Hole U1312A: 0–39.25 mbsf and Hole U1312B: 0–38.30 mbsf

Age: Holocene–late Pliocene

Subunit IB

Intervals: Sections 306-U1312A-5H-1, 125 cm, through 9H-2, 145 cm, and 306-U1312B-5H-4, 140 cm, through 9H-7, 30 cm

Depths: Hole U1312A: 39.25–78.95 mbsf and Hole U1312B: 38.30–79.70 mbsf

Age: late Pliocene

Subunit IA exhibits more variability in the magnetic susceptibility record, showing multiple excursions toward higher values (Fig. **F29**), and presents lower average and higher variability in carbonate contents than Subunit IB (Figs. **F5, F26;** Table **T24**). Furthermore, dropstones are more concentrated in Subunit IA than in Subunit IB, particularly in the upper 23 m of the sedimentary succession. Preliminary analyses of these dropstones show that they range in size from 2 to 15 mm, are subrounded to angular, and are of basic igneous and/or metamorphic (metabasalts) and sedimentary/metasedimentary (carbonates, sandstones, and mudstones) origins. Only two dropstones were identified in Subunit IB, at 77 mbsf in Hole U1312A and at 78 mbsf in Hole U1312B and are of unidentified origin.

Unit II

Intervals: Sections 306-U1312A-9H-2, 145 cm, through 25H-CC, 30 cm, and 306-U1312B-9H-7, 30 cm, through 25H-CC, 11 cm

Depths: Hole U1312A: 78.95–238.03 mbsf and Hole U1312B: 79.70–232.05 mbsf

Age: late Pliocene–late Miocene

Lithologic Unit II differs from Unit I in the loss of distinct color changes caused by cyclic terrigenous input and higher carbonate contents. The contact between the two units is gradational, and it is not easily identifiable by visual core description. This boundary mainly corresponds to reduced-amplitude fluctuations in the lightness record (Fig. **F5**).

Unit II consists of predominantly white (N9) nannofossil oozes with minor amounts of foraminifers and clay. The uppermost part of the unit contains diffuse and very faint light gray bands (10YR 7/1, 10YR 7/2, 5Y 7/1, 5Y 7/2, 2.5Y 7/2, and N7), with millimeter- and centimeter-scale thickness. The number of color bands gradually decreases downcore, and the remainder of Unit II is typically white and homogeneous. Pale green (5G 7/2) and various shades of gray (N8 and N7) streaks and bands, similar to those observed in Unit I, are frequently present through the upper part of the sequence (Fig. **F8;** Tables **T3, T4**). Calcium carbonate contents are higher than in Unit I, varying between 81 and 98 wt%, with most of the unit having >90 wt% carbonate (see Table **T24**). This confirms that pure oozes with between 5% and 10% terrigenous detritus are present in this part of the sequence. XRD data from Sample 306-U1312A-14H-4, 55–56 cm, demonstrate that calcite is the predominant component in this interval, strengthening this argument (Fig. **F10B**).

Dropstones are absent to rare in cores of Unit II. Only a total of six isolated gravels were found in Hole U1312B at 127.52, 166.33, 166.37, and 168.24 mbsf (Fig. **F5;** Table **T2**). These gravels occur near the top of individual cores in soupy intervals and consequently may not be in situ and may have fallen from the upper part of the sedimentary succession during drilling operations.

Finally, an important feature found in the sedimentary sequence is a foraminiferal sand (foraminifer ooze) bed, which occurs from 118.10 to 118.90 mbsf in Hole U1312A and from 114.11 to 114.45 mbsf in Hole U1312B. This bed has a sharp erosional base and a gradational upper contact and is normally graded, probably representing a low-density turbidite (Fig. **F11**). This bed correlates with a graded fora-

miniferal sand described at Site 608 in depth intervals of 114.69 to 114.95 mbsf (Hole 608) and 119.9 to 120.4 mbsf (Hole 608A) (Shipboard Scientific Party, 1987). A 3 cm thick isolated layer with the same characteristics was also observed at 33.26–33.29 mbsf in Hole U1312B. In Hole U1312A, a corresponding coarse-grained foraminifer ooze was not found at a similar depth interval, probably due to drilling disturbance (flow-in interval) or very local occurrence.

Toward the base of Unit I, a change in the degree of lithification of the sequence was observed; the sediments grade from ooze to firm ooze. The use of drill-over and presence of drilling-induced fractures are evidence that the bottom of Unit II is close to the transition zone from nannofossil ooze to nannofossil chalk, similar to that described at Site 608 (Shipboard Scientific Party, 1987).

Discussion

Sediments at Site U1312 mainly represent pelagic deposition during late Neogene–Quaternary times, dominantly expressed as varying mixtures of biogenic and detrital components, primarily nannofossils, foraminifers, and clay minerals. The upper Miocene–upper Pliocene sediments of Unit II are indicative of uniform stable pelagic sedimentation processes interrupted only by one large isolated episode of a turbidity-current event near 4 Ma. In contrast, a preliminary age model based on variation in the abundance of biogenic and detrital sediment characterizes the deposition of Unit I. According to biostratigraphic and paleomagnetic results, this prominent change in deposition occurred between 3.3 and 3.5 Ma. This interval marks a critical point in Earth's recent climate history. Benthic stable isotope data record a progressive but oscillatory deterioration of the northern hemisphere climate during this time interval, which gradually led to the onset of significant continental ice sheets at ~2.7 Ma (Raymo, 1992). The preliminary age model for Site U1312 indicates that the lithologic changes recorded in Unit I may be related to climate-controlled changes in detrital input during glacial–interglacial cycles, as interpreted from the lightness record (see Fig. **F23**). The growth of continental ice sheets in the northern hemisphere provided sources for the detrital sediment component in Unit I through ice rafting and eolian deposition associated with higher regional-hemispheric wind speeds (Stein and Sarnthein, 1984).

The occurrence of different biostratigraphic events suggests that the subunit boundary is placed between 1.97 and 2.74 Ma. Although this boundary cannot be constrained with precision, data from Subunit IA support more distinct glacial–interglacial cyclicity, which corresponds to the timing of major ice sheets during the late Pliocene and Pleistocene. The distinctive occurrence of dropstones found in the upper 23 m representing the last ~1 m.y. may be of great importance in identifying IRD events and possible source areas at Site U1312. In particular, the data from Hole U1312B show that these dropstones occur during glacials, as suggested by the preliminary age model based on the lightness record (see Fig. **F23**). Finally, an increased abundance and size of the dropstones are present in the interval from 13.99 to 14.43 mbsf (Fig. **F5;** Table **T2**), possibly correlating with the prominent glacial Stage 16 (see **"Stratigraphic correlation"**).

Biostratigraphy

Core catcher samples from Holes U1312A and U1312B contain rich assemblages of calcareous nannofossils and planktonic foraminifers that are generally well preserved, with the exception of some intervals from the upper Miocene. In these sediments, dissolution of nannofossils and overgrown discoasters occur and planktonic foraminifer shells are increasingly fragmented and encrusted. In contrast, silica preservation is poor in the uppermost part of each hole and the sediments are completely barren of diatoms and radiolarians in the lower part. From top to bottom, a succession of calcareous nannofossil and planktonic foraminifer events provide a reliable biostratigraphic framework that, in the upper part, is supported by the siliceous plankton biozones (Tables **T5, T6**).

According to the age of biostratigraphic events recognized in this study, a sedimentary sequence encompassing the late Miocene–Holocene was recovered from Site U1312 (Fig. **F12**). Sediments from the late Pliocene and Pleistocene contain abundant planktonic foraminifers in relation to calcareous nannofossils, whereas planktonic foraminifer abundance from lower Pliocene and Miocene sediments is reduced relative to nannofossils. In particular, Samples 306-U1312A-18H-CC and 306-U1312B-19H-CC are poor in foraminifers, probably due to dissolution in sediments from the uppermost Miocene.

Comparison of age-depth plots from Holes U1312A and U1312B show similar trends in sedimentation rate in both holes (Figs. **F13, F14**). Sedimentation rates in the late Miocene–earliest Pliocene are generally low (<3 cm/k.y.), and during much of the late Miocene rates are <1.0 cm/k.y. at Site U1312. Rates increased in the early Pliocene, reaching 8.33 cm/k.y. in Hole U1312A and 7.41 cm/k.y. in Hole U1312B. Sedimentation rates decreased significantly in the

late Pliocene, and late Pliocene and Pleistocene sedimentation rates are relatively low in both holes (1.53 and 1.69 cm/k.y., respectively).

Calcareous nannofossils

We examined all core catcher samples from Holes U1312A and U1312B for calcareous nannofossils. Several additional samples were taken from Cores 306-U1312A-5H and 19H to refine the biostratigraphy. All samples yielded abundant to very abundant nannofossil assemblages. Preservation is generally good to moderately good, particularly in the upper part of the section, although evidence of dissolution and overgrowth of discoasters begins downhole in Cores 306-U1312A-18H and 306-U1312B-18H. Samples below these cores contain moderate to moderately well preserved nannofossils. *Pseudoemiliania lacunosa* varieties dominate Pleistocene assemblages, whereas reticulofenestrids dominate Pliocene and Miocene assemblages. Some reworking is evident in both holes. Reworked specimens of *Reticulofenestra pseudoumbilicus* and *Sphenolithus abies* occur within nannofossil Zone NN16, and minor Paleogene reworking is evident within Cores 306-U1312A-25H and 306-U1312B-25H.

The sections recovered at Site U1312 yielded Pleistocene, Pliocene, and upper to uppermost middle Miocene assemblages (Tables **T7, T8**). Six Pleistocene nannofossil datums defined by Sato et al. (1999) are identified at Site U1312. The first occurrence (FO) of *Emiliania huxleyi* (0.25 Ma), which marks the base of Martini's (1971) Zone NN21, is present in Samples 306-U1312A-1H-CC and 306-U1312B-1H-CC. The last occurrence (LO) of *P. lacunosa* (0.41 Ma), which defines the base of Zone NN20, is detected in Samples 306-U1312A-2H-CC and 306-U1312B-2H-CC. Additionally, the FO of *Gephyrocapsa parallela* (0.95 Ma) occurs in Sample 306-U1312B-2H-CC but is not found in Hole U1312A. *Gephyrocapsa* spp. (large) (1.21–1.45 Ma) occurs in Sample 306-U1312A-3H-CC but is not present in Hole U1312B. The LO of *Helicosphaera sellii* (1.27 Ma) also occurs in Sample 306-U1312A-3H-CC but is not detected in Hole U1312B until Sample 306-U1312B-4H-CC. The FO of *Gephyrocapsa caribbeanica* (1.73 Ma), which we use to approximate the Pliocene/Pleistocene boundary, occurs in Samples 306-U1312A-4H-CC and 306-U1312B-4H-CC.

Sample 306-U1312B-4H-CC is problematic because it contains the co-occurrence of *Gephyrocapsa* spp. (>4 µm), *Discoaster brouweri*, and *Discoaster pentaradiatus*. According to Sato et al. (1999) and de Kaenel et al. (1999), the LO of *D. brouweri* (1.97 Ma) and the FO of *G. caribbeanica* (>4 µm) are separated by 240,000 y and thus should not co-occur. Okada (2000), however, reports medium-sized (>4 µm) *Gephyrocapsa* spp. in the uppermost Pliocene sequences from Blake Ridge, northwest Atlantic Ocean and indicates the Pleistocene medium-sized *Gephyrocapsa* datum (1.73 Ma) should be placed at the base of consistent occurrences of medium-sized *Gephyrocapsa*. Thus, we suggest Sample 306-U1312B-4H-CC is older than 2.38 Ma based on the presence of *D. brouweri* and *D. pentaradiatus*. The FO of planktonic foraminifer datum *Globorotalia inflata*, however, is also present in this sample and indicates an age younger than 2.08 Ma. Therefore, examination of samples from Core 306-U1312B-4H is necessary to determine if discoasters found in Sample 306-U1312B-4H-CC are reworked, which would yield a younger (Pleistocene) age for this sample.

Five Pliocene events dated by Sato et al. (1999) and one by Shackleton et al. (1995) occur within the sedimentary section at Site U1312. Three events from the upper Pliocene (LO of *D. brouweri*, LO of *D. pentaradiatus* [2.38 Ma], and LO of *Discoaster surculus* [2.54 Ma]) occur together in Sample 306-U1312A-5H-CC, which led us to subsample Core 5H in order to determine if a hiatus is present. Examination of the subsamples determined the LO of *D. brouweri*, which marks the base of Zone NN19, occurs in Sample 306-U1312A-5H-2, 130–131 cm. The LO of *D. pentaradiatus*, which marks the base of Zone NN18, is recorded in Sample 306-U1312A-5H-5, 125–126 cm. The LO of *D. surculus* (base of Zone NN17) also occurs in Sample 306-U1312A-5H-5, 125–126 cm. We interpret this to indicate there is not a hiatus present in Core 306-U1312A-5H, although sedimentation rates are very low. In addition, the LO of *D. surculus* co-occurs in Sample 306-U1312B-5H-CC with the LO of *Discoaster tamalis* (2.74 Ma). Within Hole U1312A, the LO of these two species is separated, as *D. tamalis* is not present until Sample 306-U1312A-6H-CC. Whereas the discoaster species used as markers for the upper Pliocene are easy to identify and generally abundant, they are susceptible to reworking. As a result, further work is necessary to resolve the differences in upper Pliocene biostratigraphy between Holes U1312A and U1312B.

The intervals from 306-U1312A-6H-CC to 11H-CC and from 306-U1312B-5H-CC to 12H-CC are characterized by the occurrence of *D. tamalis* and absence of *R. pseudoumbilicus* (>7 µm), indicating an age between 2.74 and 3.85 Ma. The LO of *R. pseudoumbilicus* (>7 µm) (3.85 Ma), which marks the base of Zone NN16, occurs in Samples 306-U1312A-12H-CC and 306-U1312B-13H-CC. This species is reworked in Zone NN16 at Site U1312. We identified the LO as the top of consistent, common occurrences of *R. pseudoumbilicus*, although the true LO is likely some-

where within Cores 306-U1312A-12H and 306-U1312B-13H.

Only one datum from the lower Pliocene is identified at Site U1312. The LO of *Amaurolithus primus* (4.56 Ma), which approximates the base of Zone NN15, is found in Samples 306-U1312A-13H-CC and 306-U1312B-15H-CC. The ceratoliths are very rare to absent at Site U1312, making it impossible to identify the lower Pliocene FO and LO of *Ceratolithus acutus*.

We identified 13 nannofossil events dated by Raffi and Flores (1995) and Backman and Raffi (1997) in the Miocene sediments at Site U1312. The LO of *Discoaster quinqueramus* (5.537 Ma), which we use to approximate the Miocene/Pliocene boundary (5.332 Ma), is tentatively found in Samples 306-U1312A-18H-CC and 306-U1312B-19H-CC. Overgrowth of discoasters within the upper Miocene sediments make it very difficult to identify this event with certainty. *Amaurolithus amplificus* (5.999–6.84 Ma) also occurs in Sample 306-U1312A-18H-CC and indicates Subzone NN11D. The FO of *A. primus* (7.392 Ma), which marks the base of Subzone NN11B, occurs with *D. quinqueramus* in Samples 306-U1312A-18H-CC and 306-U1312B-19H-CC. We took subsamples from Core 306-U1312A-19H to determine if any amauroliths were present; however, no biostratigraphic events were identified within these subsamples and further refinement of the stratigraphy is impossible at this time.

The FO of *Discoaster berggrenii* (8.281 Ma, base of Subzone NN11A) occurs in Samples 306-U1312A-19H-CC and 306-U1312B-20H-CC and coincides with rare to absent *R. pseudoumbilicus* (>7 µm). Backman and Raffi (1997) indicate *R. pseudoumbilicus* (>7 µm) is absent between 7.10 and 8.79 Ma, which coincides with the LO of *D. berggrenii* and corresponds to the data from Site U1312. Sample resolution, however, made it impossible to determine the top of the small *Reticulofenestra* interval. The FO of *Discoaster loeblichii* (8.43 Ma) is detected in Sample 306-U1312A-20H-CC and coincides with the LO of *D. berggrenii* in Sample 306-U1312B-20H-CC, as well as the rare to absent *R. pseudoumbilicus* (>7 µm) interval in both holes.

The FO of *Minylitha convallis* (9.43 Ma) is observed in Samples 306-U1312A-21H-CC and 306-U1312B-21H-CC. The LO of *Discoaster hamatus* (9.64 Ma), which defines the base of Zone NN10, occurs in Samples 306-U1312A-22H-CC and 306-U1312B-22H-CC. Catinasters are very rare at Site U1312; however, *Catinaster calyculus* is found in Hole U1312B. The LO of *C. calyculus* (9.64 Ma) occurs in Sample 306-U1312B-23H-CC, whereas the FO of *C. calyculus* (10.705 Ma) occurs in Sample 306-U1312B-24H-CC. Additionally, the FO of *Discoaster neohamatus* (10.45 Ma) and *D. hamatus* (10.48 Ma, base of Zone NN9) co-occur in Samples 306-U1312A-24H-CC and 306-U1312B-24H-CC. Thus, these cores in both holes must be younger than 10.45 Ma. *Catinaster coalitus* (10.794 Ma), which marks the base of Zone NN8, is not observed at Site U1312.

The presence of rare *Coccolithus miopelagicus* in samples from the bottom of both holes (Samples 306-U1312A-25H-CC and 306-U1312B-25H-CC) indicates we reached the LO of *C. miopelagicus* (10.947 Ma), which correlates to the uppermost middle Miocene. These cores contain rare Paleogene material (*Ellipsolithus macellus* in Hole U1312A and *Reticulofenestra umbilicus* in Hole U1312B), suggesting the possibility the occurrences of *C. miopelagicus* are reworked. If that is the case, both holes only penetrated to the lowermost upper Miocene.

Planktonic foraminifers

We studied planktonic foraminifer assemblages in all core catchers from Holes U1312A and U1312B (Tables **T9, T10**). In addition, we examined a sample from Section 306-U1312A-1H-2 and washout from the top of Section 306-U1312B-1H-1, for which only the >150 µm fraction was available. All samples were washed with tap water. Planktonic foraminifers dominate the sand fraction in all core catchers and are primarily moderately to well preserved. Poor preservation is observed in some of the Miocene samples (306-U1312A-18H-CC and 306-U1312B-19H-CC) and also in the interval from Sample 306-U1312B-23H-CC to 25H-CC. The foraminifer assemblage in most core catcher samples consists of 11 to 15 different species, with lower numbers of species observed in some of the poorly preserved samples.

The FOs of *G. inflata* and *Globorotalia truncatulinoides* are contemporaneous in Sample 306-U1312A-4H-CC. In Hole U1312B, however, *G. inflata* occurs in Sample 306-U1312B-4H-CC and *G. truncatulinoides* in Sample 3H-CC. The absence of *G. truncatulinoides* in Sample 306-U1312B-4H-CC is most probably related to hydrographic conditions because the fauna in Sample 4H-CC indicates colder, which for *G. truncatulinoides* signifies less favorable surface water temperatures than the fauna in Sample 306-U1312A-4H-CC. The FO events of both species occur in the North Atlantic and Mediterranean at 2.09 Ma (Weaver and Clement, 1987).

The LO of *Globorotalia puncticulata* is the next biostratigraphic event and occurs in Samples 306-U1312A-5H-CC and 306-U1312B-5H-CC. In Hole U1312A, it is accompanied by the LO of *Neogloboquadrina atlantica*. The LOs of both species are calibrated to the astronomical timescale in the Mediter-

ranean and dated to 2.41 Ma by Lourens et al. (1996). Because of its highly convex dorsal side, the species described as *Globorotalia* cf. *crassula* by Weaver and Clement (1987) is referred to as *Globorotalia hirsuta* during Expedition 306. Consequently, the LO of *G.* cf. *crassula* at 3.18 Ma (Weaver and Clement, 1987) is designated as "disappearance of *G. hirsuta*." This event can clearly be defined only in Hole U1312A, where it occurs in Sample 306-U1312A-6H-CC. Although based on very few specimens, we place the LO of *Sphaeroidinellopsis seminulina* in Sample 306-U1312B-7H-CC, which indicates an age of 3.19 Ma (Lourens et al., 1996). In Hole U1312A, this species last occurs in Sample 306-U1312A-11H-CC, which is not believed to be the real LO since this species is often rare in the studied samples (Tables **T9, T10**) and could therefore be present higher in the sedimentary record. As in records from the Mediterranean Sea, a well-defined gap in the occurrence of *G. puncticulata* (Lourens et al., 1996) is observed at Site U1312. The reappearance of this species occurs in Samples 306-U1312A-10H-CC and 306-U1312B-8H-CC and the disappearance in Samples 306-U1312A-12H-CC and 306-U1312B-12H-CC, respectively. In the Mediterranean, this gap occurs between 3.31 and 3.57 Ma (Lourens et al., 1996).

The last common occurrence (LcO) of *Globorotalia margaritae* defines the next biostratigraphic marker horizon and is located in Samples 306-U1312A-13H-CC and 306-U1312B-13H-CC. Weaver and Clement (1987) state this event is diachronous between the high and low latitudes. The latitude of Site U1312 is similar to that of the Mediterranean, and we therefore consider the 3.98 Ma age of the event reported by Lourens et al. (1996) to be reliable. In the lower Pliocene, the first abundant occurrence (FaO) of *G. puncticulata*, together with the FaO of *Globorotalia crassaformis*, is observed in Samples 306-U1312A-14H-CC and 306-U1312B-14H-CC. The FaO of *G. puncticulata* can be traced throughout the North Atlantic and Mediterranean and is calibrated to the astronomical timescale and dated to 4.52 Ma (Lourens et al., 1996).

The FaO of *G. margaritae* is observed in Samples 306-U1312A-17H-CC and 306-U1312B-18H-CC and occurs at ~6.0 Ma near the base of Subchron C3A.1n (F.J. Sierro, unpubl. data). In Samples 306-U1312A-18H-CC and 306-U1312B-19H-CC, two biostratigraphic events occur: (1) the preferentially sinistral to dextral coiling direction change in *Neogloboquadrina pachyderma* and (2) the first common occurrence of the *G. miotumida* group. *N. pachyderma,* which was preferentially sinistral in the late Miocene, underwent a series of changes in coiling beginning at 6.3 Ma to become dominantly dextral during the Pliocene (Hilgen and Krijgsman, 1999; Sierro et al., 2001; Hodell et al., 2001). The *G. miotumida* group, including *Globorotalia conomiozea*, expanded in the North Atlantic and Mediterranean when these species replaced the *Globorotalia menardii* 5 (dextral forms) group (Sierro, 1985; Sierro et al., 1993); however, the latter group was not observed in these samples, probably due to low sampling resolution (one sample per core) or the possible presence of a disconformity at this site. This is a distinct event that occurs at 7.24 Ma and has been used to mark the Tortonian/Messinian boundary (Sierro et al., 1993; Hilgen et al., 1995). The *G. menardii* 4 group LcO appears in Samples 306-U1312A-19H-CC and 306-U1312B-20H-CC, respectively. This event is astronomically dated to 7.51 Ma (Krijgsman et al., 1995; Hilgen et al., 1995).

From Samples 306-U1312A-20H-CC and 306-U1312B-21H-CC to the base of each hole, *N. pachyderma* is again preferentially dextral. In the Mediterranean, this species becomes dominantly dextral at 9.5 Ma (Krijgsman et al., 1995, Hilgen et al., 1995); however, several fluctuations in coiling are recorded between 7.8 and 9.55 Ma. Although a higher resolution analysis of this species is needed to accurately date this interval, an age older than 7.8 Ma is assigned to this core. This event is preceded in Samples 306-U1312A-21H-CC and 306-U1312B-22H-CC by the LO of *Globorotalia lenguaensis*, which occurs in the tropical Atlantic at 8.99 Ma (Turco et al., 2002). This species, however, is always rare, and therefore the position of this event is probably less precise. The last stratigraphic marker observed in both holes is the FO of *N. pachyderma* as its morphotype *Neogloboquadrina acostaensis*, which is present in Samples 306-U1312A-24H-CC and 306-U1312B-24H-CC. This event has been astronomically dated to 10.55 Ma (Hilgen et al., 2000) in the Mediterranean and to 9.89 Ma in the tropical Atlantic (Turco et al., 2002), with the former age probably more reliable in the North Atlantic at middle latitudes.

Globigerina nepenthes, which first appears at 11.6 Ma (Spezzaferri, 1998), occurs in Samples 306-U1312A-25H-CC and 306-U1312B-25H-CC. *Neogloboquadrina mayeri,* with its LO at 11.2 Ma (Hilgen et al., 2000), is not observed in these samples, so the age at the bottom of both holes must be younger than 11.2 Ma. In addition, specimens of *Neogloboquadrina* other than the morphotype *N. acostaensis*, including large encrusted *N. atlantica*, are still present in Samples 306-U1312A-24H-CC and 306-U1312B-24H-CC, indicating that the bottom of the hole is above the FO of the neogloboquadrinids, which is dated to 11.78 Ma (Hilgen et al., 2000). According to the planktonic foraminifer stratigraphy, Holes U1312A and U1312B

encompass the interval from the base of the Tortonian (late Miocene) to the late Quaternary.

IRD is observed in the two uppermost core catcher samples of both holes. Based on correlation of the lightness L* record with the benthic $\delta^{18}O$ stack of Lisiecki and Raymo (2005) (see **"Stratigraphic correlation"**), these samples correlate with the transition from marine isotope Stage (MIS) 11 to MIS 10 (Samples 306-U1312A-1H-CC and 306-U1312B-1H-CC) and with MIS 22 (Samples 306-U1312A-2H-CC and 306-U1312B-2H-CC). For these stages, the planktonic foraminifer fauna suggest the presence of transitional, rather than subpolar, waters, as high abundances of *G. inflata*, *N. pachyderma* (dextral), *Globigerina bulloides*, and *Globigerinella aequilateralis* appear together with minor numbers of the subtropical species *Globigerinoides ruber* and *G. crassaformis* (Tables **T9, T10**). Subtropical to tropical species of the *Globigerinoides* group are also present in rare to common abundances throughout the entire Pliocene. Samples 306-U1312A-18H-CC and 306-U1312B-17H-CC, both from the Miocene, contain heavily encrusted, relatively large sized *Neogloboquadrina* species.

Benthic foraminifers

Rare to few well preserved benthic foraminifers are present in the oozes at Site U1312 (Tables **T11, T12**). Three assemblages are distinguished based on their faunal composition.

Assemblage I (*Oridorsalis umbonatus*)

This assemblage occurs between Samples 306-U1312A-1H-CC and 14H-CC and also between Samples 306-U1312B-1H-CC and 14H-CC. *O. umbonatus* is the dominant species and is associated with *Cibicidoides wuellerstorfi*, *Globocassidulina subglobosa,* and *Melonis barleeanus*.

Assemblage II (*Nuttalides umboniferus-Pullenia bulloides-Uvigerina* spp.)

This assemblage occurs between Samples 306-U1312A-14H-CC and 19H-CC and also between Samples 306-U1312B-14H-CC and 20H-CC. It is characterized by deepwater foraminifers such as *N. umboniferus*, *P. bulloides*, *Uvigerina peregrina,* and *Uvigerina proboscidea*. The relative abundances of these species vary from sample to sample.

Assemblage III (*Astrononion stelligerum*)

This assemblage occurs below Sample 306-U1312A-19H-CC in Hole U1312A and Sample 306-U1312B-20H-CC in Hole U1312B. It is characterized by the highest relative abundance of *A. stelligerum*. *C. wuellerstorfi* and *P. bulloides* are frequently found with *A. stelligerum* in Hole U1312A.

The faunal change from Assemblage III to II occurs at ~7.246 Ma, near the Tortonian/Messinian boundary. The stratigraphic distribution of the benthic foraminifer assemblages likely reflects changes in deepwater conditions through time. Other faunal differences may possess additional paleooceanographic significance, but shipboard time constraints prohibited a more detailed investigation.

Diatoms

We investigated diatoms in smear slides from 50 core catcher samples and 125 depth intervals in core sections from Holes U1312A and U1312B (Tables **T13, T14**). Trace numbers of diatoms are generally present within the upper 60 m in Hole U1312A and the upper 90 m in Hole U1312B, corresponding to the Pliocene–Pleistocene interval. The next two to three cores below these levels are marked by dissolution and a decrease in diatom abundance. Below Samples 306-U1312A-11H-CC and 306-U1312B-12H-CC, the core catchers are almost completely devoid of diatoms. Silicoflagellates are generally present with the diatoms.

The generally low abundance of diatoms in the upper one-third of Holes U1312A and U1312B made placement of defined datums (Baldauf, 1987) difficult, and the almost complete lack of diatoms in the lower two-thirds of both holes made it impossible.

The base of the *Fragilariopsis doliolus* Zone, defined by the LO of *Fragilariopsis reinholdii* (0.48–0.45 Ma), occurs in Samples 306-U1312A-2H-CC and 306-U1312B-3H-CC (ignoring a single, probably reworked specimen in Sample 306-U1312B-2H-CC). *Rhizosolenia curvirostris* occurs in samples taken from the first sections of Core 306-U1312B-1H, suggesting an age of at least 0.3 Ma.

The *F. reinholdii* Zone is not present in the Hole U1312A material. In Hole U1312B, this zone spans from Samples 306-U1312B-3H-CC to 306-U1312B-6H-CC, based on the co-occurrence of *F. doliolus* (FO = 1.9 Ma), *F. reinholdii*, and *Fragilariopsis fossilis* (LO = ~0.5 Ma).

The upper part of the *Alveus marinus* Zone is present from Samples 306-U1312A-3H-CC to 5H-CC based on the occurrence of *F. reinholdii* and *F. fossilis* without *F. doliolus*. This zone is not readily apparent in Hole U1312B. The bottom of the *A. marinus* Zone is not identified, as the LO of the zonal marker *Fragilariopsis jouseae* (2.66–2.83 Ma) is not observed in material from Site U1312. *Thalassiosira convexa* last occurs in the lower part of the *A. marinus* Zone (2.58–2.68

Ma) and gives a secondary datum to indicate the beginning of this zone.

Because of the rarity and poor preservation of diatoms in the lower two-thirds of both holes, the assignment of biostratigraphic zones is tentative. The absence of *F. doliolus,* continued presence of *F. reinholdii* and *F. fossilis*, and occasional occurrence of *T. convexa* indicate the oldest diatom-containing intervals of both cores belong somewhere between the *A. marinus* and *T. convexa* Zones (6.2–1.9 Ma). This interval spans from Samples 306-U1312A-6H-CC to 10H-CC and from 306-U1312B-7H-CC to 11H-CC. Below Samples 306-U1312A-10H-CC and 306-U1312B-11H-CC, the core catchers are essentially devoid of diatoms.

The diatom flora in the upper six core catchers of both holes is diverse considering the preservation. A total of 42 diatom species are identified, along with several types of silicoflagellates. The assemblage is dominated by warm-water flora, as observed by Baldauf (1987), including *Coscinodiscus radiatus, Hemidiscus cuneiformis, Thalassiosira oestrupii* group, *A. marinus, Thalassionema nitzschioides* group, *F. reinholdii, F. fossilis*, and species of the *Thalassiosira* genus with a linear areolae array. *Chaetoceros* resting spores are often present, indicating high productivity. Both holes contain plentiful *Thalassiothrix* fragments, indicating influence of colder waters. Several samples from Hole U1312B contain *Actinocyclus curvatulus*, also indicating a cold-water influence. In both holes, coastal diatoms such as *Paralia sulcata* and *Raphoneis* are observed in the upper three core catchers. Additionally, *Fragilariopsis* aff. *pseudocylindrus* is present in Sample 306-U1312A-3H-CC, which suggests transport of coastal diatoms to open waters.

Radiolarians

We examined radiolarians in all core catcher samples from Holes U1312A and U1312B. Only eight samples (306-1312B-1H-CC through 4H-CC, 6H-CC, and 8H-CC through 10H-CC) include identifiable radiolarian specimens (Tables **T15, T16**). These samples generally contain rare to few poorly preserved radiolarians, but common, well preserved specimens are present in Sample 306-U1312B-3H-CC. This sample contains numerous species, 60 of which are listed in Table **T15.**

According to Ciesielski and Bjørklund (1995), *Cycladophora davisiana* first occurs in the middle latitude North Atlantic at 2.59 Ma in Sample 94-609-19X-CC, 2–4 cm. Haslett (1994, 2004) recognized this species in the same site (Sample 94-609-18X-CC) at 2.44 Ma. The two age models applied by Haslett (1994, 2004) and Ciesielski and Bjørklund (1995) are in close agreement; therefore, we assume the FO of *C. davisiana* is close to 2.59 Ma.

In Hole U1312B, *C. davisiana* is observed in all core catcher samples from Sample 306-U1312B-1H-CC to 4H-CC, whereas 5H-CC is barren of radiolarians. In Sample 306-U1312B-6H-CC, where radiolarians are abundant, *C. davisiana* is absent. This indicates the FO of *C. davisiana* is somewhere in Core 306-U1312B-5H. The maximum age for Sample 306-U1312B-4H-CC is therefore 2.59 Ma.

Motoyama (1997) demonstrated at DSDP Site 192 that *C. davisiana* evolved from *Cycladophora sakaii* in the northwest Pacific. The oldest specimens assignable to *C. davisiana* are observed in Sample 19-192-18R-1, 50–52 cm (4.2 Ma), with a typical rich *C. davisiana* population occurring at ~2.7–2.3 Ma. This indicates *C. davisiana* evolved in the northwest Pacific and then spread to the rest of the world ocean. Ciesielski and Bjørklund (1995) reported the FO of *C. davisiana* at 2.99–3.08 Ma in the Labrador Sea in Sample 105-646B-25X-CC. They suggested that *C. davisiana* evolved in the Labrador Sea and migrated through the Arctic Ocean into the North Pacific (2.62–2.64 Ma; Stage 114) before migrating into the Norwegian Sea (2.63–2.53 Ma) and then the North Atlantic (2.59–2.44 Ma; Stage 109–102). According to the new results by Motoyama (1997), however, the most likely route of migration is from the northwest Pacific to the Labrador Sea via the Arctic Ocean.

Paleomagnetism

Archive halves of all cores recovered at Site U1312 were measured on the three-axis cryogenic magnetometer at 5 cm intervals. The natural remanent magnetization (NRM) was measured before (NRM step) and after stepwise alternating-field (AF) demagnetization in peak fields of up to 20 mT. Cores 306-U1312A-1H through 9H and 19H through 21H were AF demagnetized at peak fields of 10 and 20 mT. Cores 306-U1312A-10H through 18H and 22H through 25H were AF demagnetized at a peak field of 20 mT. All cores from Hole U1312B were AF demagnetized at a peak field of 20 mT.

Downcore variations in magnetic intensity in Holes U1312A and U1312B are shown in Figure **F15.** Data associated with intervals identified as physically disturbed were removed. NRM intensities after 20 mT AF demagnetization are in the range of 10^{-3} A/m above 40 mbsf and below 220 mbsf in both holes (Fig. **F15**). Intensities are one order of magnitude lower (in the range of 10^{-4} A/m) in the 40–100 mbsf depth interval and two orders of magnitude lower (in the range of 10^{-5} A/m) between 100 and 210 mbsf. Inclination and declination data (after 20 mT

AF demagnetization) are shown in Figure F16. Declination values have been corrected using Tensor tool data, which were available starting with Cores 306-U1312A-3H and 306-U1312B-2H. Both holes display similar directional changes, although the top 75 m of Hole U1312A was affected by severe core deformation because of poor weather conditions, leading to considerable data editing.

The distribution of inclination values at Site U1312, before AF demagnetization, reflects mostly downward drill string overprint (Fig. F17). The distribution obtained after AF demagnetization at 20 mT can be characterized as a combination of two log-normal distributions centered at approximately –50° and +65°, respectively. These values are close to the expected values for a geocentric axial dipole (I_{GAD} = ±61.7°), which suggests that most of the drill string overprint was removed at 20 mT. Nevertheless, the distributions are large due to the presence of low-intensity intervals affected by noise. The distributions are also slightly offset toward more positive values, possibly due to the presence of some intervals that are still affected by the drill string overprint.

The magnetostratigraphy was constructed based on the succession of polarity reversals recorded at Site U1312 (Fig. F18). The Brunhes/Matuyama reversal occurs at 18.40 mbsf in Hole U1312A and 16.95 mbsf in Hole U1312B. The next normal polarity interval is the Jaramillo Subchron, which corresponds to the 20.90–24.80 mbsf depth interval in Hole U1312B. The reversals present in the underlying sediments were more difficult to characterize. In conformity with the biostratigraphy (see "Biostratigraphy"), the Gauss/Matuyama boundary was placed at 51.60 mbsf in Hole U1312B. Identification of the Olduvai Subchron in the preceding depth interval (25–51 mbsf) was nearly impossible. There are a few short intervals with directions corresponding to normal polarities in this depth range, but these may reflect remaining drill string overprint as the signal is highly variable and thus noisy. Among these intervals, the one that is the most compatible with the biostratigraphy is located at the top of Core 306-U1312-6H and has a length of ~45 cm. If this short interval does correspond to the Olduvai Subchron, however, its length is considerably shortened and sedimentation rates must be very low (i.e., ~0.25 cm/k.y.). The Gauss/Gilbert boundary is tentatively placed at 72.2 mbsf in Hole U1312B, although a significant part of the Gauss interval (Chron C2An) is missing due to coring-induced deformation in Core 306-U1312-8H. The magnetostratigraphy is unclear in the depth interval associated with low NRM intensities (gray region in Fig. F18). It becomes interpretable again below ~200 mbsf, where a long interval of normal polarity is tentatively identified as Chron 5, which would place the bottom of Hole U1312A at ~11 Ma.

Depths of the polarity transitions identified in the two holes at Site U1312 and their possible correlation to the magnetic polarity timescale (Cande and Kent, 1995) are listed in Table T17.

Stratigraphic correlation

All cores recovered from Hole U1312A were measured for magnetic susceptibility at 5 cm resolution using the "Fast Track" magnetic susceptibility core logger (MSCL) soon after recovery. Below ~80 mbsf, magnetic susceptibility decreased to noise level because of the high carbonate content of the sediments. Therefore, only the uppermost 14 cores were measured with the MSCL in Hole U1312B. Initial correlation based on these data did not influence coring operations because so much of the upper portion of Hole U1312A was highly disturbed. In essence, any core recovered from Hole U1312B was important for filling both gaps between cores and long intervals from Hole U1312A that contained deformed core, mainly in the form of flow-in. Later GRA density, NGR, magnetic susceptibility, magnetic intensity, and color reflectance data became available from the various multisensor tracks and was included in building the composite section. Magnetic intensity of the NRM after AF demagnetization in peak fields of 20 mT (see "Paleomagnetism") measured at 5 cm interval and color reflectance parameter L* measured at 2 cm intervals proved most useful for correlating between holes at Site U1312.

As noted above, coring deformation was severe in much of the upper portion of Hole U1312A, particularly in Cores 306-U1312A-1H through 5H, but also in other intervals downhole. The deformation was mainly the result of large ship heave experienced during operations in Hole U1312A. Weather conditions were more favorable during coring in Hole U1312B, which resulted in excellent core quality with the exception of Core 306-U1312B-8H and a few other core sections from deeper in the hole. As at other Ocean Drilling Program and IODP drill sites, the tops of cores were also often disturbed. A list of the disturbed intervals is provided in Table T18. For between-hole correlation and building a spliced section, we removed the data from these disturbed intervals.

Because of the core disturbance in the uppermost cores from Hole U1312A, it is not possible to construct a complete splice for the entire section, and potential breaks can occur where cores had to be ap-

pended (see Table T18). In the 0–32.5 meters composite depth (mcd) interval, the splice is built from Cores 306-U1312B-1H through 3H, and so the mcd scale for this interval is equivalent to the mbsf scale of Hole U1312B (Fig. F19). A comparison with Core 306-U1312A-2H revealed that there is probably little or no gap or overlap between Cores 306-U1312B-2H and 3H. Interestingly, significant relative compression and expansion of the sedimentary section occurs between the holes, which is particularly evident in the interval from 12 to 18 mbsf (Fig. F19). Because coring deformation is low for both holes in this interval and because the holes are only separated by 28 m, the different relative compression and expansion is surprising. Flow-in appears absent in this interval, so possibly there are real lateral variations in sedimentation rates or deformation that is not apparent to the eye.

The core break between Cores 306-U1312B-4H and 5H was filled by splicing with Core 306-U1312A-4H (Figs. F20A, F21A), but at 42 mcd Core 306-U1312B-6H had to be appended to Core 306-U1312B-5H. Another potential gap occurs at 68 mcd because the break between Cores 306-U1312A-7H and 8H could not be closed by an equivalent section of Core 306-U1312B-8H, all of which is disturbed. From 68.05 to 158.89 mcd, NRM intensity and color patterns match relatively well between Holes U1312A and U1312B, and all core breaks could be filled, resulting in a complete splice for this interval (Figs. F20B, F21B). A possible exception occurs where the basal portion of Core 306-U1312A-8H is tied to the top portion of Core 306-U1312B-9H because the between-hole correlations are poor. Directly below this, however, the basal portion of Core 306-U1312B-9H has several distinct lightness anomalies that correlate very well with Core 306-U1312A-9H.

Below 158.89 mcd, which corresponds to the bottom of Core 306-U1312B-16H, stratigraphic correlation was difficult because the high-resolution records show only minor amplitude changes because of a very uniform sediment composition. Because of this, we did not continue to build a spliced stratigraphic section, as it might mislead rather than assist future studies. Possibly other data sets collected postcruise will assist in between-hole correlation of this very homogeneous interval. In our composite section, we are able to correlate Cores 306-U1312B-24H and 25H to the long-wavelength increase in magnetic intensity evident, and more completely recovered, in Hole U1312A (Fig. F22). The correlation is crude, however, as it is only based on long-wavelength features in the signal, which probably constrain the correlation to no better than ±0.5 m.

Core offsets and composite depths are listed in Table T19, whereas the sections of core used for the splice are identified in Table F20. Further lithologic features and magnetic reversal boundaries have been identified in both holes drilled at Site U1312 and were used as constraints in the construction of the composite depth scale. These are listed in Table T21.

We noticed that marine oxygen isotope stages of the last 1.5 m.y. as displayed in the global benthic oxygen isotope stack by Lisiecki and Raymo (2005) are mirrored in the lightness parameter L*, which mainly reflects the carbonate content at Site U1312. Despite the fact that the L* splice is not complete, its stratigraphic potential is demonstrated by the preliminary correlation shown in Figure F23. Sedimentation rates derived from this correlation vary between 0.5 and 3.5 cm over the past 1.5 m.y.

Geochemistry

Inorganic geochemistry

A total of eight interstitial water samples were extracted from 5 cm whole-round sediment sections from Hole U1312A with a resolution of one sample per core for the first six cores and thereafter one sample per core for 306-U1312A-9H and 12H covering a depth of 110.5 mbsf. Interstitial water samples were processed for routine shipboard geochemical analyses. For details of the interstitial water extraction procedure and analytical methods, see "Geochemistry" in the "Site U1312–U1315 methods" chapter. The concentrations of dissolved elements in Hole U1312A are given in Table T22, and their downhole profiles are illustrated in Figure F24. Cores 306-U1312A-1H to 10H (0–95 mbsf) exhibited frequent flow-in structures, probably caused by excessive heaving during coring, especially in the upper five cores (Table T18). Interstitial water data measured from these disturbed intervals are identified in Table T22 and indicated by open circles in Figure F24. Despite the apparent physical core disturbance in the upper cores, concentrations of some elements appear not to be affected, as shown in their downhole profiles (e.g., Mn). However, only the data points denoted by solid circles are utilized here for the downhole description. A noticeable change in most profiles shown in Figure F24 is observed below the boundary between the lithologic Units I and II.

Chlorinity, salinity, alkalinity, and pH

Chloride concentrations in Hole U1312A show a maximum value of ~570 mM at 34.5 mbsf, followed by a general downhole trend in decreasing values to 553 mM at 110.5 mbsf (Fig. F24A). The chlorinity maximum observed at 34.5 mbsf may correlate with those found by previous workers at 40–50 mbsf (see

"Geochemistry" in the Site U1302/U1303, U1304, U1305, U1306, U1307, and U1308 chapters). Chlorinity maxima at this depth have been attributed to a remnant of higher salinity bottom water masses during the LGM preserved in the sediment pore spaces (e.g., McDuff, 1985; Adkins et al., 2002; Adkins and Schrag, 2003). The overall downhole trends of our shipboard interstitial water chlorinity data in the upper ~100 m of the sediment columns are similar to those reported during Expedition 303 see "Geochemistry" in the Site U1302/U1303, U1304, U1305, U1306, U1307, and U1308 chapters) and from other deep-sea sections. This implies that conservative chemical proxies preserved in the interstitial water samples collected from Hole U1312A may record properties of bottom water masses that prevailed during the LGM. The downhole salinity profile shows a similar trend to Cl^- decreasing from 35 to 33 g/kg between 34.5 and 110 mbsf (Fig. **F24B**).

Alkalinity increases with depth from 3.73 to 4.77 mM in the upper 82 mbsf, followed by a decrease to 3.96 mM at 110.5 mbsf (Fig. **F24C**). These values are comparatively lower than those reported from Hole U1308A (see **"Geochemistry"** in the "Site U1308" chapter). The pH profile in Hole U1312A does not exhibit any significant downhole trend, with values ranging from 7.01 to 7.41 (Fig. **F24D**).

Sodium, potassium, magnesium, and calcium

The interstitial water Na^+, K^+, and Mg^{2+} concentrations in Hole U1312A range from 432 to 454.3 mM, 8.4 to 9.4 mM, and 41.2 to 47.1 mM, respectively, and their downhole profiles exhibit trends that are roughly similar to that of Cl^- except for an increase in value between 82 and 110.5 mbsf (Fig. **F24E**).

Iron, boron, barium, lithium, manganese, and strontium

Fe^{2+} concentrations in Hole U1312A exhibit downhole decreasing values from ~9.6 µM at 34.45 mbsf to 2.4 µM at 110.5 mbsf, with an interval of increased value (9.0 µM) at 82 mbsf (Fig. **F24I**). B concentrations, mostly as boric acid (H_3BO_3), in the interstitial water samples of Hole U1312A exhibit a downhole increasing trend (Fig. **F24J**).

Ba^{2+} concentrations are very low (<1.0 µM) and it was challenging to obtain sensible values using inductively coupled plasma–atomic emission spectroscopy. In order to make the slope more sensitive to pore water Ba^{2+} concentrations, the intensity of the standard of the Ba^{2+} values needed to be tuned to the lower end of the calibration curve. Without performing this regression, obtained Ba^{2+} values would be too unrealistic to be valid (Table **T22**). However, shifting the intercept to zero made the calibration curve more sensitive to the lower values and allowed us to obtain more realistic Ba^{2+} values, listed as Ba^{2+}* in Table **T22.** Downcore Ba^{2+}* values show an increasing trend from 0.26 to 0.69 µM between 34.5 and 82 mbsf (Fig. **F24K**). Values then decrease to 0.39 µM at 110.5 mbsf. The highest Ba^{2+}* value was measured at 82 mbsf, near the boundary between lithologic Units I and II.

The Li^+ and Sr^{2+} profiles show opposite trends to each other. Li^+ concentrations in Hole U1312A are highest in the shallowest samples and decrease with depth, while the reverse is observed with Sr^{2+} values (Fig. **F24L, F24N**). Sr^{2+} is usually expelled in the pore water from the carbonate constituents in the sediments during dissolution and reprecipitation. This is one hypothesis for the downhole increase of Sr^{2+} (Baker et al., 1982; De Carlo, 1992). Mn^{2+} concentrations are also higher in the shallowest samples but decrease rapidly with depth (Fig. **F24M**).

Dissolved silica and sulfate

Dissolved silica (H_4SiO_4) concentrations in Hole U1312A range from 425.3 to 640.9 µM, and its downhole profile exhibits an initial trend in increasing values to a depth of 53.45 mbsf followed by decreasing values thereafter to the deepest sample measured (Fig. **F24O**). The lowest dissolved silica concentration (425 µM) was measured at 110.45 mbsf, coinciding with an interval composed of white nannofossil ooze sediments (see **"Lithostratigraphy"** and **"Biostratigraphy"**). The elevated dissolved silica contents between 34.5 and 53.5 mbsf likely reflect the initial presence of biogenic silica in the sediments and its subsequent dissolution.

Sulfate (SO_4^{2-}) concentrations show a moderate decrease with depth and its downhole profile appears to parallel that of pH (Fig. **F24P, F24D**).

Organic geochemistry

Volatile hydrocarbons

Headspace gas analysis was conducted as part of the standard protocol required for shipboard safety and pollution prevention monitoring. A total of 25 headspace samples from Hole U1312A with a sample resolution of one sample per core were analyzed (Table **T23**). Methane was the only hydrocarbon gas detected at the site. The concentrations of methane in Hole U1312A are relatively constant and at a natural background level (1.7–3.8 ppmv). Slight fluctuations in methane concentrations of ~3 ppmv are observed in the upper ~130 mbsf. However, the concentration of methane below 140 mbsf remains uniform at ~2 ppmv (Fig. **F25**).

Sedimentary bulk geochemistry

Sediment samples for the analysis of solid-phase bulk inorganic C, total C, and total N (TN) were collected from the working halves from Hole U1312A at a resolution of two samples per core. In addition, splits of sediments from interstitial water squeeze cake (see **"Geochemistry"** in the "Site U1312–U1315 methods" chapter) samples were also used for investigations of solvent-extractable organic matter (see below) as well as for bulk geochemical analyses. Data from the bulk geochemical analysis performed on 58 samples are shown in Table **T24.** See **"Geochemistry"** in the "Site U1312–U1315 methods" chapter for analytical methods and the derivation of total organic carbon (TOC) values. Descriptions and discussion of data and subsets follows with reference to the identified lithologic units (see **"Lithostratigraphy"**). Note that the geochemical data may have suffered from flow-in and distortion during coring (see **"Stratigraphic correlation;"** Table **T18**) with respect to sample depth assignments and absolute values.

Downhole variations of calcium carbonate contents for Hole U1312A are shown in Figure **F26.** For comparison, $CaCO_3$ data from Site 608 drilled at the same location were also plotted. $CaCO_3$ for Hole U1312A is very high, averaging 90.4 wt% with a range from 58.9 to 98.3 wt%. Notable fluctuations in carbonate content between 59 and 95 wt% are recognized in the upper ~40 mbsf (lithologic Subunit IA), and the lowest carbonate contents for Hole U1312A are found within this unit. On average, the $CaCO_3$ concentration for Subunit IA is 84 wt%. In Subunit IB, carbonate contents generally increase downcore from a minimum value of ~65 wt% at 40 mbsf toward values of ~95 wt% at 70 mbsf. The boundary between lithologic Units I and II in Hole U1312A is confined as a local minimum in $CaCO_3$ at ~80 mbsf and is in accordance with the earlier findings from Site 608 (Ruddiman, Kidd, Thomas, et al., 1987). Being dominantly composed of a white nannofossil ooze with only a minor amount of clay, Unit II of Hole U1312A displays relatively constant (90–98 wt%) and high (average = 95 wt%) carbonate contents, except two low values (~82 wt%) at 81.95 and 110.45 mbsf.

TOC and TN contents range from 0 to 0.9 wt% and from 0.08 to 0.18 wt%, respectively (Fig. **F27**). On average, TOC and TN are 0.13 and 0.1 wt%, respectively, in Hole U1312A. Despite low mean TOC contents, the upper 80 mbsf (lithologic Unit I) shows higher variability in TOC, occasional peak values as high as 0.9 wt%, and an average of 0.3 wt%. In contrast, Unit II is characterized by extremely low TOC concentrations (<0.1 wt%).

TN concentrations are low overall and relatively uniform; downcore fluctuations are noiselike and might therefore result from measurements at the lower end of instrumental precision. However, a slight gradient in TN from ~0.15 wt% at the top toward the average 0.1 wt% value at the boundary between lithologic Units I and II is obvious. This is in line with the decreasing abundance of clay content over the same depth range (see **"Lithostratigraphy;"** Fig. **F5**). Therefore, sedimentary TN in Hole U1312A might result from the tendency of clay to absorb ammonium ions generated during the degradation of organic matter (Müller, 1977). Because of this and TOC contents <0.2 wt% for most of the samples from Hole U1312A, TOC/TN ratios, often used as an indicator for the nature of organic matter in sediments (i.e., marine versus terrestrial derived) (Emmerson and Hedges, 1988; Meyers, 1994), were not calculated.

Sedimentary organic geochemistry

In Hole U1312A, eight samples were collected for geochemical analyses of the solvent extractable organic matter. These were splits of the remaining sediments after interstitial water squeeze-out as described in **"Geochemistry"** in the "Site U1312–U1315 methods" chapter. The bulk data corresponding to these samples are shown in Table **T24** and are underlined. Because of the dominant presence of $CaCO_3$ and the generally low TOC, only five out of the eight samples were processed. Because of the low organic carbon contents, the total organic solvent extracts of these samples were completely colorless. Therefore, the total extracts were submitted directly to gas chromatograph (GC)-mass spectrometer (MS) analysis without further silica gel separation. Sedimentary organic compounds were only detected in one sample at 24.95 mbsf (see below). In all other samples investigated, no *n*-alkanes or alkenones could be detected, or they were below the detection limit of the GC-MS system used. Sample 306-U1312A-3H-4, 145–150 cm, revealed the presence of a series of hopanes, as shown by the *m/z* 191 extracted ion chromatogram in Figure **F28.** The carbon atom number distribution of these compound types ranges from C_{26} (T_S) to C_{35} with the C_{30} homolog most abundant and a regular decrease from C_{31} to C_{35} homohopanes. The isomerizations of these compounds at C_{17} and C_{22} (i.e., the observed 17(α) H-configuration and the dominance of 22S over 22R isomers for C_{31}–C_{35} hopanes) clearly indicate that they do not occur in their biological configuration but rather in a thermodynamically more stable configuration. Such "mature" isomeric hopane mixtures are typically found in oils and source rocks (e.g., Peters

and Moldowan, 1993; Killops and Killops, 2004). Their occurrence in Hole U1312A at 24.95 mbsf (>0.78 Ma, based on the occurrence of the Brunhes/Matuyama reversal at 18.40 mbsf; see "Paleomagnetism" and Table T17) thus can be interpreted as contributions of organic matter derived from ancient sedimentary source rocks, possibly eroded by glaciers and transported by icebergs to the site location. Recently, comparable hopane mixtures have been shown to occur specifically within Heinrich layers 2 and 3 from samples of the Labrador Sea and also in the western and northern North Atlantic (Rashid and Grosjean, 2004). The identification of this mature hopane mixture in Hole U1312A may thus support the occurrence of "Heinrich-type" sedimentation prior to ~0.8 Ma.

Physical properties

Physical property measurements were carried out at Site U1312 following the procedures described in "Physical properties" in the "Site U1312–U1315 methods" chapter. Magnetic susceptibility measurements were made with both the MSCL and MST system. Additionally, GRA density and NGR were measured with the multisensor system. Discrete *P*-wave velocities were measured (*P*-wave sensor 3 [PWS3]–measuring perpendicular to the core axis) on each section, and moisture and density measurements were made on two discrete samples per core, usually at the top of the first and the bottom of the sixth sections.

Whole-core magnetic susceptibility

The magnetic susceptibility records derived during coring operations at Site 1312 show a highly variable record in the upper 40 m because of variations in clay content. Magnetic susceptibility measurements obtained from the MSCL and MST generally show similar trends and display multiple excursions toward higher values in the upper section of each hole (Fig. F29) and consistent with the presence of clays. In the lower section of Hole U1312A, the MST shows more coherent and negative values than the MSCL. Site U1312 has peak magnetic susceptibility values of ~8×10^{-3} SI units and minimum values approaching the instrument noise level, with most values ranging from 0.4×10^{-3} to 1.6×10^{-3} SI.

GRA density

Sediments from Site U1312 show a general increase in bulk density downcore consistent with a downcore decrease in water content (Fig. F30). GRA density varies between 1.5 and 1.8 g/cm³. Discrete bulk densities show similar trends but are offset toward lower values relative to GRA densities.

Porosity

Dry and wet water content, as well as grain densities, were determined from discrete samples (Fig. F31). Both dry and wet water contents decrease in the upper 40 m and then are relatively constant downcore. Grain density values are relatively constant, with a value of ~2.7 g/cm³. Porosity measurements were calculated from the discrete samples. Porosity varies between ~55% and 70% (Fig. F32). Porosity decreases from 70% at the seafloor to ~60% at a depth of 40 mbsf. This pattern is consistent with compaction and is inversely correlated to density.

P-wave velocity

Discrete measurements of *P*-wave velocity (PWS3) were performed on cores from Site U1312. *P*-wave velocities generally vary between 1500 and 1600 m/s (Fig. F33); however, there are several departures to lower values of ~1400 m/s. Trends in *P*-wave velocities are in general correlated with trends in density.

Natural gamma radiation

Natural gamma ray counts range from 10 to 35 cps, with the majority of the values between 10 and 15 cps (Fig. F34) in the lower part of the hole. NGR values also mimic the trends seen in the magnetic susceptibility and GRA density data. NGR counts average ~15–20 cps from 0 to 50 mcd, whereas they average ~10 cps from 50 to 275 mcd.

Discussion

The physical properties measured on cores from Site U1312 show the greatest variability in the upper 40 m consistent with greater clay content. Below 40 m, the carbonate content exceeds 90 wt%.

References

Adkins, J.F., and Schrag, D.P., 2003. Reconstructing last glacial maximum bottom water salinities from deep-sea sediment pore fluid profiles. *Earth Planet Sci. Lett.,* 216:109–123. doi:10.1016/S0012-821X(03)00502-8

Adkins, J.F., McIntyre, K., and Schrag, D.P., 2002. The salinity, temperature and $\delta^{18}O$ of the glacial deep ocean. *Science,* 298:1769–1773. doi:10.1126/science.1076252

Backman, J., and Raffi, I., 1997. Calibration of Miocene nannofossil events to orbitally tuned cyclostratigraphies from Ceara Rise. *In* Shackleton, N.J., Curry, W.B., Richter, C., and Bralower, T.J. (Eds.), *Proc. ODP, Sci. Results,* 154: College Station, TX (Ocean Drilling Program), 83–99. [PDF]

Baker, P.A., Gieskes, J.M., and Elderfield, H., 1982. Diagenesis of carbonates in deep-sea sediments—evidence from Sr^{2+}/Ca^{2+} ratios and interstitial dissolved Sr^{2+} data. *J. Sediment. Petrol.,* 52:71–82.

Baldauf, J.G., 1987. Diatom biostratigraphy of the middle- and high-latitude North Atlantic Ocean, Deep Sea Drilling Project Leg 94. *In* Ruddiman, W.F., Kidd, R.B., Thomas, E., et al., *Init. Repts. DSDP,* 94 (Pt. 2): Washington (U.S. Govt. Printing Office), 729–762.

Baldauf, J.G., Thomas, E., Clement, B., Takayama, T., Weaver, P.P.E., Backman, J., Jenkins, G., Mudie, P.J., and Westberg-Smith, M.J., 1987. Magnetostratigraphic and biostratigraphic synthesis, Deep Sea Drilling Project Leg 94. *In* Ruddiman, W.F., Kidd, R.B., Thomas, E., et al., *Init. Repts. DSDP,* 94 (Pt. 2): Washington (U.S. Govt. Printing Office), 1159–1205.

Cande, S.C., and Kent, D.V., 1995. Revised calibration of the geomagnetic polarity timescale for the Late Cretaceous and Cenozoic. *J. Geophys. Res.,* 100:6093–6095. **doi:10.1029/94JB03098**

Ciesielski, P.F., and Bjørklund, K.R., 1995. Ecology, morphology, stratigraphy, and the paleoceanographic significance of *Cycladophora davisiana davisiana*. Part II: stratigraphy in the North Atlantic (DSDP Site 609) and Labrador Sea (ODP Site 646B). *Mar. Micropaleontol.*, 25:67–86. **doi:10.1016/0377-8398(94)00027-K**

De Carlo, E.H., 1992. Geochemistry of pore water and sediments recovered from the Exmouth Plateau. *In* von Rad, U., Haq, B.U., et al., *Proc. ODP, Sci. Results,* 122: College Station, TX (Ocean Drilling Program), 295–308.

de Kaenel, E., Siesser, W.G., and Murat, A., 1999. Pleistocene calcareous nannofossil biostratigraphy and the western Mediterranean sapropels, Sites 974 to 977 and 979. *In* Zahn, R., Comas, M.C., and Klaus, A. (Eds.), *Proc. ODP, Sci. Results,* 161: College Station, TX (Ocean Drilling Program), 159–183. [**HTML**]

Emerson, S., and Hedges, J.I., 1988. Processes controlling the organic carbon content of open ocean sediments. *Paleoceanography,* 3:621–634.

Haslett, S.K., 1994. Plio–Pleistocene radiolarian biostratigraphy and paleoceanography of the mid-latitude North Atlantic (DSDP Site 609). *Geol. Mag.*, 131:57–66.

Haslett, S.K., 2004. Late Neogene–Quaternary radiolarian biostratigraphy: a brief review. *J. Micropaleont.*, 23:39–47.

Hilgen F.J., and Krijgsman, W., 1999. Cyclostratigraphy and astrochronology of the Tripoli diatomite formation (Pre-evaporite Messinian, Sicily, Italy). *Terra Nova*, 11:16–22. **doi:10.1046/j.1365-3121.1999.00221.x**

Hilgen, F.J., Krijgsman, W., Langereis, C.G., Lourens, L.J., Santarelli, A., and Zachariasse, W.J., 1995. Extending the astronomical (polarity) time scale into the Miocene. *Earth Planet. Sci. Lett.,*136:495–510. **doi:10.1016/0012-821X(95)00207-S**

Hilgen, F.J., Krijgsman, W., Raffi, I., Turco, E., and Zachariasse, W.J., 2000. Integrated stratigraphy and astronomical calibration of the Serravallian/Tortonian boundary section at Monte Gibliscemi (Sicily, Italy). *Mar. Micropaleontol., 3*8:181–211. **doi:10.1016/S0377-8398(00)00008-6**

Hodell, D.A., Curtis, J.H., Sierro, F.J., and Raymo, M.E., 2001. Correlation of late Miocene to early Pliocene sequences between the Mediterranean and North Atlantic. *Paleoceanogr.*, 16:164–178. **doi:10.1029/1999PA000487**

Killops, S., and Killops, V., 2004. *Introduction to Organic Geochemistry* (second ed.): Cambridge (Blackwell Publishing).

Krijgsman, W., Hilgen, F.J., Langereis, C.G., Santaralli, A., and Zachariasse, W.J., 1995. Late Miocene magnetostratigraphy, biostratigraphy and cyclostratigraphy in the Mediterranean. *Earth Planet. Sci. Lett.*, 136:475–494. **doi:10.1016/0012-821X(95)00206-R**

Krijgsman, W., Hilgen, F.J., Raffi, I., Sierro, F.J., and Wilson, D.S., 1999. Chronology, causes and progression of the Messinian salinity crisis. *Nature (London, U. K.),* 400:652–655. **doi:10.1038/23231**

Lisiecki, L.E., and Raymo, M.E., 2005. A Pliocene–Pleistocene stack of 57 globally distributed benthic $\delta^{18}O$ records. *Paleoceanography,* 20. **doi:10.1029/2004PA001071**

Lourens, L.J., Antonarakou, A., Hilgen, F.J., Van Hoof, A.A.M., Vergnaud-Grazzini, C., and Zachariasse, W.J., 1996. Evaluation of the Plio–Pleistocene astronomical timescale. *Paleoceanography,* 11:391–414. **doi:10.1029/96PA01125**

Martini, E., 1971. Standard Tertiary and Quaternary calcareous nannoplankton zonation. *In* Farinacci, A. (Ed.), *Proc. 2nd Int. Conf. Planktonic Microfossils Roma:* Rome (Ed. Tecnosci.), 2:739–785.

McDuff, R.E., 1985. The chemistry of interstitial waters, Deep Sea Drilling Project Leg 86. *In* Heath, G.R., Burckle, L.H., et al., *Init. Repts. DSDP,* 86: Washington (U.S. Govt. Printing Office), 675–687.

Meyers, P.A., 1994. Preservation of elemental and isotopic source identification of sedimentary organic matter. *Chem. Geol.,* 114:289–302. **doi:10.1016/0009-2541(94)90059-0**

Motoyama, I., 1997. Origin and evolution of *Cycladophora davisiana* Ehrenberg (Radiolaria) in DSDP Site 192, Northwest Pacific. *Mar. Micropaleontol.,* 30:45–63. **doi:10.1016/S0377-8398(96)00047-3**

Müller, P.J., 1977. C/N ratios in Pacific deep sea sediments: effect of inorganic ammonium and organic nitrogen compounds sorbed by clays. *Geochim. Cosmochim. Acta,* 41:765–776. **doi:10.1016/0016-7037(77)90047-3**

Okada, H., 2000. Neogene and Quarternary calcareous nannofossils from the Blake Ridge, Sites 994, 995, and 997. *In* Paull, C.K., Matsumoto, R., Wallace, P.J., and Dillon, W.P. (Eds.), *Proc. ODP, Sci. Results,* 164: College Station, TX (Ocean Drilling Program), 331–341. [**HTML**]

Peters, K.E., and Moldowan, J.M., 1993. *The Biomarker Guide: Interpreting Molecular Fossils in Petroleum and Ancient Sediments:* Englewood Cliffs, NJ (Prentice Hall).

Pflaumann, U., Sarnthein, M., Chapman, M., de Abreu, L., Funnell, B., Huels, M., Kiefer, T., Maslin, M., Schulz, H., Swallow, J., van Kreveld, S., Vautravers, M., Vogelsang, E., and Weinelt, M., 2003. Glacial North Atlantic: sea-surface conditions reconstructed by GLAMAP 2000. *Paleoceanography,* 18(3). **doi:10.1029/2002PA000774**

Raffi, I., and Flores, J.-A., 1995. Pleistocene through Miocene calcareous nannofossils from eastern equatorial Pacific Ocean. *In* Pisias, N.G., Mayer, L.A., Janecek, T.R., Palmer-Julson, A., and van Andel, T.H. (Eds.), *Proc. ODP, Sci. Results,* 138: College Station, TX (Ocean Drilling Program), 233–286.

Rashid, H., and Grosjean, E., 2004. Detecting the source of Heinrich layers: an organic geochemical study. *Eos. Trans. AGU, 85(17), Joint Assembly Suppl.,* Abstract GC13A-04.

Raymo, M.E., 1992. Global climate change: a three million year perspective. *In* Kukla, G.J., and Went, E. (Eds.), *Start of a Glacial*. NATO ASI Ser. I: Berlin (Springer-Verlag), 3:207–223.

Raymo, M.E., Oppo, D.W., Flower, B.P., Hodell, D.A., McManus, J.F., Venz, K.A., Kleiven, K.F., and McIntyre, K., 2004. Stability of North Atlantic water masses in face of pronounced climate variability during the Pleistocene. *Paleoceanography,* 19. **doi:10.1029/2003PA000921**

Raymo, M.E., Ruddiman, W.F., Backman, J., Clement, B.M., and Martinson, D.G., 1989. Late Pliocene variation in Northern Hemisphere ice sheets and North Atlantic deep water circulation. *Paleoceanography,* 4:413–446.

Ruddiman, W.F., Backmann, J., Baldauf, P., Hooper, L., Keigwin, K., Miller, K., Raymo, M., and Thomas, E., 1987. Leg 94 paleoenvironmental synthesis. *In* Ruddiman, W.F. Kidd, R.B., Thomas, E., et al., *Init. Repts. DSDP,* 94: Washington (U.S. Govt. Printing Office), 1207–1215.

Ruddiman, W.F., Kidd, R.B., Thomas, E., et al., 1987. *Init. Repts. DSDP,* 94 (Pts. 1 and 2): Washington (U.S. Govt. Printing Office).

Ruddiman, W.F., Raymo, M., and McIntyre, A., 1986. Matuyama 41,000-year cycles: North Atlantic Ocean and Northern Hemisphere ice sheets. *Earth Planet. Sci. Lett.,*80:117–129. **doi:10.1016/0012-821X(86)90024-5**

Ruddiman, W.F., Raymo, M.E., Martinson, D.G., Clement, B.M., and Backman, J., 1989. Pleistocene evolution: Northern Hemisphere ice sheets and North Atlantic Ocean. *Paleoceanography,* 4:353–412.

Sato, T., Kameo, K., and Mita, I., 1999. Validity of the latest Cenozoic calcareous nannofossil datums and its application to the tephrochronology. *Earth Sci.,* 53:265–274.

Shackleton, N.J., Crowhurst, S., Hagelberg, T., Pisias, N.G., and Schneider, D.A., 1995. A new late Neogene time scale: application to Leg 138 sites. *In* Pisias, N.G., Mayer, L.A., Janecek, T.R., Palmer-Julson, A., and van Andel, T.H. (Eds.), *Proc. ODP, Sci. Results,* 138: College Station, TX (Ocean Drilling Program), 73–101.

Shipboard Scientific Party, 1987. Site 608. *In* Ruddiman, W.F., Kidd, R.B., Thomas, E., et al., *Init. Repts. DSDP,* 94 (Pt. 1): Washington (U.S. Govt. Printing Office), 149–246.

Sierro, F.J., 1985. The replacement of the "*Globorotalia menardii*" group by the "*Globorotalia miotumida*" group: an aid to recognizing the Tortonian/Messinian boundary in the Mediterranean and adjacent Atlantic. *Mar. Micropaleontol*, 9:525–535. **doi:10.1016/0377-8398(85)90016-7**

Sierro, F.J., Flores, J.A., Civis, J., González-Delgado, J.A., and Frances, G., 1993. Late Miocene globorotaliid event-stratigraphy and biogeography in the NE-Atlantic and Mediterranean. *Mar. Micropaleontol.,* 21:143–168. **doi:10.1016/0377-8398(93)90013-N**

Sierro, F.J., Hilgen, F.J., Krijgsman, W., and Flores, J.A., 2001. The Abad composite (SE Spain): a Messinian reference section for the Mediterranean and the APTS. *Paleogeogr., Paleoclimatol., Paleoecol.,* 168:141–169. **doi:10.1016/S0031-0182(00)00253-4**

Stein, R., and Sarnthein, M., 1984. Late Neogene events of atmospheric and oceanic circulation offshore Northwest Africa: high resolution record from deep-sea sediments. *Paleoecol. Africa*, 16:9–36.

Spezzaferri, S., 1998. Planktonic foraminifer biostratigraphy and paleoenvironmental implications of Leg 152 sites (East Greenland Margin). *In* Saunders, A.D., Larsen, H.C., and Wise, S.W., Jr. (Eds.), *Proc. ODP, Sci. Results,* 152: College Station, TX (Ocean Drilling Program), 161–189. [**PDF**]

Turco, E., Bambini, A.M., Foresi, L., Iaccarino, S., Lirer, F., Mazzei, R., and Salvatorini, G., 2002. Middle Miocene high resolution calcareous plankton biostratigraphy at Site 926 (Leg 154, equatorial Atlantic Ocean): palaeoecological and palaeobiogeographical implications. *Geobios, Memoire special*, 24:257–276. **doi:10.1016/S0016-6995(02)00064-5**

Weaver, P.P.E., and Clement, B.M., 1987. Magnetobiostratigraphy of planktonic foraminiferal datums, DSDP Leg 94, North Atlantic. *In* Ruddiman, W.F., Kidd, R.B., Thomas, E., et al., *Init. Repts. DSDP,* 94: Washington (U.S. Govt. Printing Office), 815–829.

Westberg-Smith, M.J., and Riedel, W.R., 1984. Radiolarians from the western margin of the Rockall Plateau: Deep Sea Drilling Project Leg 81. *In* Roberts, D.G., Schnitker, D., et al., *Init. Repts. DSDP,* 81: Washington (U.S. Govt. Printing Office), 479–501.

Publication: 9 September 2006
MS 306-111

Figure F1. Sites U1312 and U1313 drilled during Expedition 306 at locations of Site 607 and 608. Site 609 was redrilled during Expedition 303 (Site U1308).

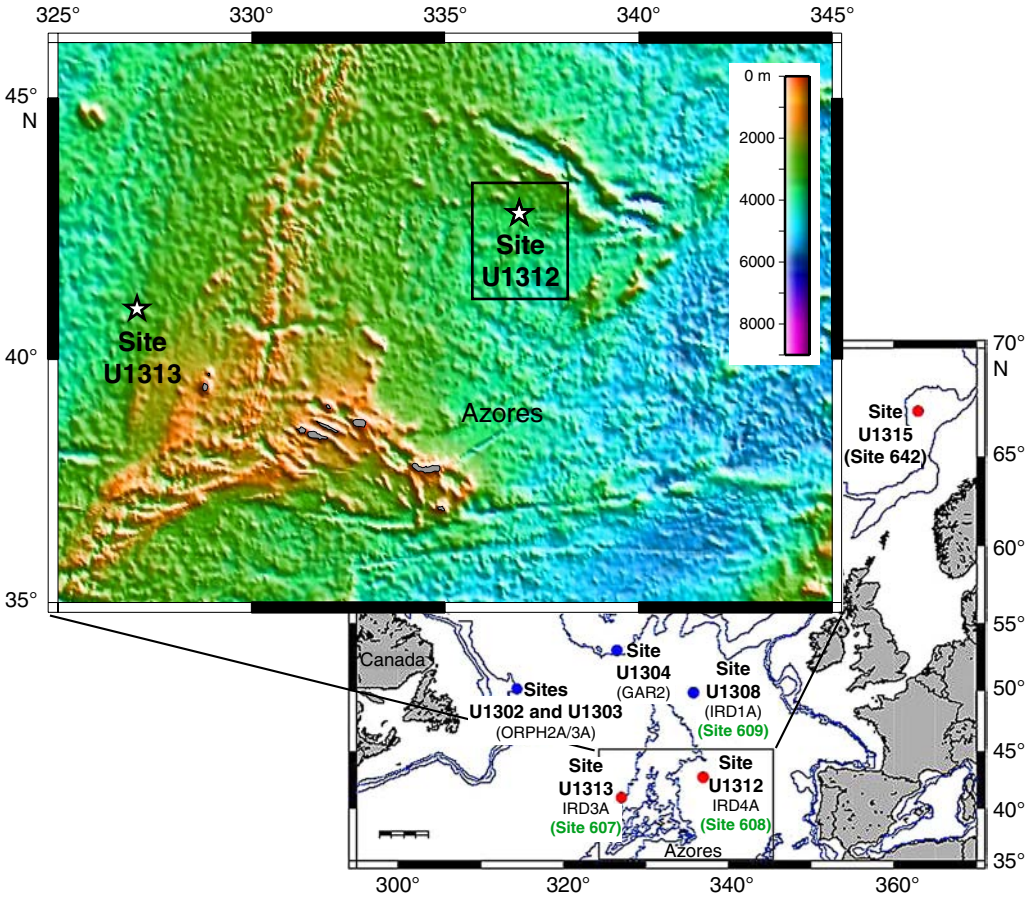

Figure F2. Seismic profile across location of Site 608 (Ruddiman, Kidd, Thomas, et al., 1987).

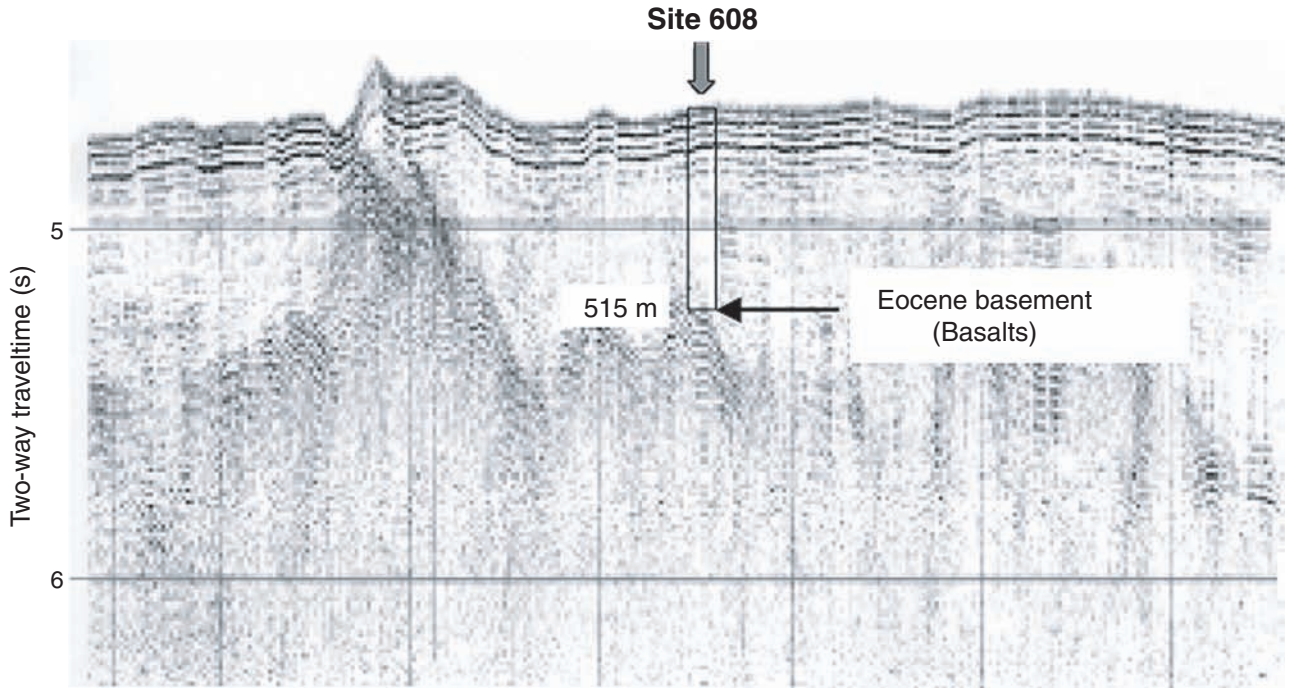

Figure F3. Glacial Atlantic Ocean Mapping (GLAMAP) 2000 sea-surface temperature (SST) reconstruction of the glacial Atlantic (SST anomalies; i.e., Last Glacial Maximum [LGM] minus modern) for northern summer (Pflaumann et al., 2003).

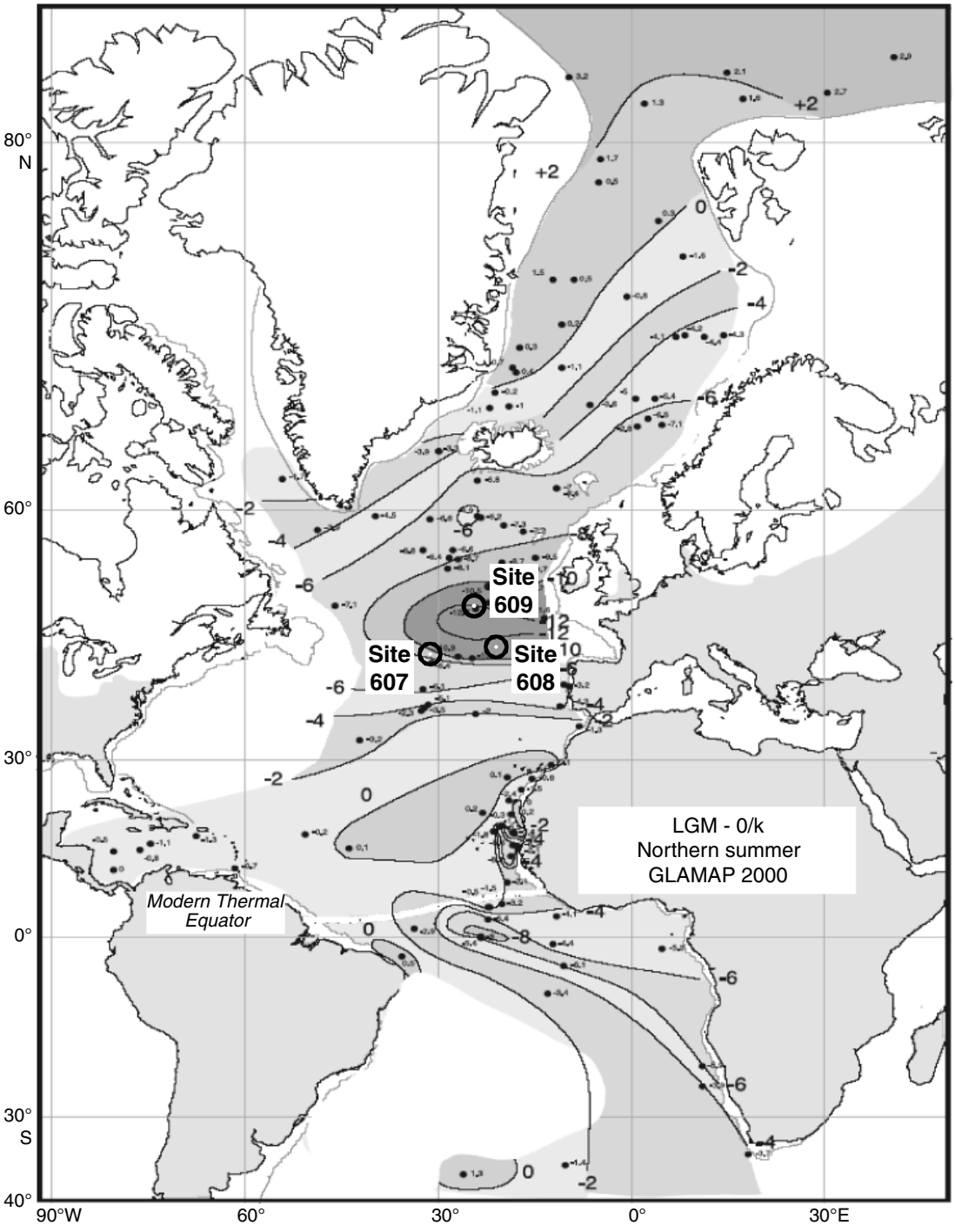

Figure F4. Abundances of nannofossils, foraminifers, and clay minerals in Holes U1312A and U1312B, plotted as a function of depth. Differences between the two holes in the uppermost 20 m (e.g., clay mineral percentages) can be related to the presence of moderate drilling disturbance (flow-in) present in Hole U1312A.

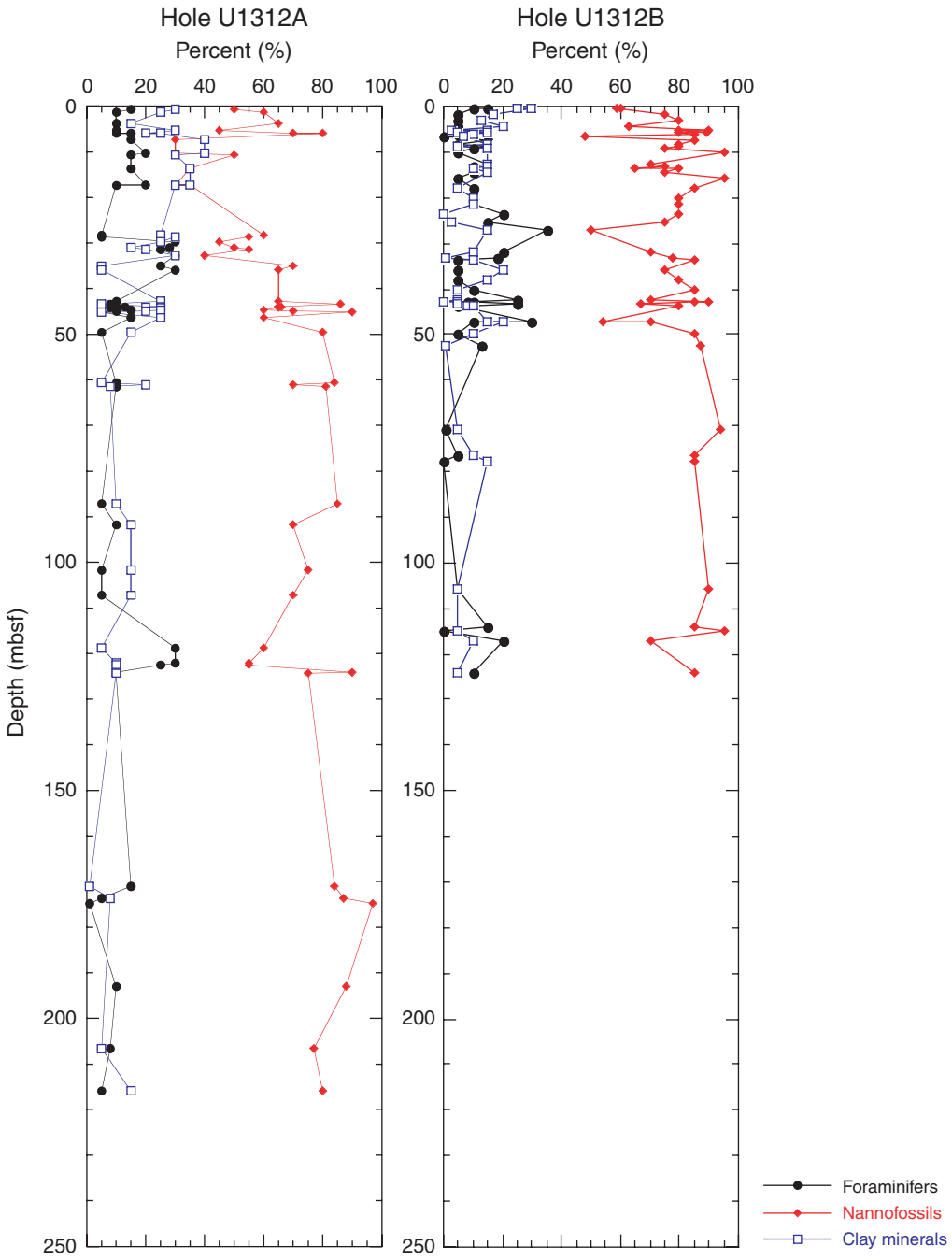

Figure F5. Graphic summary of core recovery at Site U1312 with the lithologic units and the lithologies recovered in Hole U1312B. The occurrence of gravel-sized grains is schematically represented next to the lithologic log as solid circles. The interval of maximum occurrence of dropstones at ~14 mbsf is marked by a large solid circle. Sediment lightness values determined from color reflectance data and total carbonate contents are also shown.

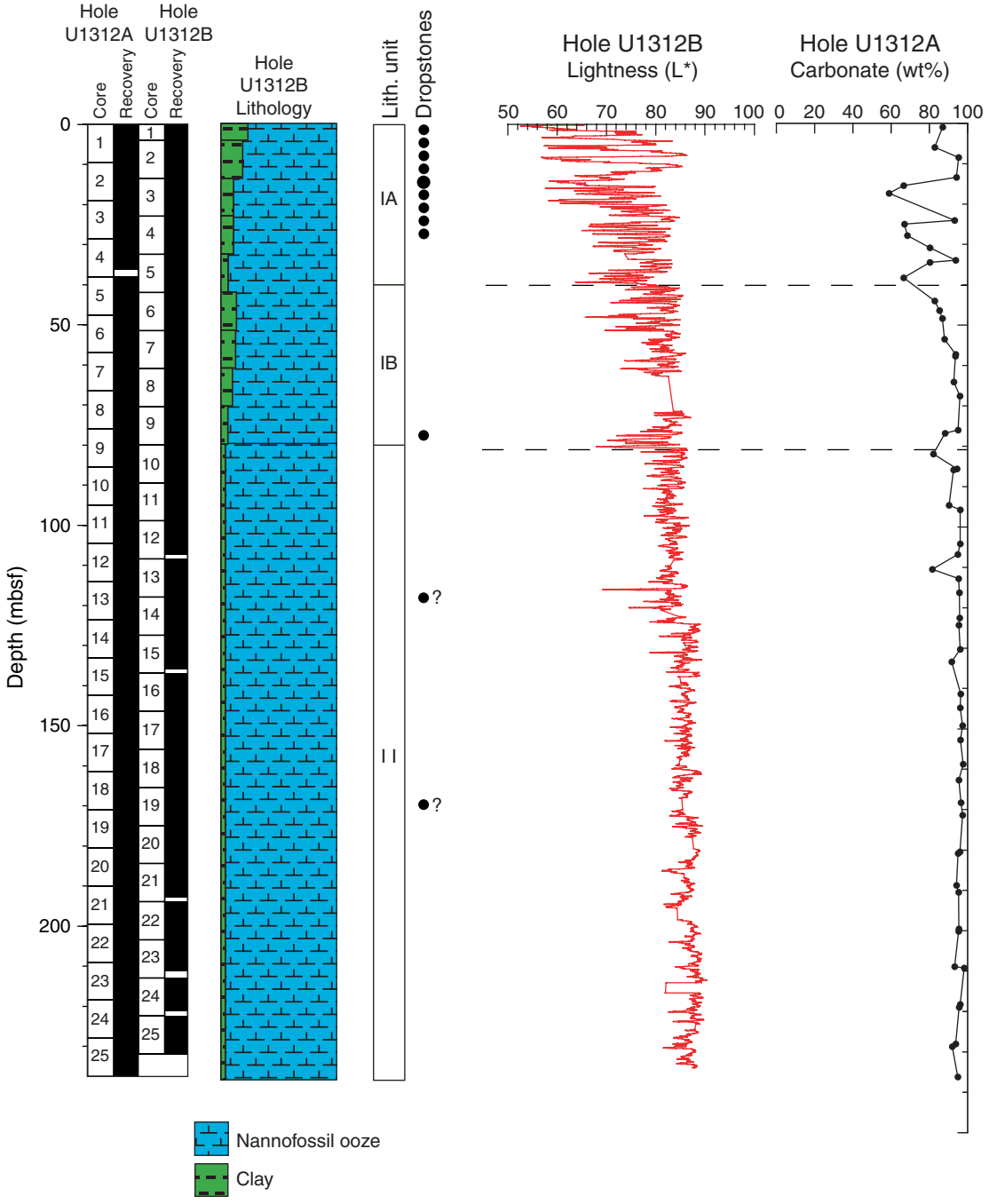

Figure F6. Color changes (interval 306-U1312A-2H-6, 7–47 cm; 17.07–17.47 mbsf).

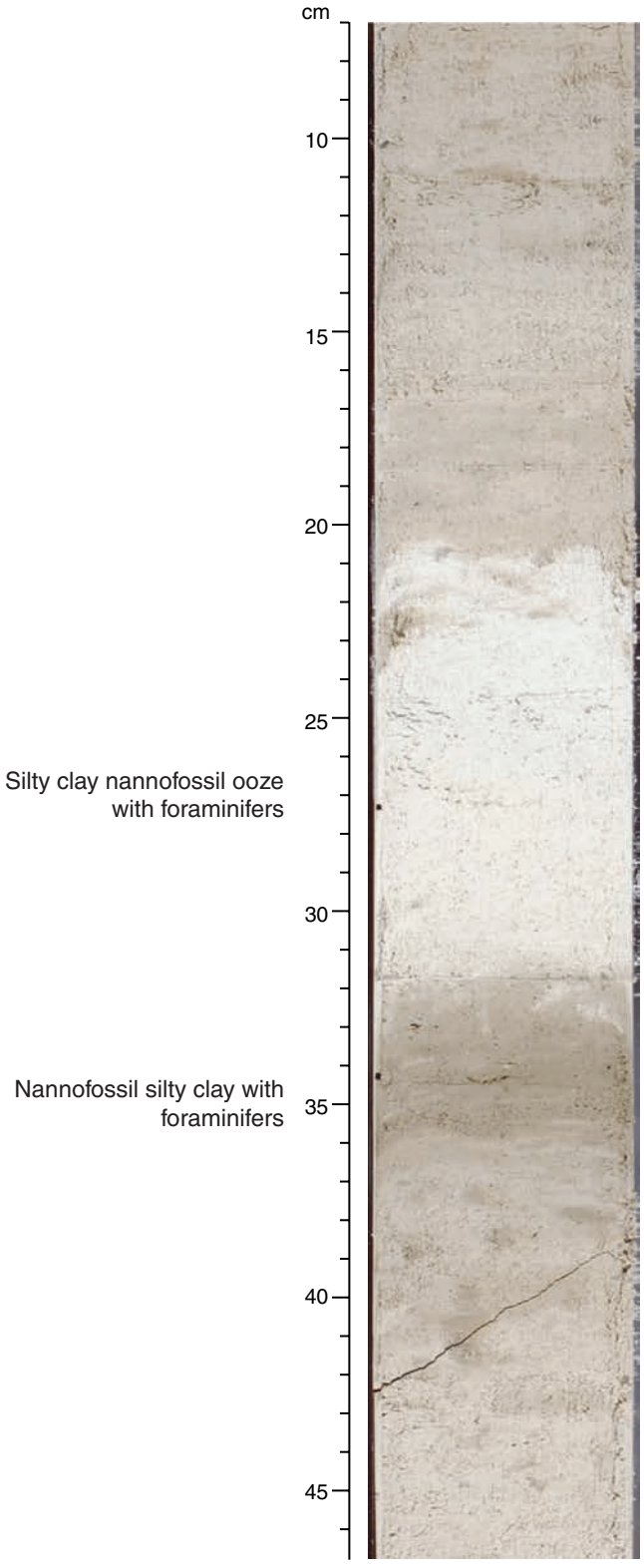

Figure F7. Pale green color banding (interval 306-U1312A-7H-4, 21.5–48.5 cm; 61.715–62.985 mbsf).

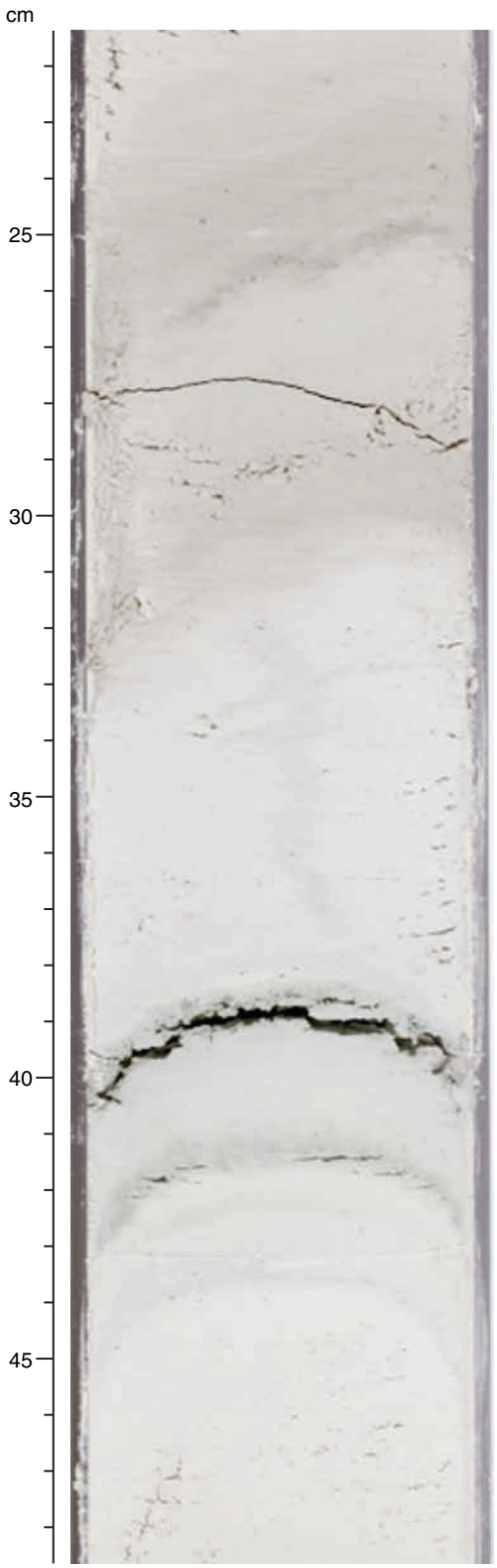

Figure F8. Schematic distribution of pale green color bands at Site U1312. The occurrence of these color bands is correlative between Holes U1312A and U1312B.

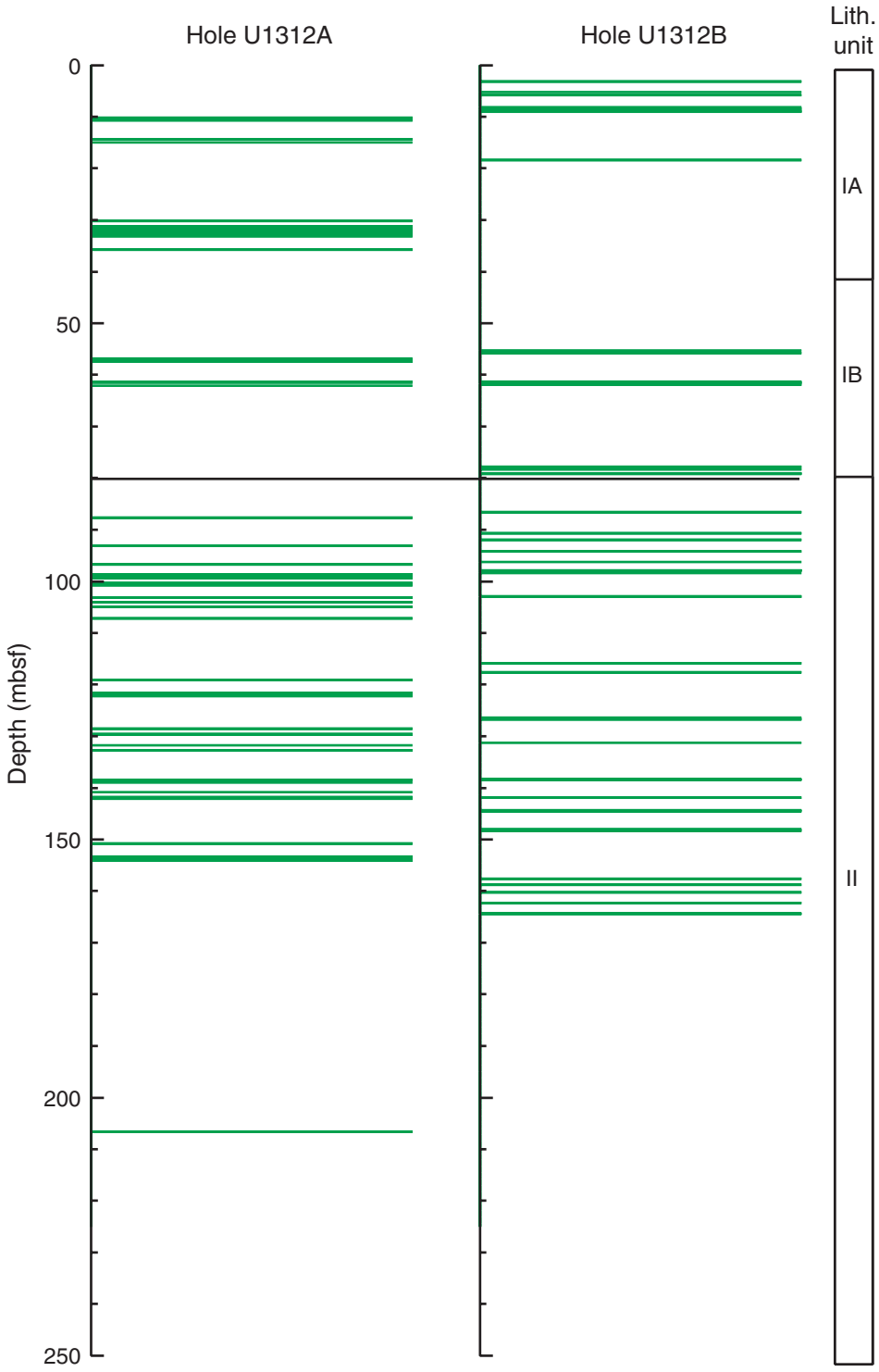

Figure F9. Detrital carbonate layer (interval 306-U1312B-2H-2, 88–107 cm; 6.28–6.47 mbsf).

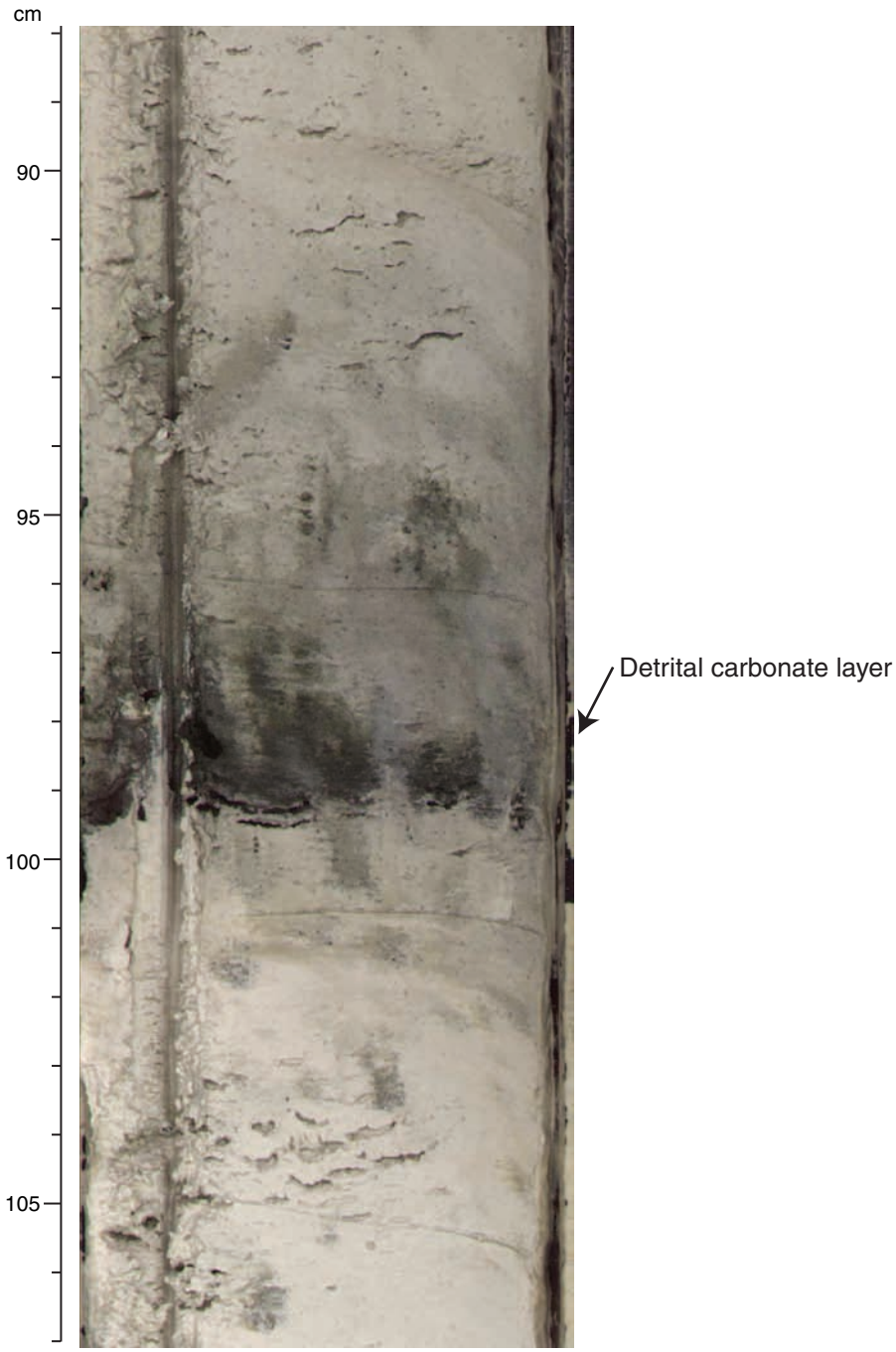

Figure F10. XRD data from (**A**) Sample 306-U1312B-2H-CC, 13–14 cm, showing the presence of detrital calcite, dolomite, and quartz and (**B**) Sample 306-U1312A-14H-4, 55–56 cm, showing the presence of calcite in this interval. IRD = ice-rafted debris.

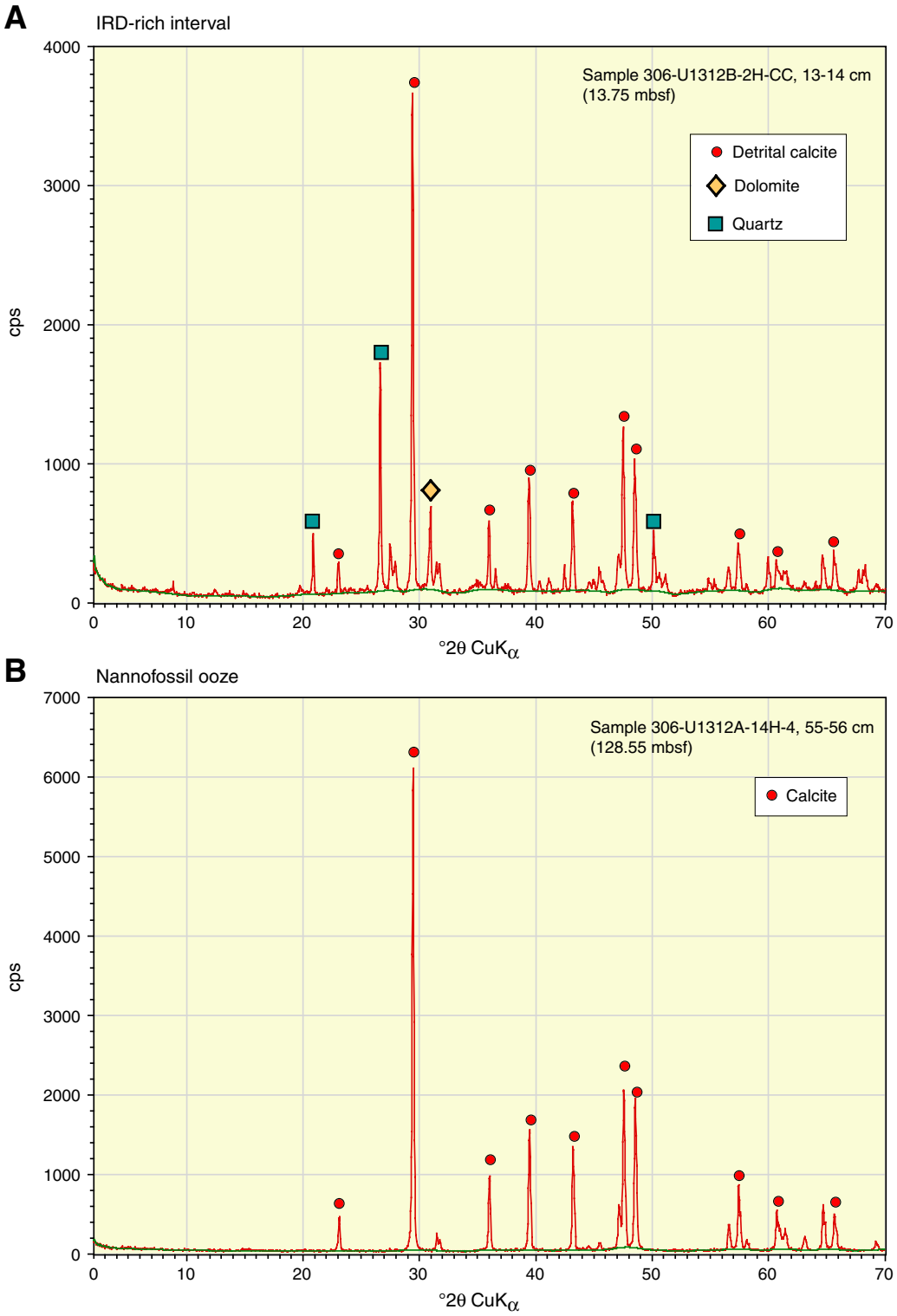

Figure F11. Soupy foraminifer nannofossil ooze with a sharp erosional contact at the base, identified as a turbidite (interval 306-U1312A-13H-4, 18–47 cm; 118.68–118.97 mbsf).

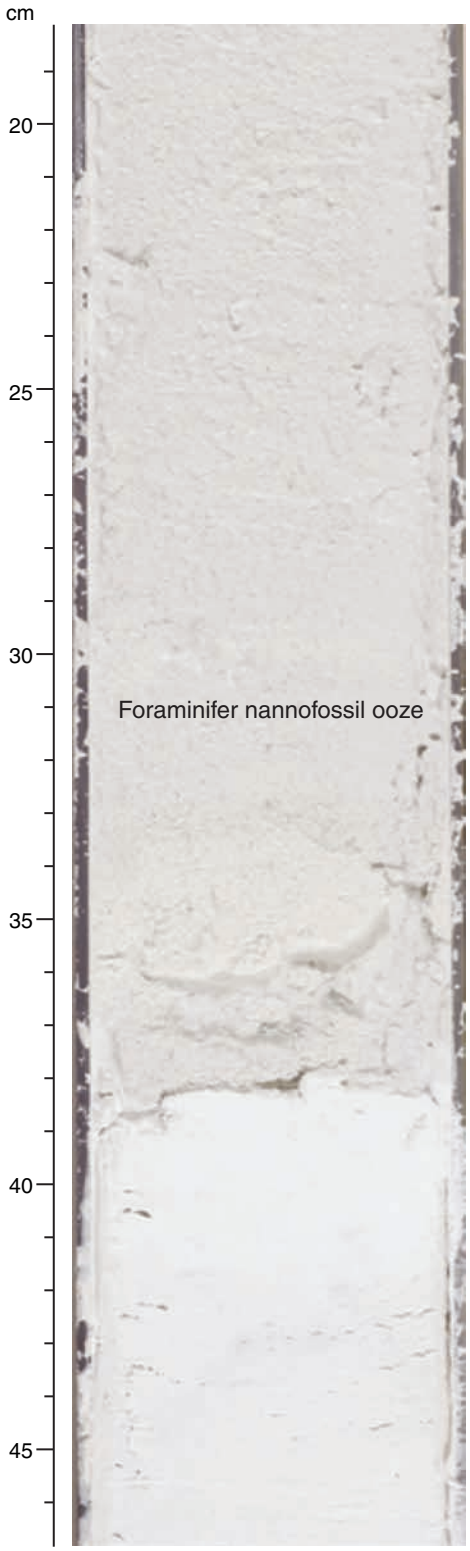

Figure F12. Plot of core recovery from Holes U1312A and U1312B and location of biostratigraphic events defined in this study with their corresponding position on the magnetic polarity timescale defined by Cande and Kent (1995). FO = first occurrence, FaO = first abundant occurrence, FcO = first common occurrence, LO = last occurrence, LcO = last common occurrence, s = sinistral, d = dextral. Calcareous nannofossil event datums from Raffi and Flores (1995), Shackleton et al. (1995), Backman and Raffi (1997), and Sato et al. (1999). Planktonic foraminifer event datums from Weaver and Clement (1987), Sierro et al. (1993), Krijgsman et al. (1995, 1999), Lourens et al. (1996), Spezzaferri (1998), and Hilgen et al. (2000). Diatom event datums compiled by Baldauf (1987). Radiolarian event datums compiled from Westberg-Smith and Riedel (1984) and Haslett (1994, 2004).

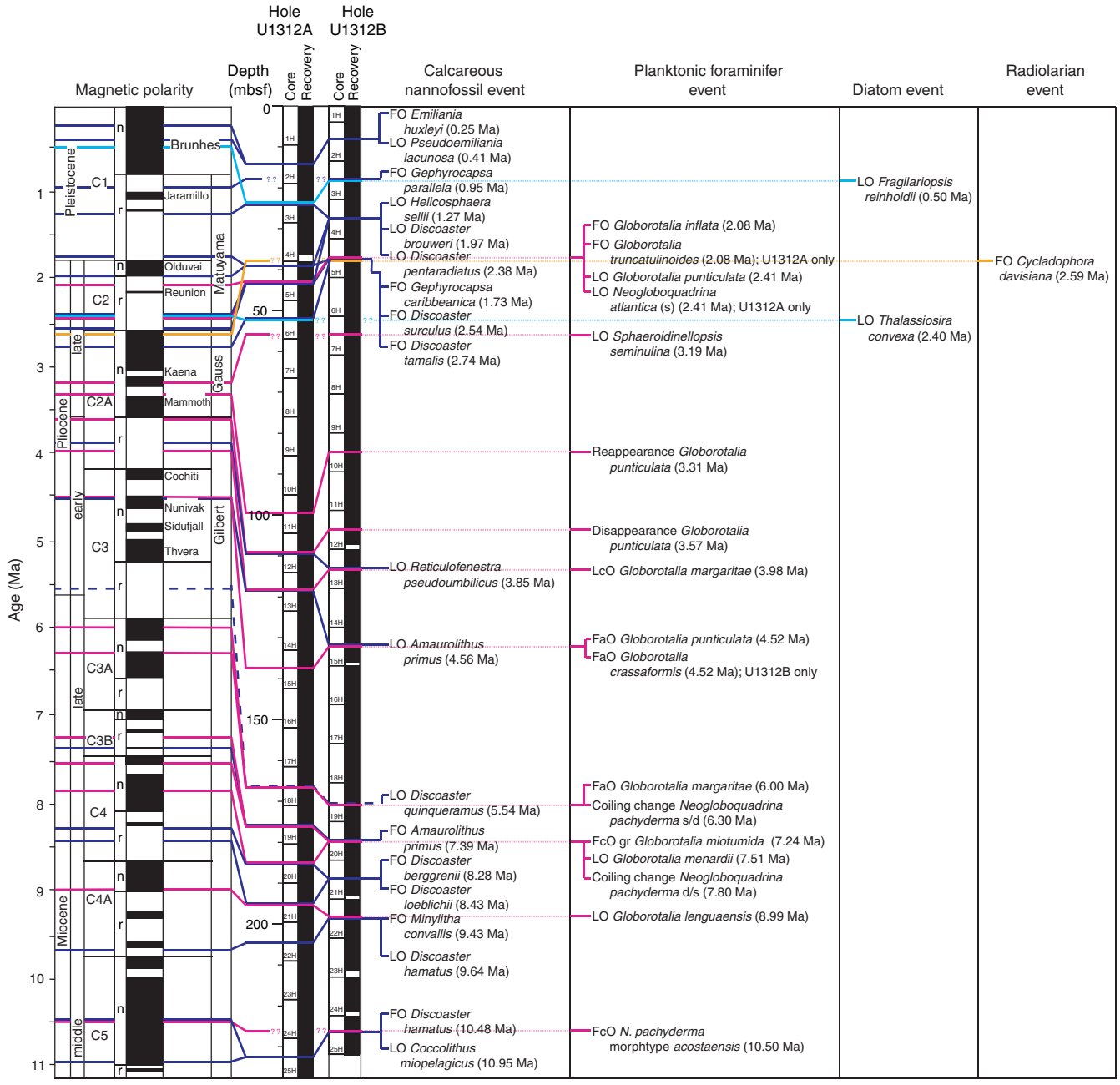

Figure F13. Age vs. depth plot and average sedimentation rates for different intervals of time in Hole U1312A. The datum levels used to construct the curve are given in Table T5.

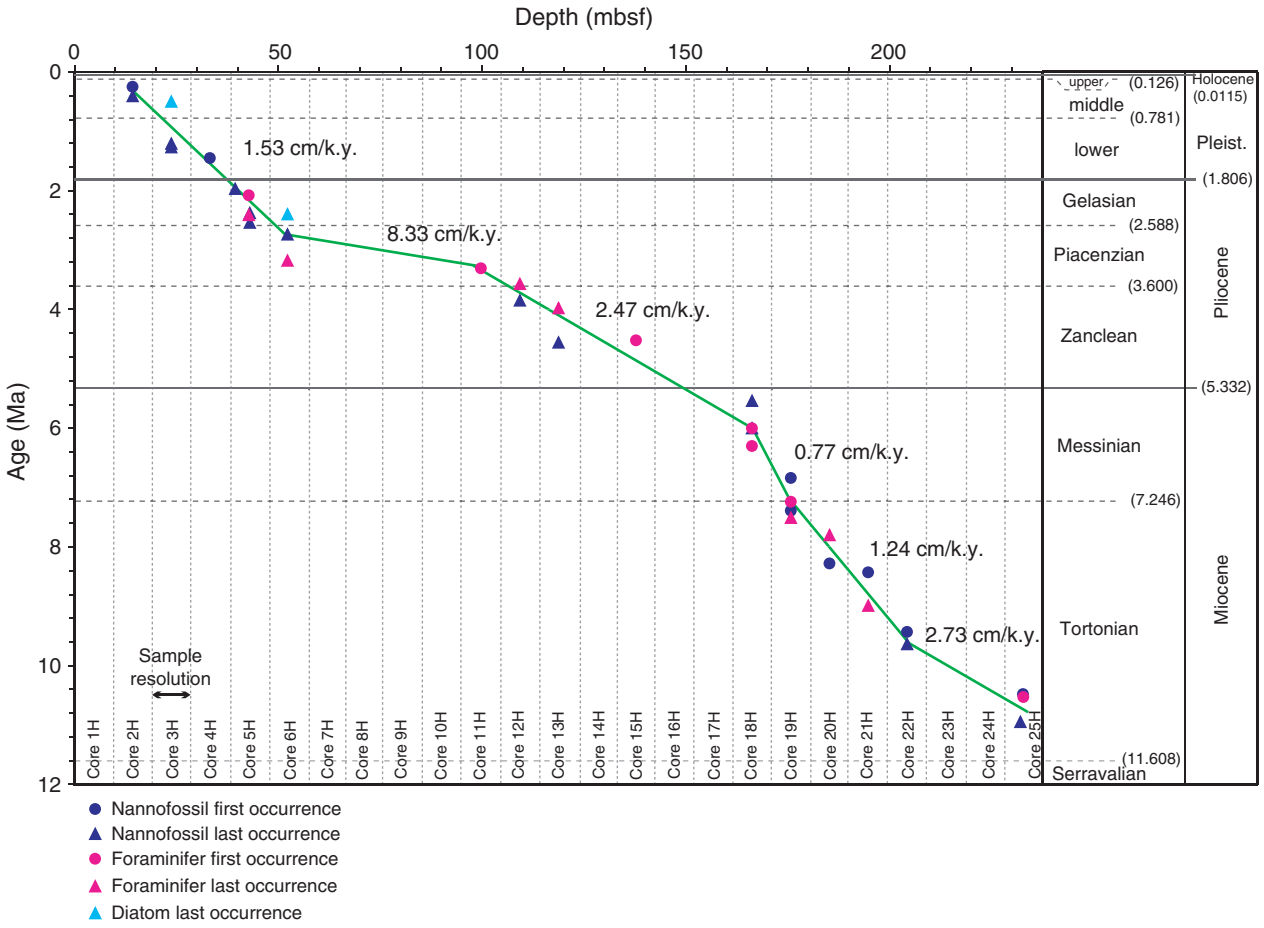

Figure F14. Age vs. depth plot and average sedimentation rates for different intervals of time in Hole U1312B. The datum levels used to construct the curve are given in Table T6.

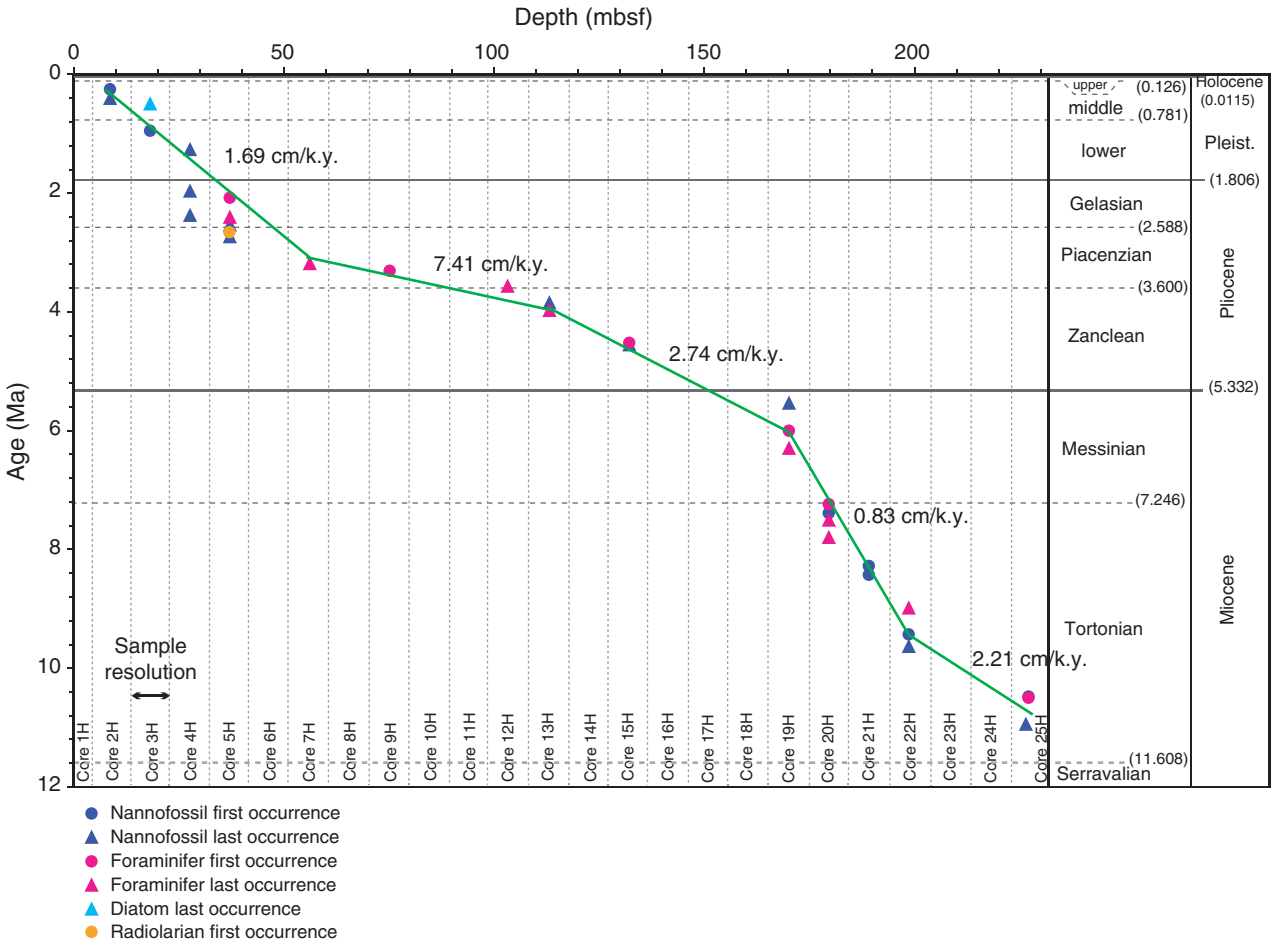

Figure F15. NRM intensity before (green) and after (red) AF demagnetization at 20 mT vs. depth.

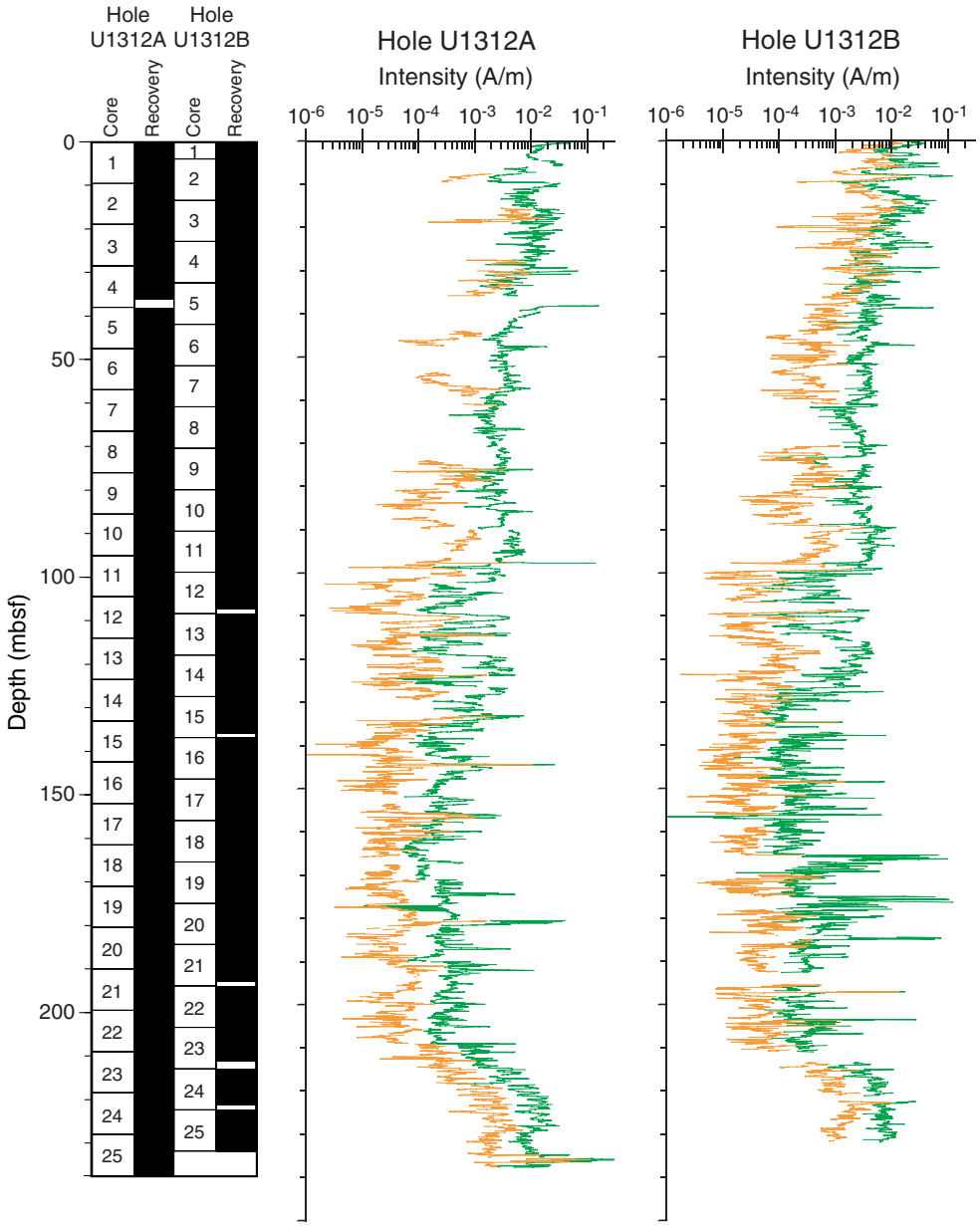

Figure F16. Inclination and declination of remanent magnetization after 20 mT AF demagnetization vs. depth. Declination values have been corrected using Tensor tool data.

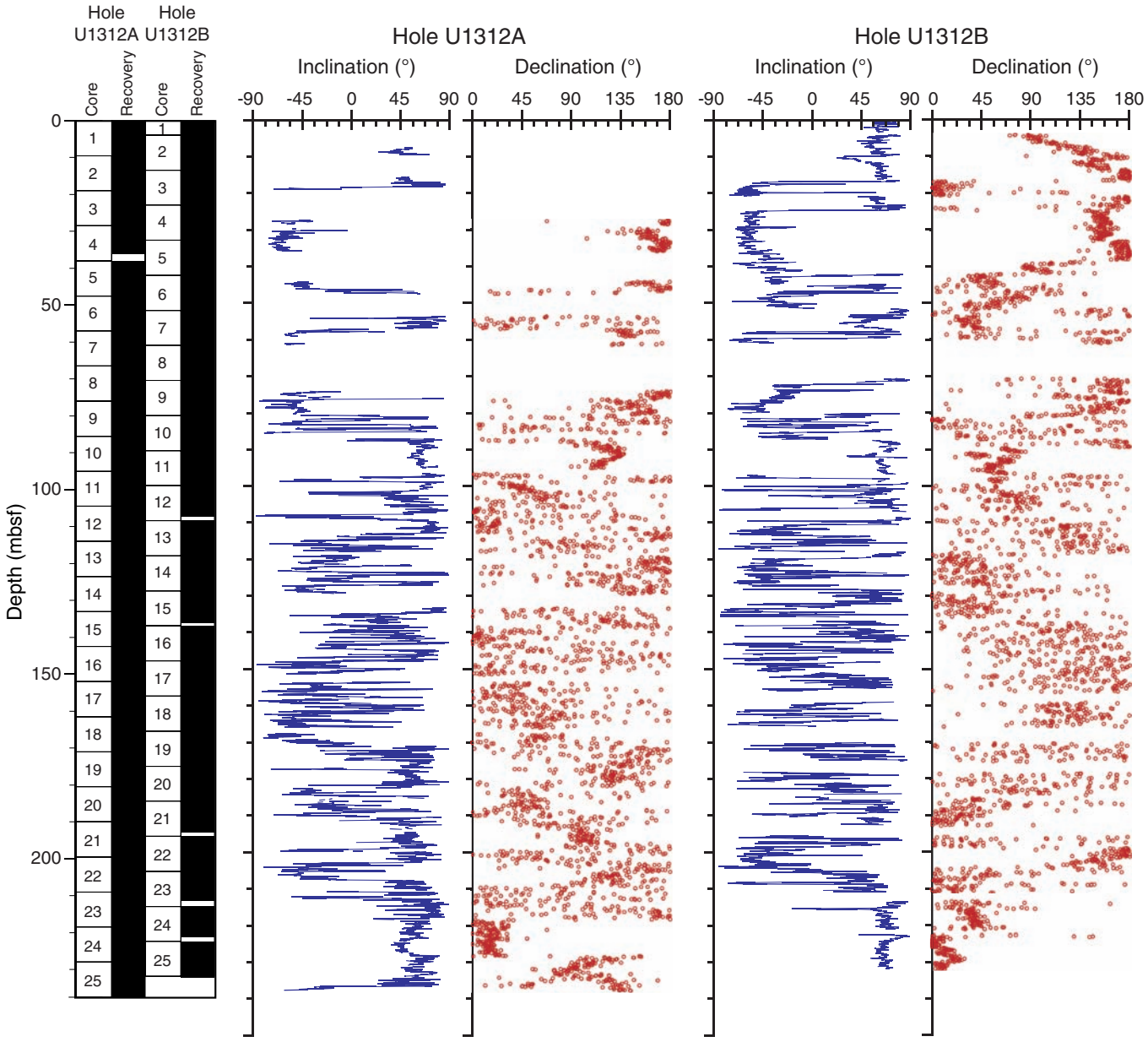

Figure F17. A. Inclination histograms with natural remanent magnetization (NRM) data acquired before alternating-field (AF) demagnetization. **B.** Inclination histograms with data acquired after 20 mT AF demagnetization. I_{GAD} = expected inclination for a geocentric axial dipole.

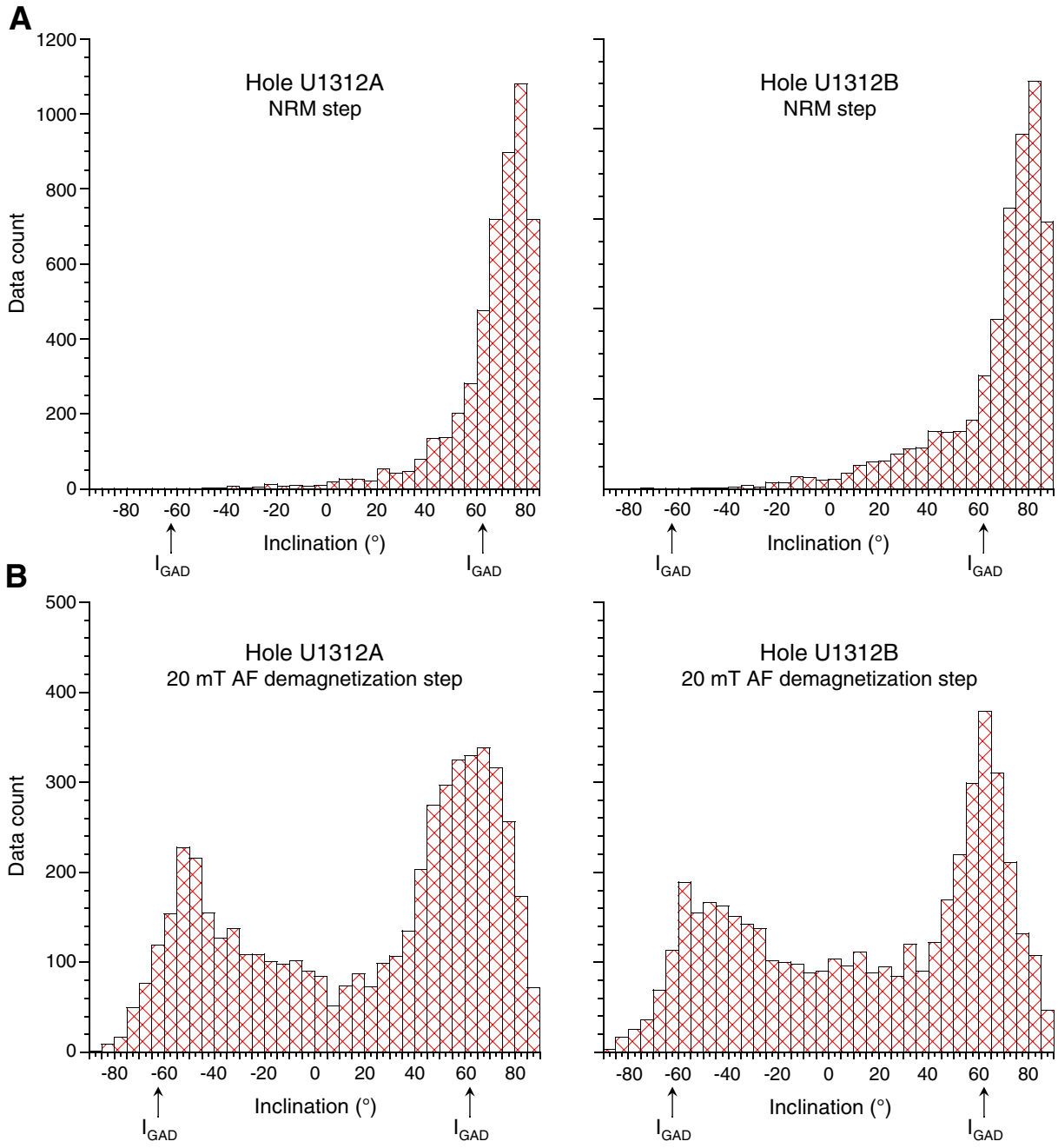

Figure F18. Inclination after 20 mT AF demagnetization vs. depth for Holes U1312A and U1312B and the paleomagnetic polarity interpretation for Hole U1312B (black = normal polarity, white = reversed polarity, gray = undetermined polarity) referenced to the geomagnetic polarity timescale (Cande and Kent, 1995). A possible tie to the reference polarity timescale for the bottom of Hole U1312A is indicated by a red line. Uncertain ties are labeled using a question mark.

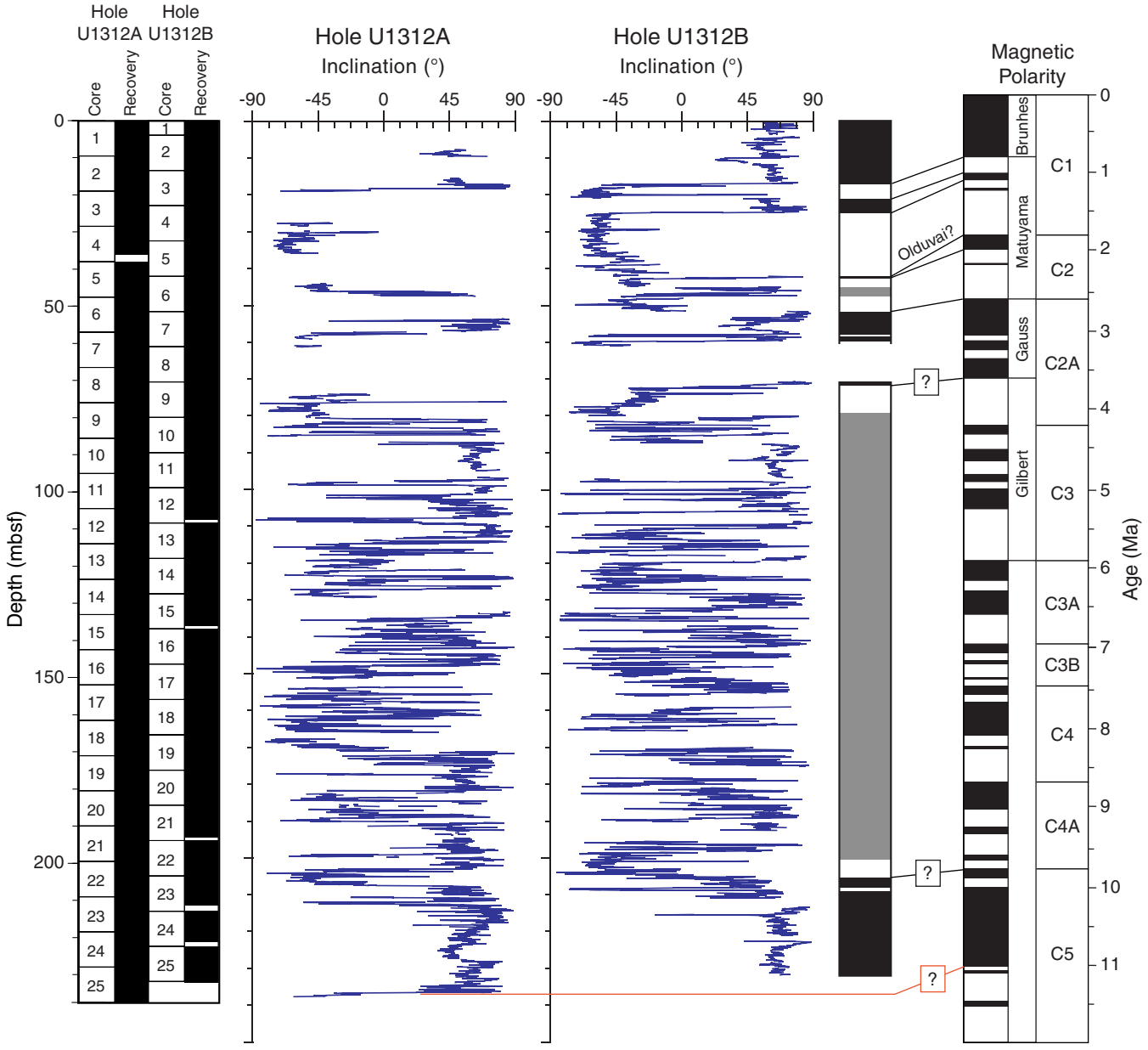

Figure F19. Lightness (L*) data for the interval from 12 to 18 mcd illustrating the lack of a significant gap between Cores 306-U1312B-2H and 3H and relative compression and expansion that occur between holes. For display purposes, 25 has been subtracted from the L* values from Hole U1312B.

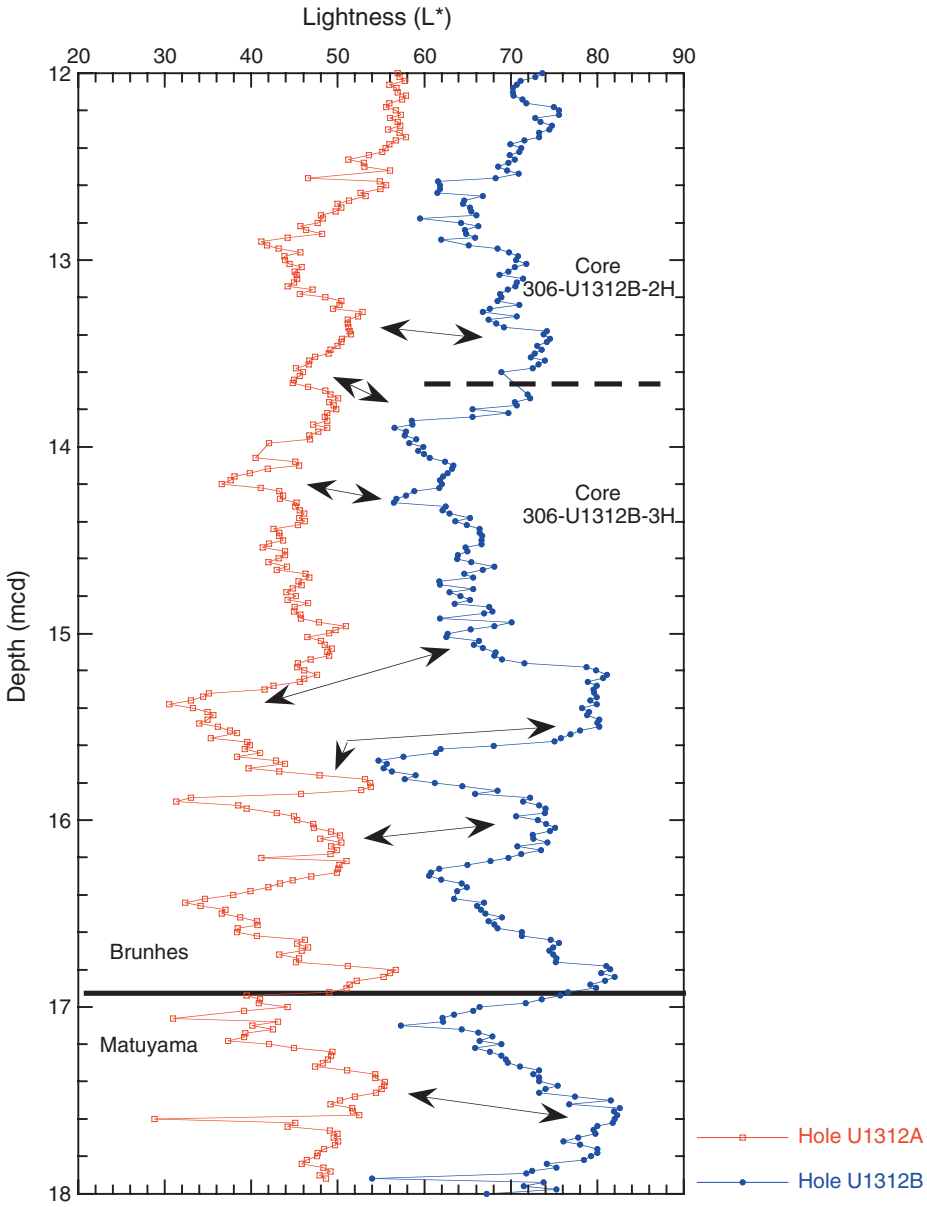

Figure F20. NRM intensity vs. mcd for Holes U1312A and U1312B. Upper panels show composite magnetic intensity record indicating which hole was used to form the splice. Numbers in the lower panel indicate core number. **A.** 0–80 mcd. (Continued on next page.)

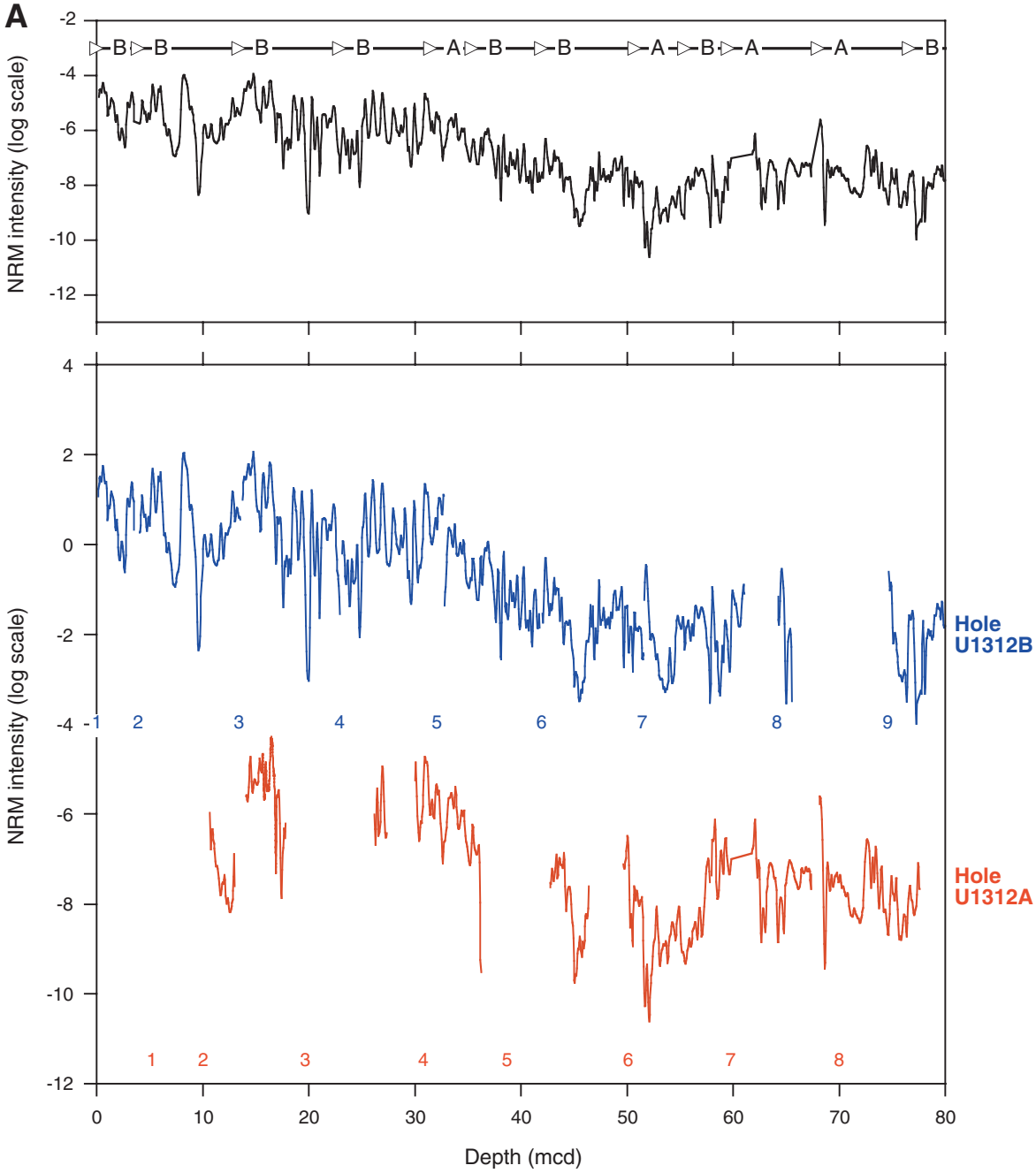

Figure F20 (continued). B. 80–160 mcd.

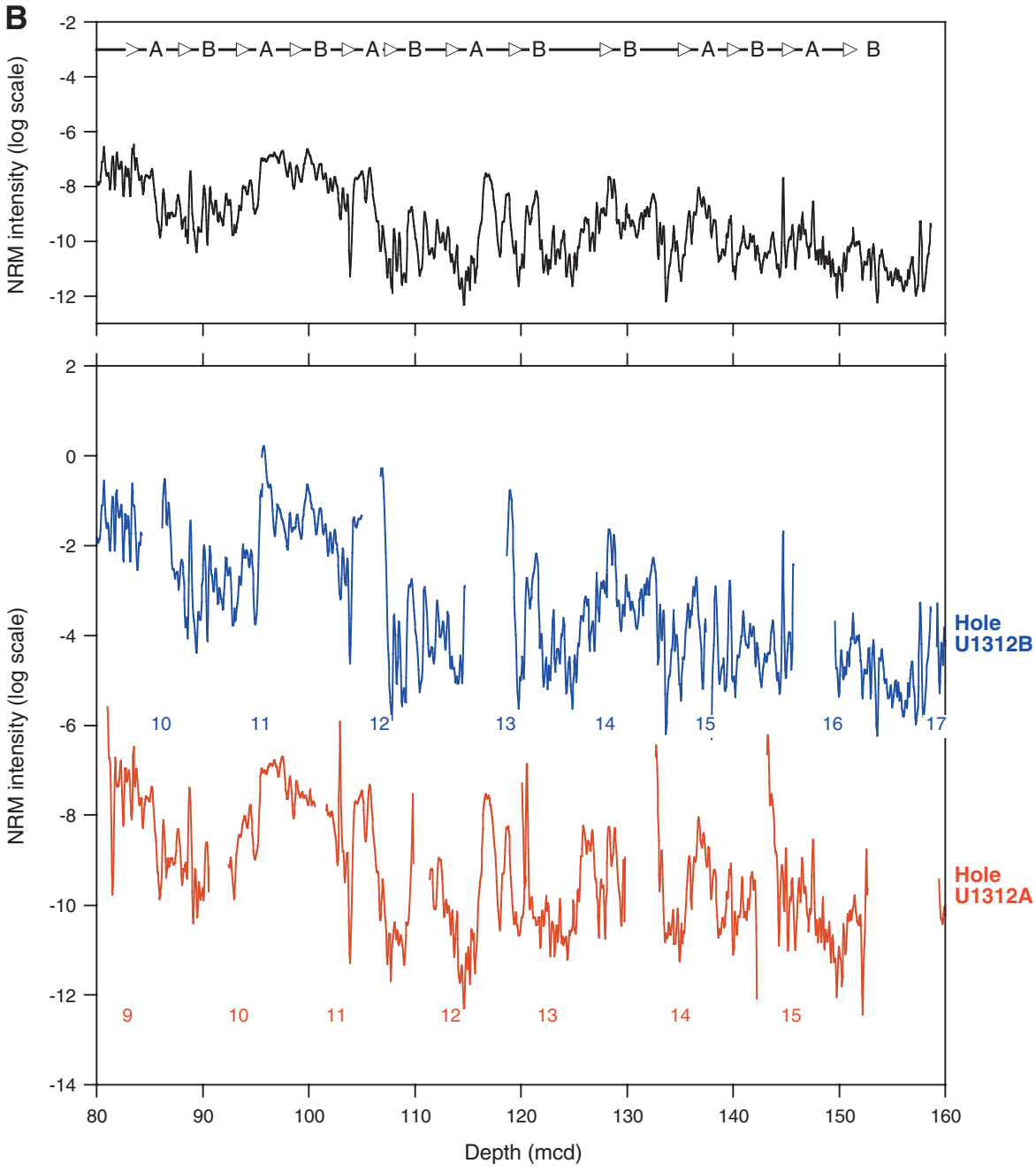

Figure F21. Color parameter L* vs. mcd for Holes U1312A and U1312B. Upper panels show composite L* record indicating which hole was used to form the splice. Numbers in the lower panels indicate core number. **A.** 0–80 mcd. (Continued on next page.)

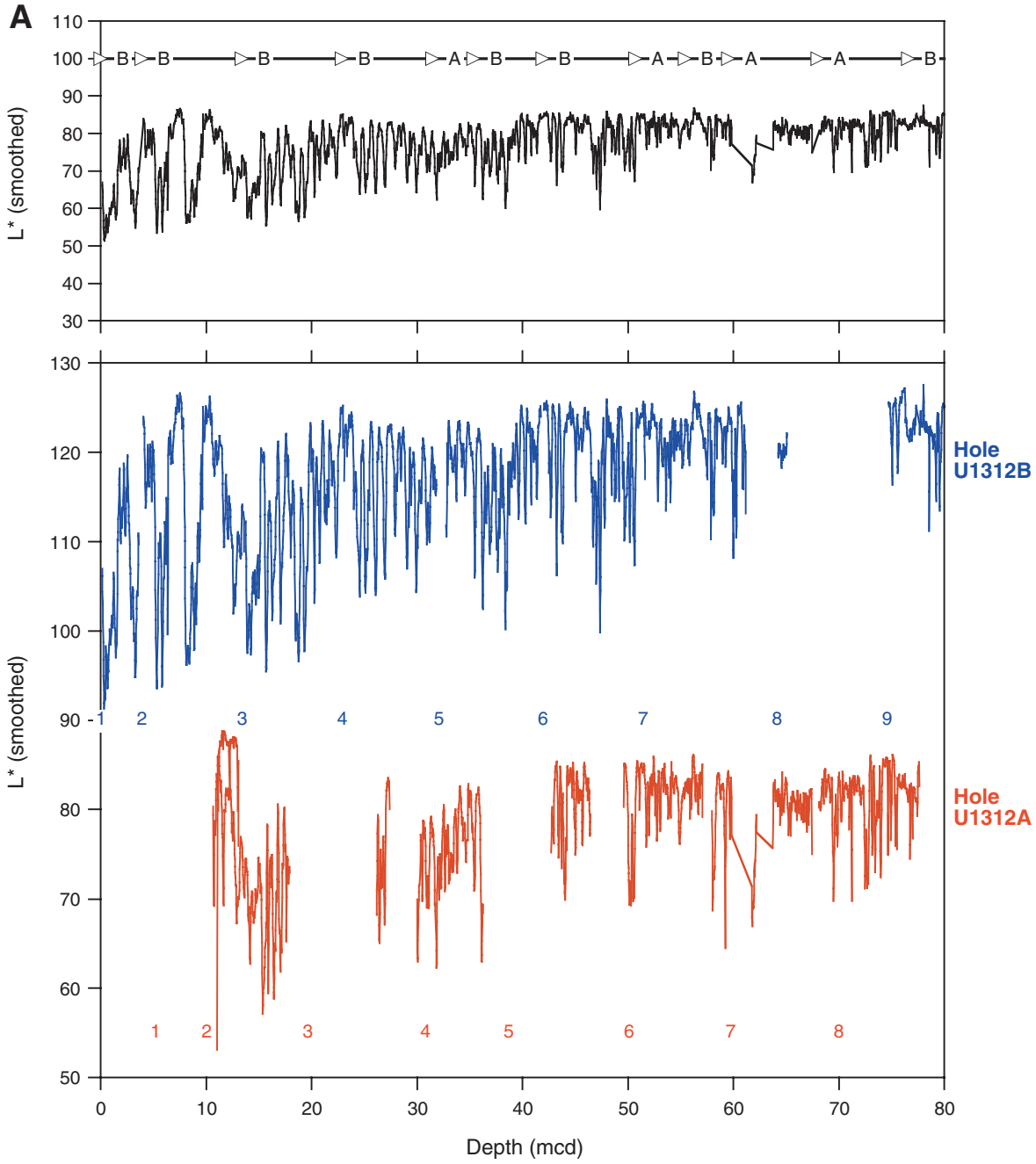

Figure F21 (continued). B. 80–160 mcd.

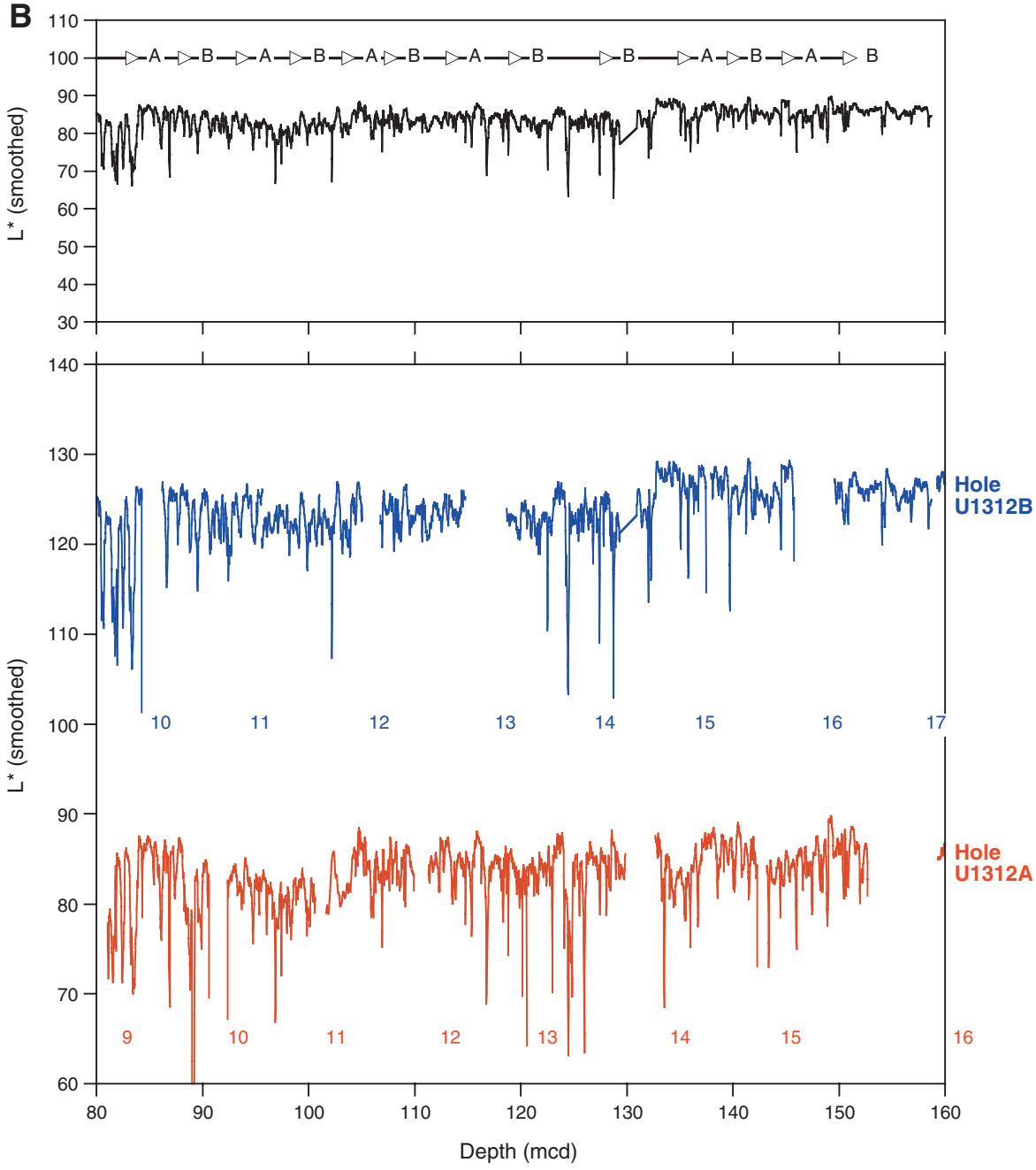

Figure F22. Possible correlation of Cores 306-U1312B-24H and 25H to the long-wavelength increase in natural remanent magnetic (NRM) intensity displayed in Hole U1312A.

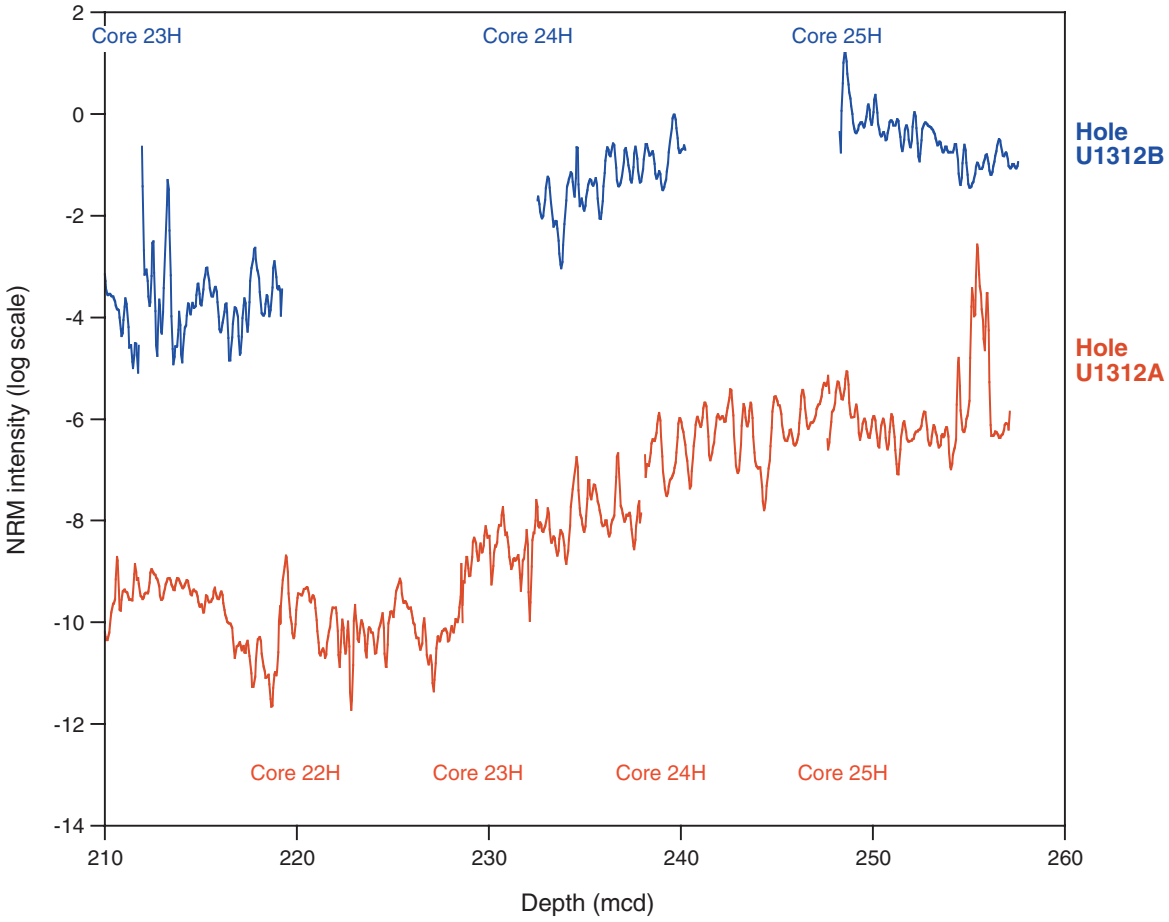

Figure F23. Preliminary correlation between lightness (L*) measured in Hole U1312B (lower panel) and the global benthic oxygen isotope stack (upper panel). Numbers indicate marine oxygen isotope stages (Lisiecki and Raymo, 2005).

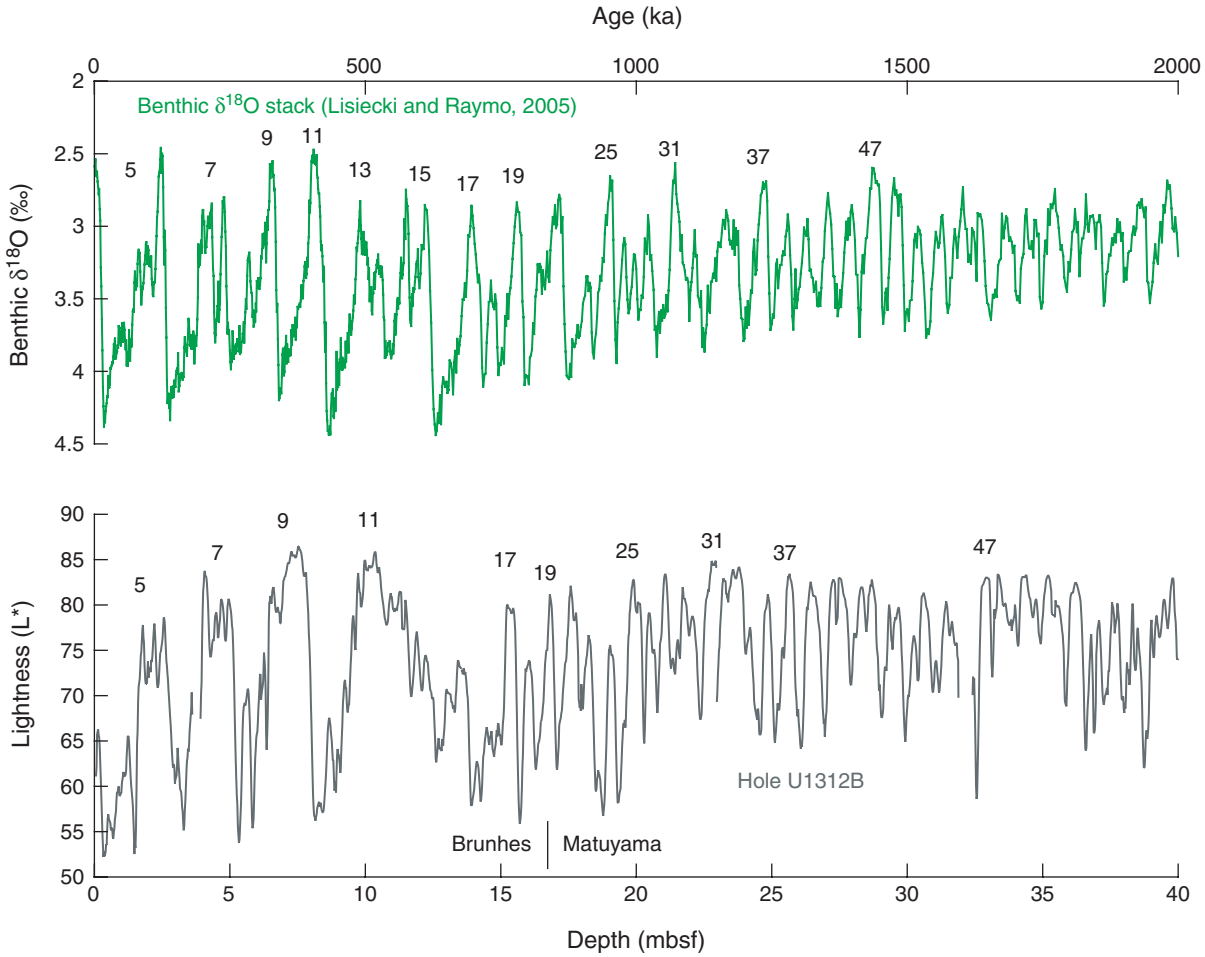

Figure F24. Downhole profiles of chemical constituents in interstitial waters from Hole U1312A. **A.** Chloride. **B.** Salinity. **C.** Alkalinity. **D.** pH. **E.** Sodium. **F.** Potassium. **G.** Magnesium. **H.** Calcium. **I.** Iron. **J.** Boron. **K.** Barium. **L.** Lithium. **M.** Manganese. **N.** Strontium. **O.** Silica. **P.** Sulfate. Open circles = flow-in interval, shaded circles = mildly disturbed, solid circles = no visual disturbance. Dotted line = boundary between lithologic Subunits IA and IB, solid line = boundary between lithologic Units I and II.

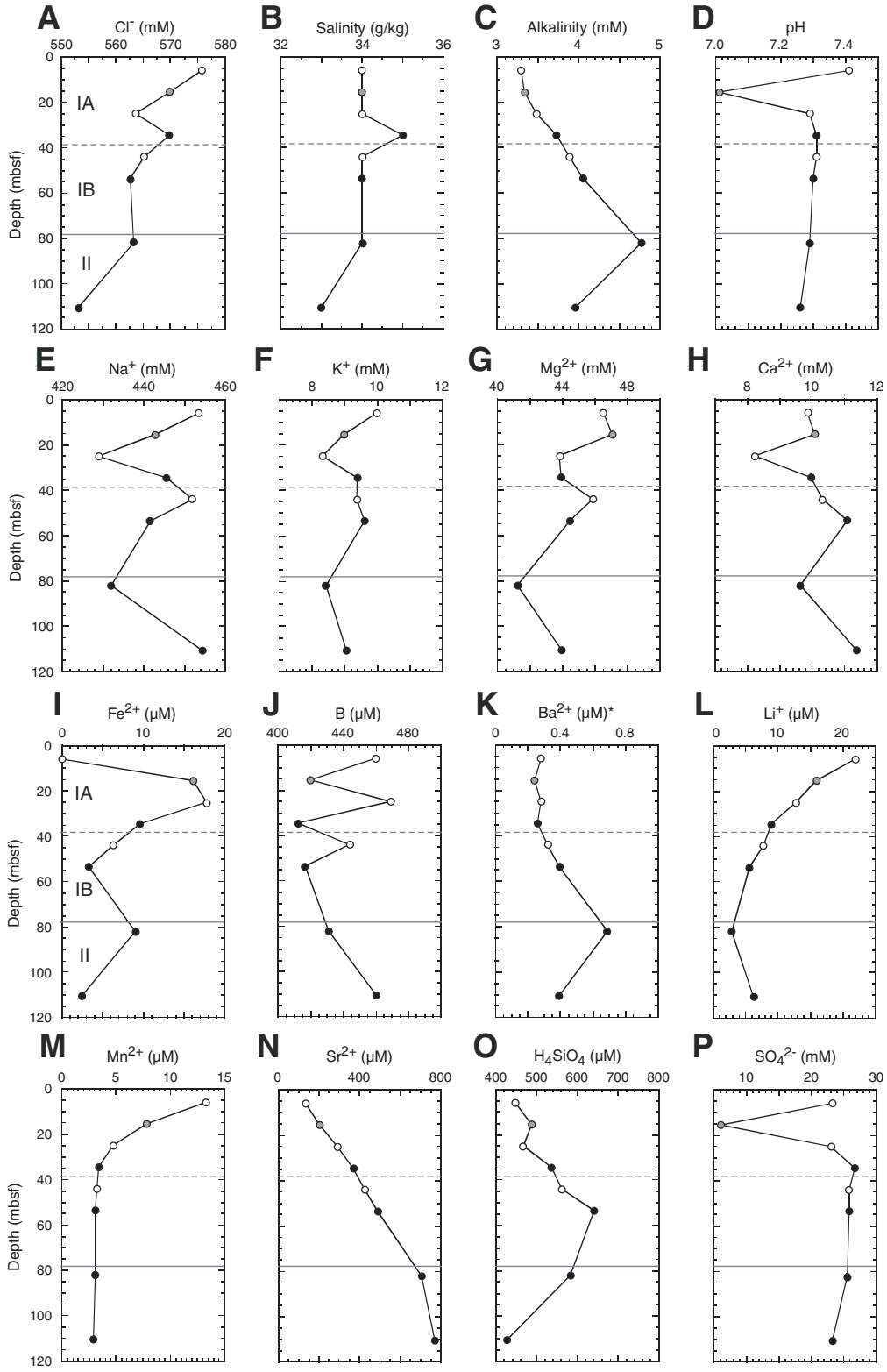

Figure F25. Headspace methane concentrations for Hole U1312A.

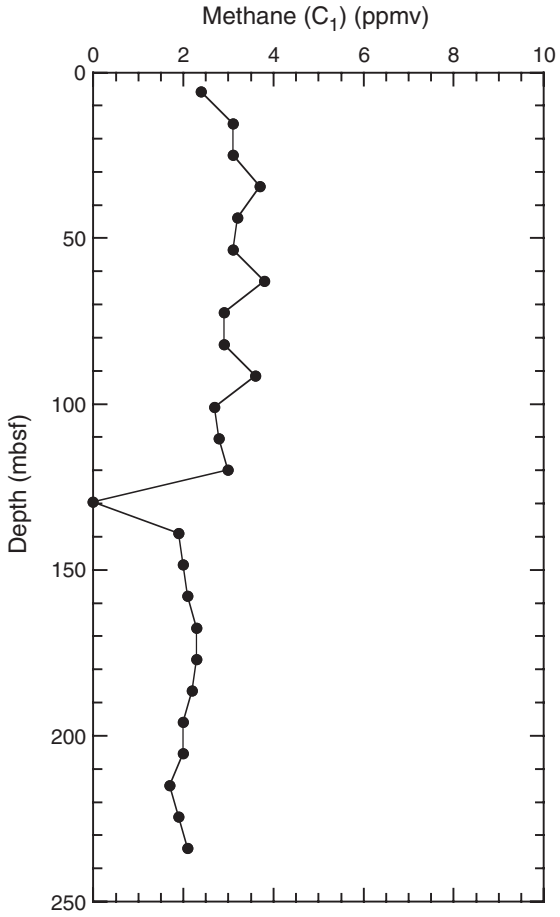

Figure F26. Calcium carbonate content for Hole U1312A compared to contents from Site 608. Lithologic units and subunits are shown.

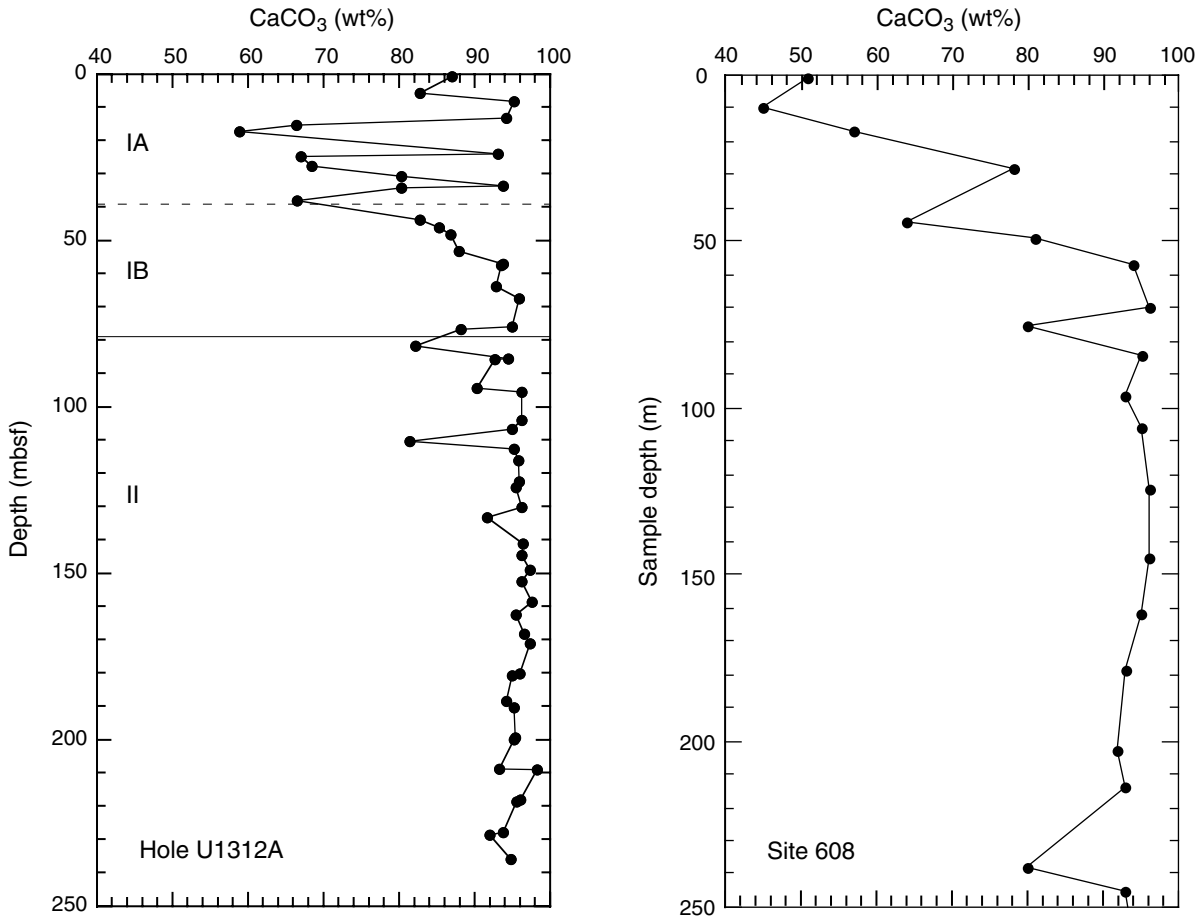

Figure F27. Total organic carbon (TOC) and total nitrogen (TN) for Hole U1312A.

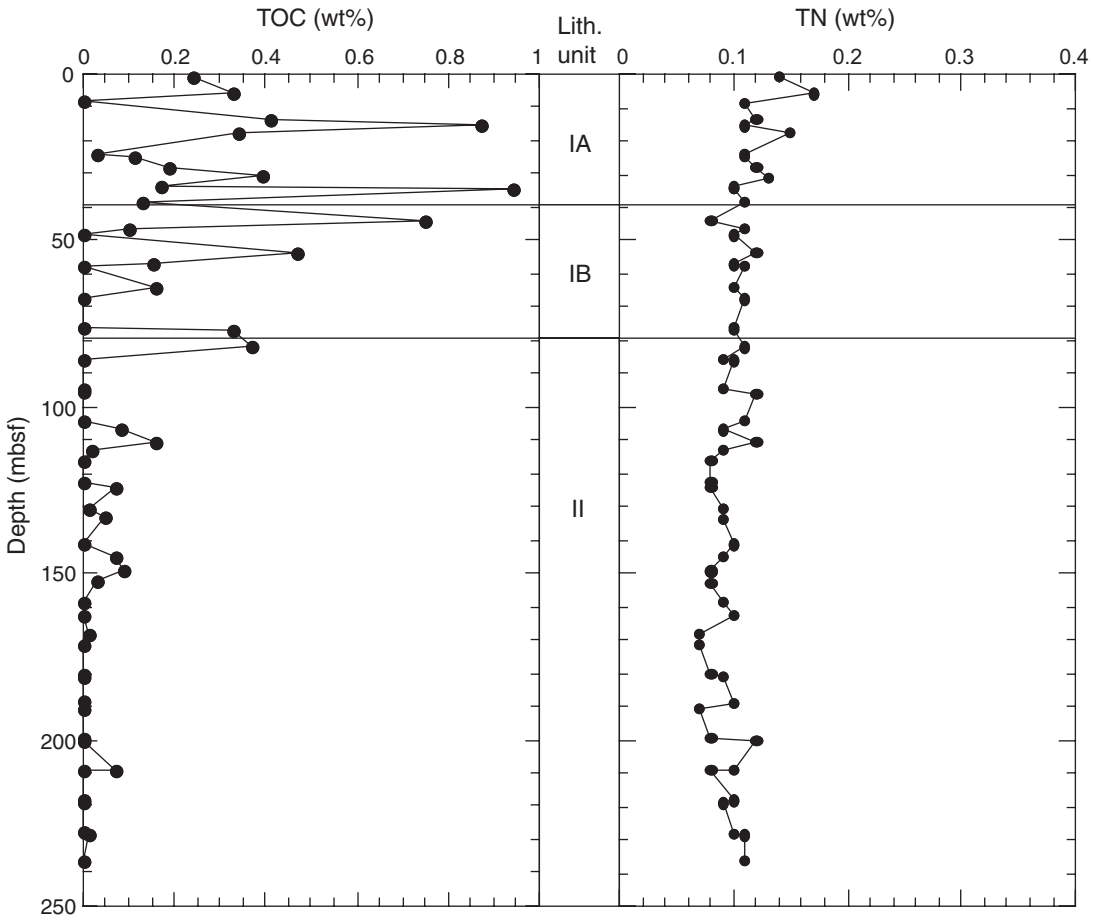

Figure F28. Partial ion chromatogram at *m*/*z* 191 (hopanoid hydrocarbons) from Sample 306-U1312A-3H-4, 145–150 cm. T_s = 22,29,30-trinorneohopane, T_m = 22,29,30-trinorhopane, X = contaminant. 17α(H) indicates isomerization at C_{17}, S and R refer to side-chain isomerization.

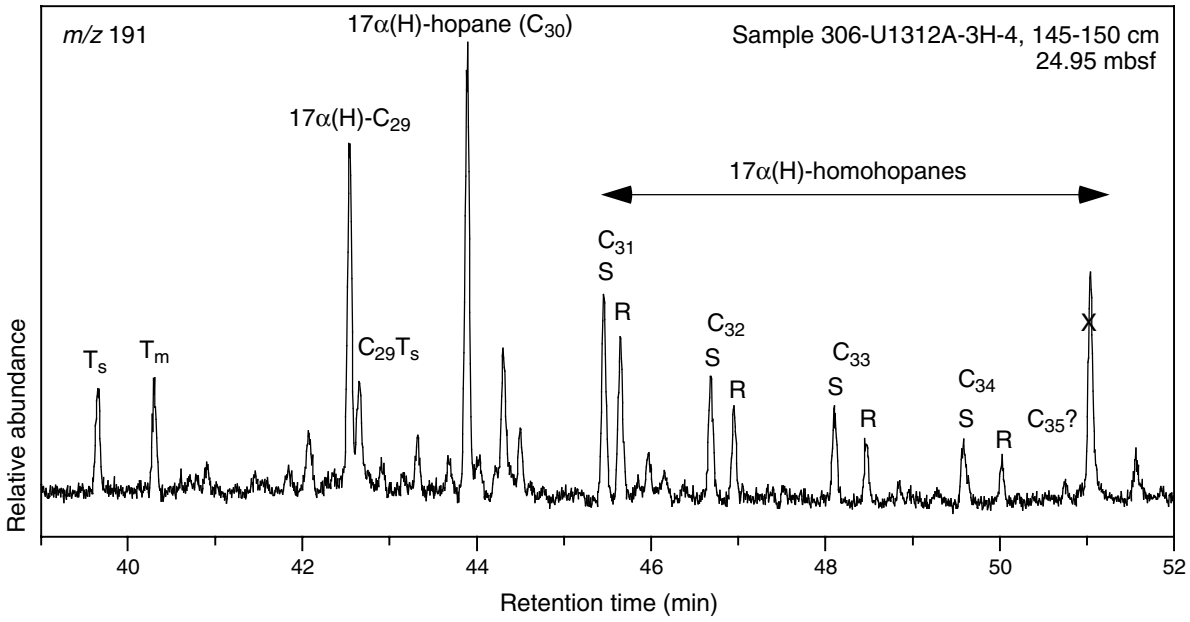

Figure F29. Magnetic susceptibility records. Red = MST, black = MSCL. Multiply values by 6×10^{-5} to obtain SI units.

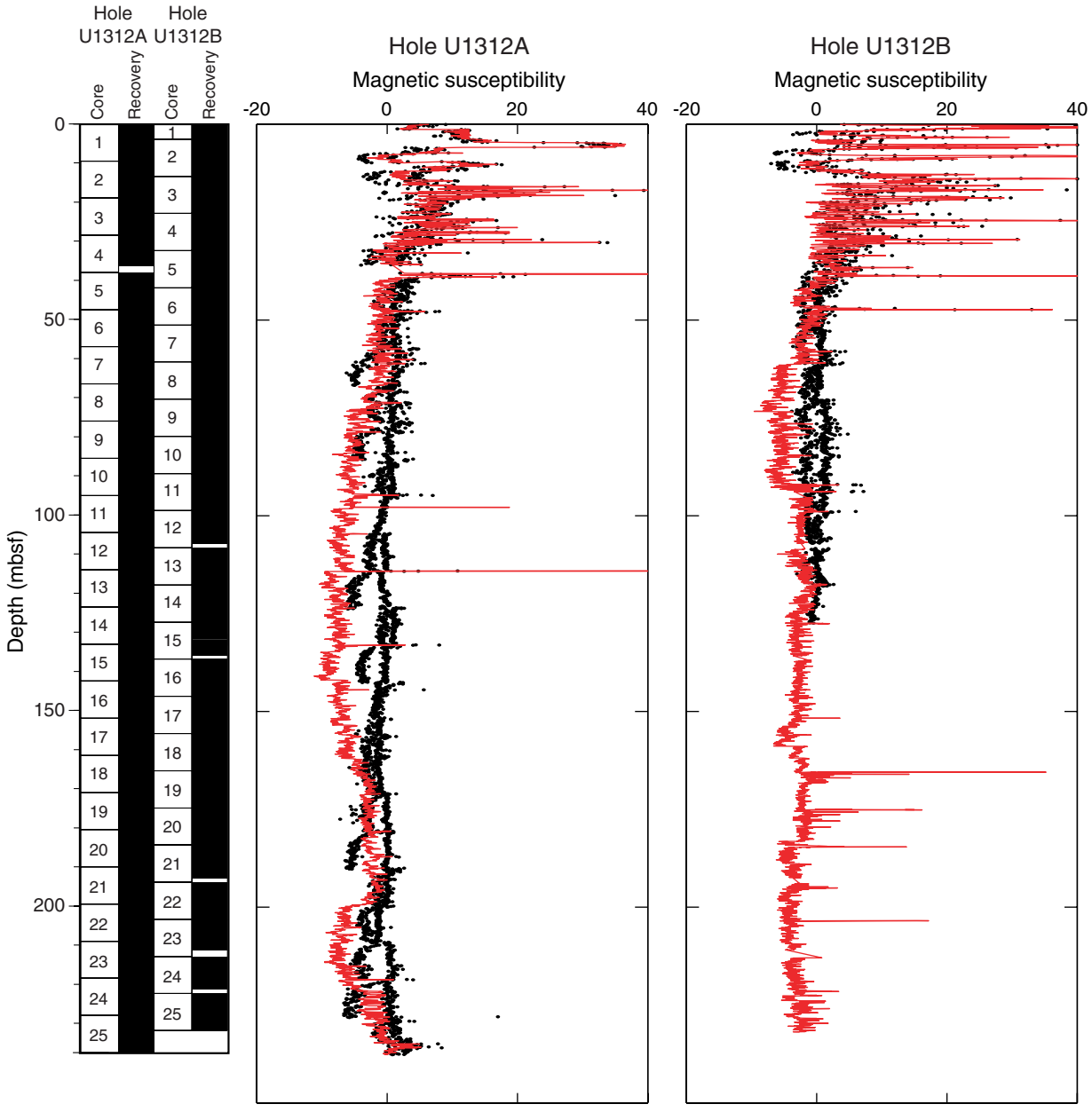

Figure F30. Combined GRA density measurements from the MST and bulk density from discrete measurements (blue circles).

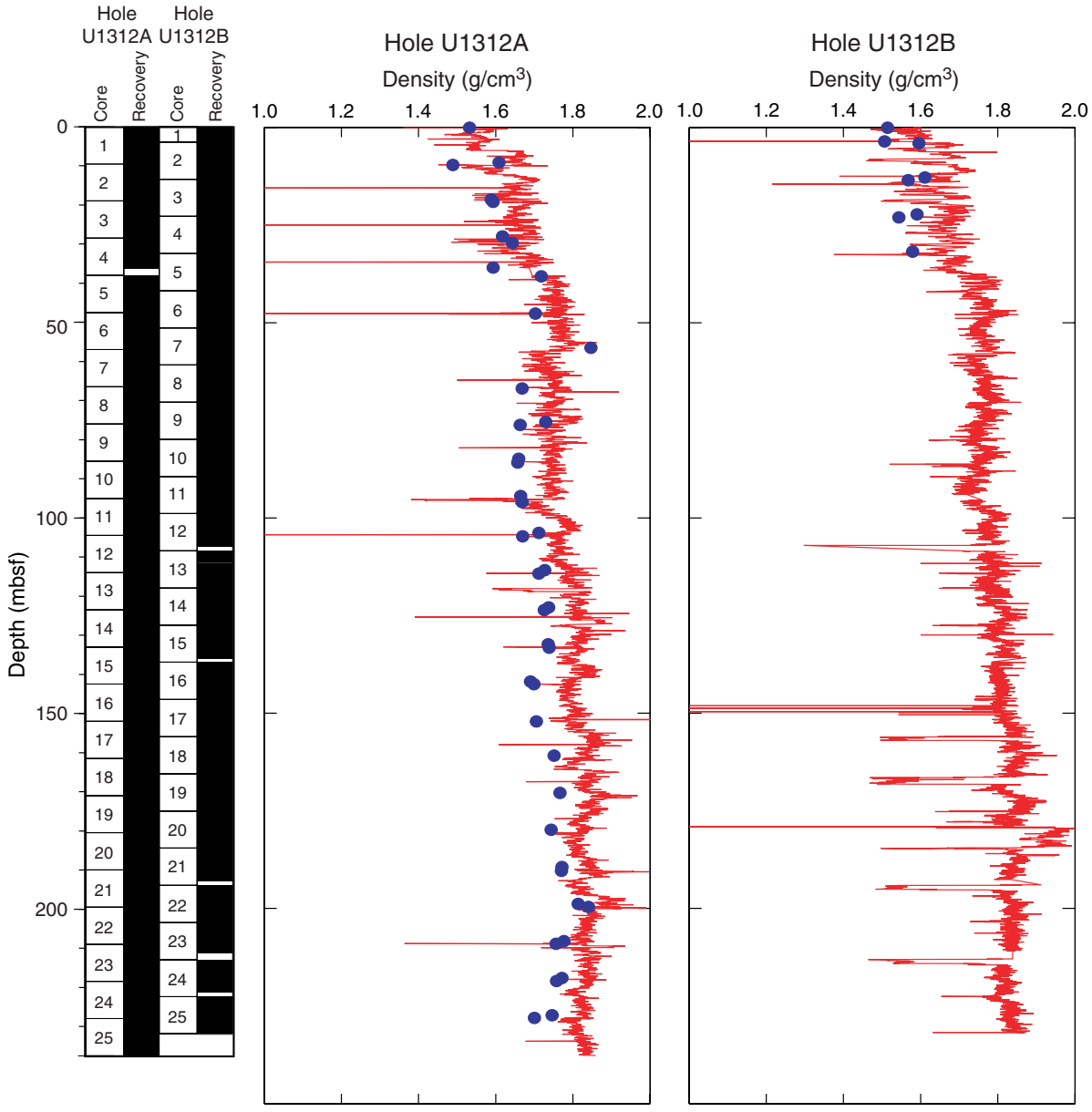

Figure F31. Dry and wet water contents and grain density for Hole U1312A.

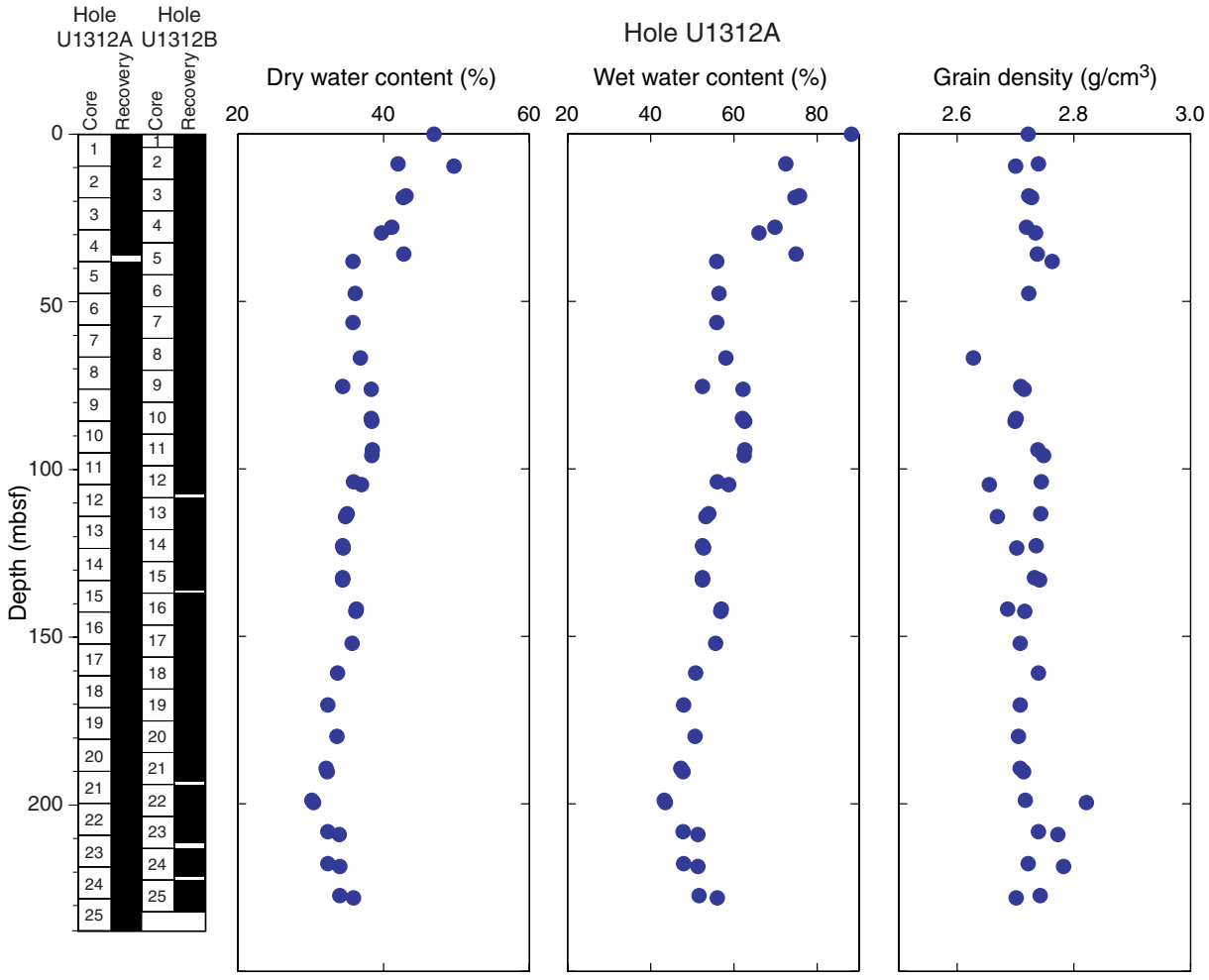

Figure F32. Porosity values.

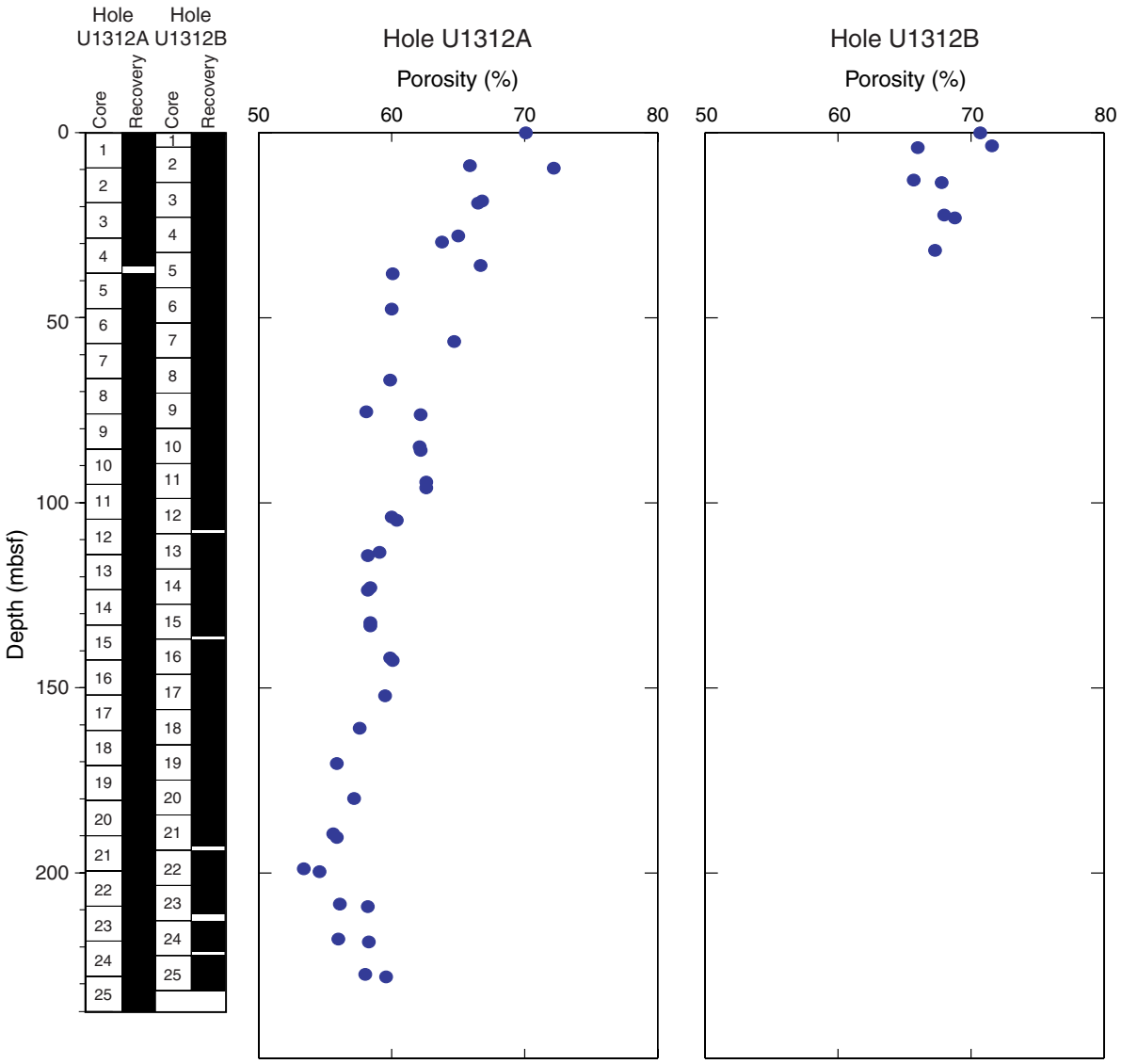

Figure F33. Downcore PWS3 velocity records.

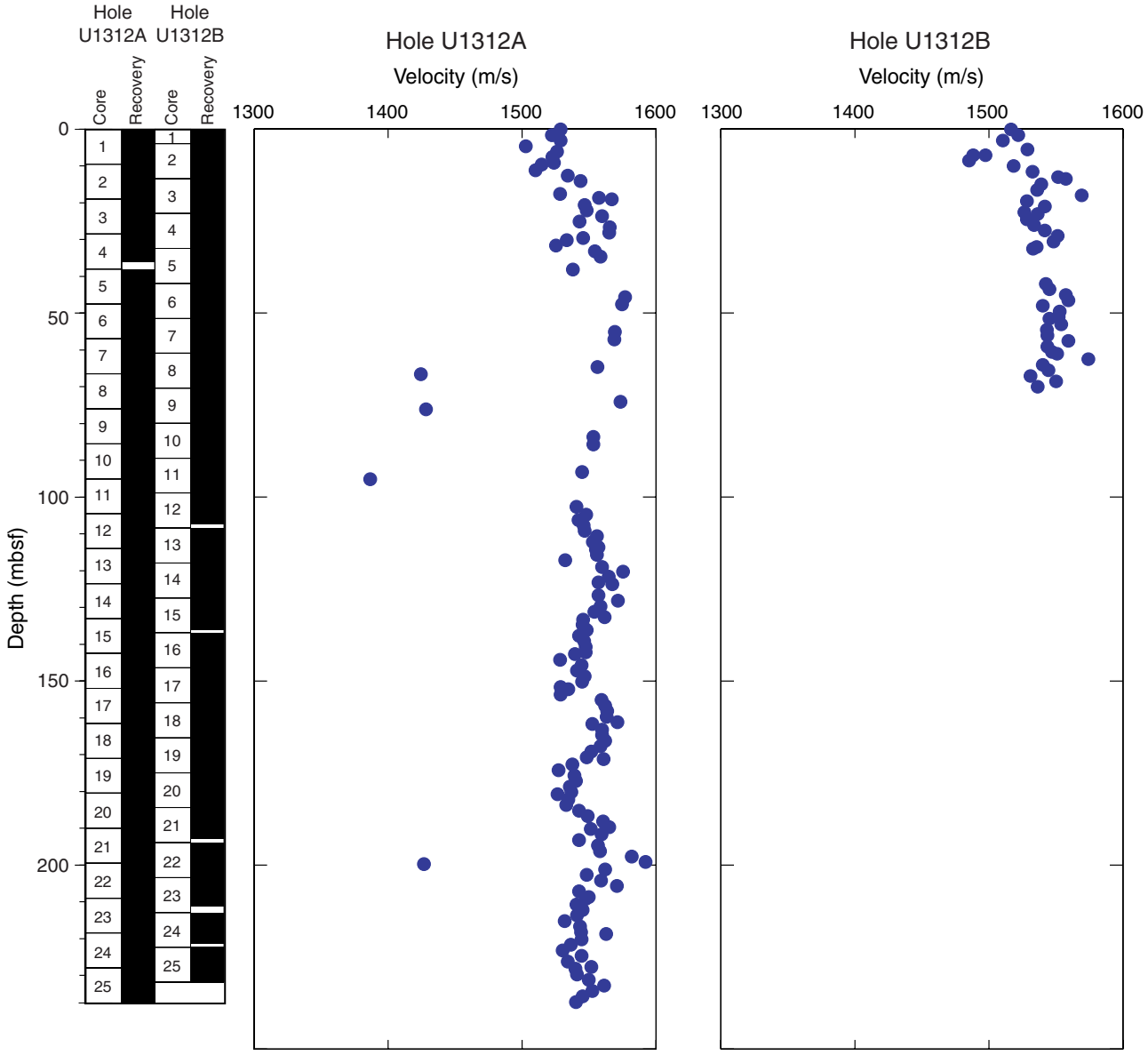

Figure F34. Natural gamma ray (NGR) counts from the MST.

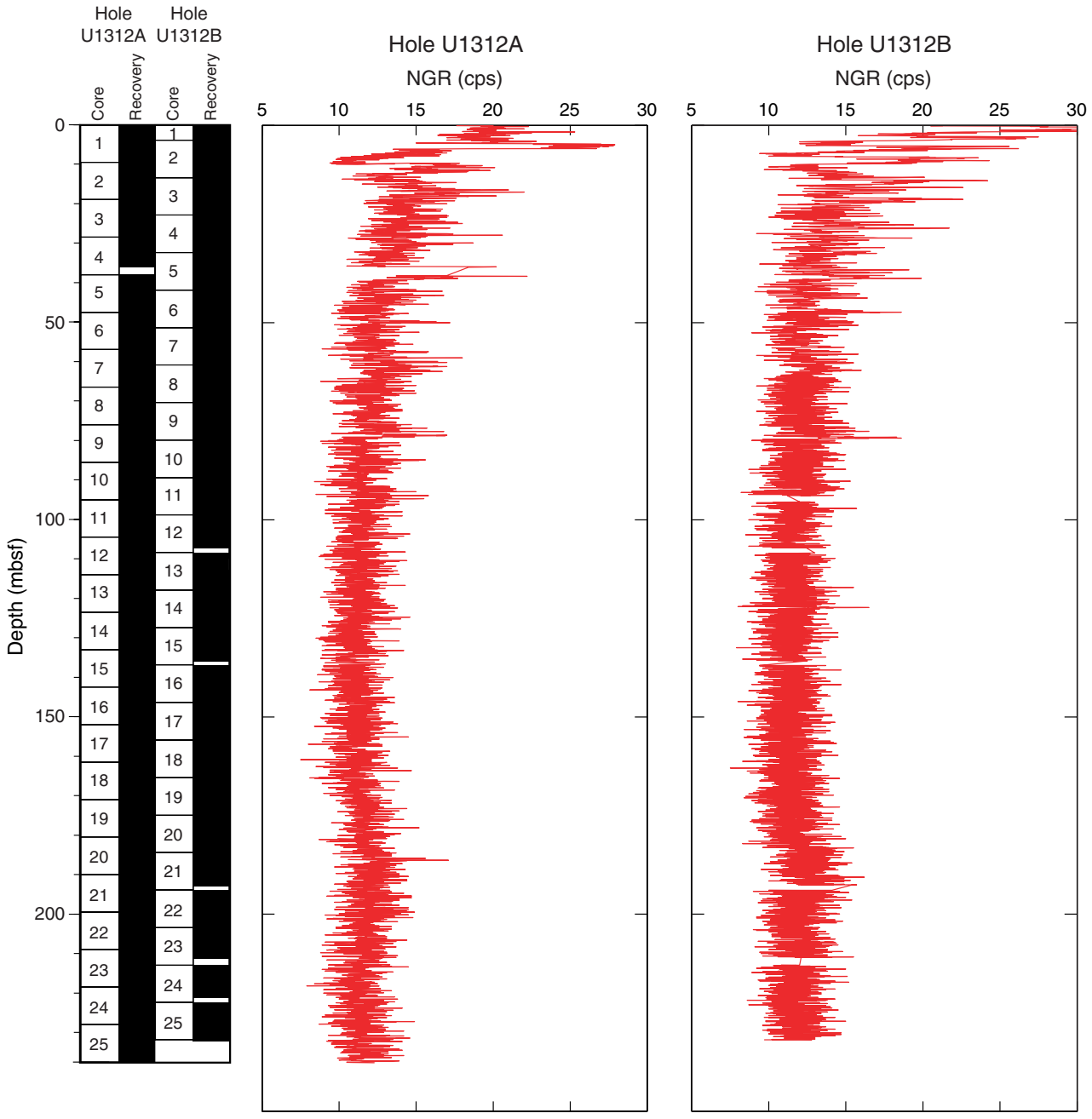

Table T1. Coring summary, Site U1312. (Continued on next page).

Hole U1312A
Latitude: 42°50.2040′N
Longitude: 23°5.2506′W
Time in hole (h): 47.25
Seafloor (drill pipe measurement from rig floor, mbrf): 3533
Distance between rig floor and sea level (m): 10.9
Water depth (drill pipe measurement from sea level, m): 3522.1
Total depth (drill pipe measurement from rig floor, mbrf): 3770.5
Total penetration (mbsf): 237.5
Total length of cored section (m): 237.5
Total core recovered (m): 248.07
Core recovery (%): 104.45
Total number of cores: 25

Hole U1312B
Latitude: 42°50.2150′N
Longitude: 23°5.2652′W
Time in hole (h): 59.00
Seafloor (drill pipe measurement from rig floor, mbrf): 3533
Distance between rig floor and sea level (m): 10.9
Water depth (drill pipe measurement from sea level, m): 3522.7
Total depth (drill pipe measurement from rig floor, mbrf): 3765.5
Total penetration (mbsf): 231.9
Total length of cored section (m): 231.9
Total core recovered (m): 236.84
Core recovery (%): 102.13
Total number of cores: 25

Core	Date (Mar 2005)	Local time (h)	Depth (mbsf) Top	Depth (mbsf) Bottom	Length (m) Cored	Length (m) Recovered	Recovery (%)	Comments
306-U1312A-								
1H	11	1000	0.0	9.5	0.0	10.1	106.1	Oriented, nonmagnetic core barrel
2H	11	1115	9.5	19.0	9.5	10.2	106.9	Oriented, nonmagnetic core barrel
3H	11	1225	19.0	28.5	9.5	10.1	106.0	Oriented, nonmagnetic core barrel
4H	11	1330	28.5	38.0	9.5	7.7	81.2	Oriented, nonmagnetic core barrel
5H	11	1425	38.0	47.5	9.5	10.1	106.0	Oriented, nonmagnetic core barrel
6H	11	1535	47.5	57.0	9.5	10.2	106.8	Oriented, nonmagnetic core barrel
7H	11	1630	57.0	66.5	9.5	10.0	105.6	Oriented, nonmagnetic core barrel
8H	11	1730	66.5	76.0	9.5	10.0	105.1	Oriented, nonmagnetic core barrel
9H	11	1825	76.0	85.5	9.5	9.9	104.6	Oriented, nonmagnetic core barrel
10H	11	1925	85.5	95.0	9.5	10.0	105.3	Oriented, nonmagnetic core barrel
11H	11	2030	95.0	104.5	9.5	10.1	106.1	Oriented, nonmagnetic core barrel
12H	11	2125	104.5	114.0	9.5	10.0	105.4	Oriented, nonmagnetic core barrel
13H	11	2220	114.0	123.5	9.5	10.1	106.5	Oriented, nonmagnetic core barrel
14H	11	2320	123.5	133.0	9.5	10.0	105.6	Oriented, nonmagnetic core barrel
15H	12	0025	133.0	142.5	9.5	10.0	104.8	Oriented, nonmagnetic core barrel
16H	12	0125	142.5	152.0	9.5	9.5	100.1	Oriented, nonmagnetic core barrel
17H	12	0230	152.0	161.5	9.5	10.1	106.7	Oriented, nonmagnetic core barrel
18H	12	0330	161.5	171.0	9.5	10.0	105.6	Oriented, nonmagnetic core barrel
19H	12	0420	171.0	180.5	9.5	10.0	104.9	Oriented, nonmagnetic core barrel
20H	12	0520	180.5	190.0	9.5	10.1	106.4	Oriented, nonmagnetic core barrel
21H	12	0620	190.0	199.5	9.5	10.1	106.0	Oriented, nonmagnetic core barrel
22H	12	0740	199.5	209.0	9.5	10.0	105.4	Drillover
23H	12	0945	209.0	218.5	9.5	9.7	101.7	Drillover
24H	12	1155	218.5	228.0	9.5	10.2	106.8	Drillover
25H	12	1540	228.0	237.5	9.5	10.0	105.6	Drillover
			Cored totals:		228.00	248.07	104.45	
306-U1312B-								
1H	12	2135	0.00	3.90	3.90	3.92	100.50	Oriented, nonmagnetic core barrel
2H	12	2245	3.90	13.40	9.50	9.98	105.10	Oriented, nonmagnetic core barrel
3H	12	2330	13.40	22.90	9.50	9.77	102.80	Oriented, nonmagnetic core barrel
4H	13	0020	22.90	32.40	9.50	10.15	106.80	Oriented, nonmagnetic core barrel
5H	13	0115	32.40	41.90	9.50	10.14	106.70	Oriented, nonmagnetic core barrel
6H	13	0205	41.90	51.40	9.50	10.17	107.10	Oriented, nonmagnetic core barrel
7H	13	0300	51.40	60.90	9.50	10.10	106.30	Oriented, nonmagnetic core barrel
8H	13	0400	60.90	70.40	9.50	10.15	106.80	Oriented, nonmagnetic core barrel
9H	13	0450	70.40	79.90	9.50	10.12	106.50	Oriented, nonmagnetic core barrel
10H	13	0540	79.90	89.40	9.50	9.90	104.20	Oriented, nonmagnetic core barrel
11H	13	0635	89.40	98.90	9.50	9.89	104.10	Oriented, nonmagnetic core barrel
12H	13	0730	98.90	108.40	9.50	9.65	101.60	Oriented, nonmagnetic core barrel

Table T1 (continued).

Core	Date (Mar 2005)	Local time (h)	Depth (mbsf) Top	Depth (mbsf) Bottom	Length (m) Cored	Length (m) Recovered	Recovery (%)	Comments
13H	13	0820	108.40	117.90	9.50	9.88	104.00	Oriented, nonmagnetic core barrel
14H	13	0910	117.90	127.40	9.50	9.76	102.70	Oriented, nonmagnetic core barrel
15H	13	1010	127.40	136.90	9.50	8.59	90.40	Oriented, nonmagnetic core barrel
16H	13	1055	136.90	146.40	9.50	9.56	100.60	Oriented, nonmagnetic core barrel
17H	13	1200	146.40	155.90	9.50	10.10	106.30	Oriented, nonmagnetic core barrel
18H	13	1510	155.90	165.40	9.50	9.99	105.20	Oriented, nonmagnetic core barrel
19H	13	1650	165.40	174.90	9.50	10.13	106.60	Oriented, nonmagnetic core barrel
20H	13	1745	174.90	184.40	9.50	9.76	102.70	Oriented, nonmagnetic core barrel
21H	13	1845	184.40	193.90	9.50	8.50	89.50	Oriented, nonmagnetic core barrel
22H	13	1940	193.90	203.40	9.50	9.74	102.50	Oriented, nonmagnetic core barrel
23H	13	2045	203.40	212.90	9.50	7.82	82.30	Oriented, nonmagnetic core barrel
24H	13	2140	212.90	222.40	9.50	9.42	99.20	Oriented, nonmagnetic core barrel
25H	13	2330	222.40	231.90	9.50	9.65	101.60	Drillover
			Cored totals:		231.90	236.84	102.08	

Table T2. Isolated gravel data, lithology, diameter, and shape, Holes U1312A and U1312B.

Core, section	Depth (mbsf)	Comments
306-U1312A-		
1H-7	9.78	Carbonate clast, d = 2–3 mm, subangular
1H-CC	9.91	Carbonate clast, d = 2 mm, subangular
2H-7	19.06	Basalt (?) clast, d = 10 mm, angular
9H-1	76.60	Sandstone (?) clast, d = 8 mm, subrounded
306-U1312B-		
1H-3	3.05	Carbonate clast, d = 3 mm, angular
1H-3	3.56	Unidentified clast, green, d = 7 mm
2H-2	6.00	Unidentified clast, green, d = 8 mm
2H-3	7.90	Unidentified clast, mudstone (?) or basalt (?), d = 4 mm
2H-6	11.80–11.90	Unidentified clast, d = 2 mm
2H-6	12.24	Sandstone (?) clast, d = 15 mm
2H-6	12.84	Sandstone (?) clast, d = 6 mm
2H-7	13.28	Sandstone (?) clast, d = 13 mm, subrounded
2H-CC	13.74	Unidentified clast, mudstone (?) or basalt (?), d = 2 mm
3H-1	13.99	Basalt (?) clast, d = 12 mm, angular
3H-1	14.01	Mudstone (?) clast, d = 2.5 mm, angular
3H-1	14.02	Mudstone (?) clast, d = 2 mm, angular
3H-1	14.36	Sandstone (?) clast, d = 8 mm, subrounded
3H-1	14.4	Sandstone (?) clast, d = 8 mm, subrounded
3H-1	14.41	Sandstone (?) clast, d = 9 mm, subrounded
3H-1	14.42	Sandstone (?) clast, d = 8 mm, subrounded
3H-1	14.42	Sandstone (?) clast, d = 7 mm, subrounded
3H-1	14.43	Sandstone (?) clast, d = 5 mm, subrounded
3H-3	16.98	Unidentified clast, d = 3 mm, angular
3H-3	17.00	Unidentified clast, d = 3 mm, angular
3H-3	17.04	Unidentified clast, d = 3 mm, angular
3H-3	17.05	Unidentified clast, d = 3 mm, angular
3H-4	18.48	Unidentified clast, d = 2 mm, angular
3H-4	18.75	Unidentified clast, d = 3 mm, angular
3H-4	19.33	Unidentified clast, d = 3 mm, angular
3H-6	21.95	Unidentified clast, d = 2 mm, angular
4H-1	23.04	Unidentified clast, black, d > 10 mm, angular
9H-6	78.89	Sandstone clast, d = 8 mm, subrounded
15H-1	127.52	Unidentified clast, rounded, in fall-in?
19H-1	166.33	Unidentified clast, in fall-in?
19H-1	166.33	Unidentified clast, in fall-in?
19H-1	166.37	Unidentified clast, in fall-in?
19H-2	168.24	Unidentified clast, in fall-in?
19H-2	168.24	Unidentified clast, in fall-in?

Note: d = diameter.

Table T3. Occurrence of pale green bands, Hole U1312A.

Core, section, interval (cm)	Depth (mbsf) Top	Bottom	Munsell color
306-U1312A-			
2H-1, 68	10.18	10.23	Olive green band or patch 5Y 5/2
2H-1, 78	10.28	10.33	Olive green band or patch 5Y 5/2
2H-1, 117	10.67	10.8	Light greenish gray band 5GY 7/Y
2H-4, 37	14.37	14.65	Light green 10YR 7/1
2H-4, 104	15.04	15.15	Light green 10 YR 7/1
4H-2, 20	30.2	30.25	Greenish gray 5Y 6/1
4H-2, 128	31.28	31.39	Light greenish gray 5GY 7/1
4H-3, 3	31.53	31.58	Light green 5GY 7/1
4H-3, 69	32.19	32.195	Greenish band
4H-3, 75	32.25	32.255	Greenish band
4H-3, 122	32.72	32.76	Light green 5G 7/1
4H-3, 126	32.76	32.765	Green
4H-3, 130	32.8	32.83	Green
4H-3, 143	32.93	32.935	Green
4H-4, 4	33.04		Light green
4H-4, 6	33.06		Light green
4H-4, 13	33.13	33.15	Light greenish gray 5GY 7/1
4H-5, 124	35.74	35.94	Light greenish gray 5GY 7/1
6H-7, 41	56.91	56.92	Light greenish gray 5G 7/1
6H-CC, 16	57.44	57.45	Light greenish gray 5G 7/1
7H-3, 139	61.39		Pale green 5G 6/2
7H-3, 144	61.44		Pale green 5G 6/2
7H-3, 147	61.47	61.48	Pale green 5G 6/2
7H-4, 64	62.14	62.19	Pale green 5G 6/2
10H-2, 67	87.67	87.68	Pale green 5G 7/2
10H-6, 16	93.16	93.18	
11H- 3, 27	96.77	96.78	Light greenish gray 5G 7/1
11H-3, 66	98.66	98.67	Light bluish gray 5B 7/1
11H-3, 77	98.77	98.79	Light bluish gray 5B 7/1
11H-3, 85	98.85	98.87	Light bluish gray 5B 7/1
11H-3, 97	98.97	98.98	Light greenish gray 5G 7/1
11H-3, 135	99.35	99.36	Light greenish gray 5G 7/1
11H-3, 143	99.43	99.44	Light greenish gray 5G 7/1
11H-4, 84	100.34	100.36	Light bluish gray 5B 7/1
11H-4, 129	100.79	100.81	Light bluish gray 5B 7/1
11H-6, 74	103.24	103.26	Light greenish gray 5G 7/1
11H-7, 4	104.04	104.05	Light bluish gray 5B 7/1
12H-1, 44	104.94	104.95	Light greenish gray 5B 7/1
12H-2, 115	107.15	107.25	Light greenish (bluish) gray 5B(G) 7/1
13H-4, 58	122.08	119.09	Light greenish green
13H-6, 17	121.67		Light green
13H-6, 22	121.72		Light green
13H-6, 28	121.78		Light green
13H-6, 44	121.94		Light greenish gray
13H-6, 45	121.95		Light greenish gray
13H-6, 48	121.98		Light greenish gray
13H-6, 52	122.02		Light greenish gray
13H-6, 58	122.08	122.09	Greenish gray 5BG 6/1
13H-6, 68	122.18		Light greenish gray 5G 7/1
13H-6, 69	122.19	122.20	Light greenish gray 5G 7/1
13H-6, 74	122.24	122.25	Light greenish gray 5G 7/1
14H-4, 55	128.55	128.56	Light greenish gray 5B 7/1
14H-5, 8	129.58		Light greenish gray 5B 7/1
14H-5, 1	129.6		Light greenish gray 5B 7/1
14H-6, 8	131.8	131.85	Light greenish gray 5B 7/1
14H-7, 19	132.69	132.73	Light greenish gray 5B 7/1
15H-4, 98	138.48	138.52	Light greenish gray 5G 7/1
15H-4, 143	138.93	138.95	Light greenish gray 5G 7/1
15H-6, 4	140.9	140.92	Light greenish gray 5G 8/1
15H-6, 130	141.8		Light greenish gray 5G 8/1
15H-7, 15	142.15	142.16	Light greenish gray 5B 7/1
16H-6, 79	150.79	150.8	Light greenish gray 5GY 8/1
17H-1, 132	153.32	153.33	Light greenish gray 5G
17H-2, 20	153.7		Light greenish gray 5GY 8/1
17H-2, 56	154.06		Light greenish gray 5GY 8/1
17H-2, 57.5	154.075	154.08	Light greenish gray 5GY 8/1
22H-5, 112	206.62		Greenish gray 5G 6/1

Table T4. Occurrence of pale green bands, Hole U1312B.

Core, section, interval (cm)	Depth (mbsf) Top	Bottom	Munsell color
306-U1312B-			
1H-3, 18	3.18	3.2	Greenish brown 2.5Y 5/2
2H-1, 129	5.19	5.4	Gray, grades up into greenish brown
2H-2, 40	5.8	5.9	Olive 5Y 5/3
2H-3, 118	8.08	8.2	Greenish brown 10YR 5/2
2H-4, 7	8.47	8.55	Greenish brown 10YR 5/2
2H-4, 28	8.68		Greenish gray 5GY 5/1
2H-4, 56	8.96		Greenish gray 5GY 5/1
2H-4, 66	9.06		Greenish gray 5GY 5/1
2H-4, 52	18.42	18.9	Greenish brown 10YR 5/2
7H-3, 84	55.24		Light greenish gray 5G 7/1
7H-3, 134	55.74		Pale green 5G 7/2
8H-1, 47	61.37		Pale green 5G 7/2
8H-1, 61	61.51		Pale green 5G 7/2
8H-1, 83	61.73		Pale green 5G 7/2
8H-1, 95	61.85		Pale green 5G 7/2
8H-1, 96	61.86		Pale green 5G 7/2
9H-5, 142	77.82	77.85	Bluish gray 5B 5/1
9H-6, 40	78.30	78.42	Light greenish gray 5GY 7/1
9H-6, 114	79.04	79.13	Light greenish gray 5G 7/1
9H-6, 123	79.13	79.35	Light greenish gray 5G 7/1?
10H-5, 68	86.58	86.59	Light greenish gray 5G 7/1
11H-1, 129	90.69	90.7	Light greenish gray 5G 7/1
11H-2, 109	91.99	92	Light greenish gray 5G 7/1
11H-4, 31	94.21	94.25	Light greenish gray 5G 7/1
11H-5, 89	96.29	96.3	Light greenish gray 5G 7/1
11H-6, 97	97.87		
11H-6, 101	97.91		
11H-6, 104	97.94		
11H-6, 148	98.38	98.385	Light greenish gray 5G 7/1
12H-3, 104	102.94		
12H-3, 109	102.99	103	Light greenish gray 5G 7/1
13H-5, 147	115.87	115.88	Light greenish gray 5G 7/1
13H-7, 23	117.63	117.7	Light greenish gray (5G 7/1) and white
14H-6, 98	126.38		Light greenish gray 5GY 8/1
14H-6, 125.5	126.655	126.66	Light greenish gray 5GY 8/1
14H-6, 133	126.73	126.76	Light greenish gray 5GY 8/1
15H-3, 95	131.35		Pale green 5G 7/2
16H-2, 3	138.43		Pale green 5G 7/2
16H-2, 5	138.45		Pale green 5G 7/2
16H-4, 48	141.88	141.91	Pale green 5G 7/2
16H-5, 149	144.39		Pale green 5G 7/2
16H-6, 16	144.56	144.58	Pale green 5G 7/2
17H-2, 18	148.08		Pale green 5G 7/2
17H-2, 44	148.34		Pale green 5G 7/2
18H-2, 21	157.61		Pale green 5G 7/2
18H-2, 136	158.76		Pale green 5G 7/2
18H-3, 139	160.29		Pale green 5G 7/2
18H-5, 36	162.26		Pale green 5G 7/2
18H-6, 101	164.41		Pale green 5G 7/2
18H-6, 108	164.48		Pale green 5G 7/2

Table T5. Calcareous nannofossil, planktonic and benthic foraminifer, and diatom biostratigraphic events, Hole U1312A.

Core, section, interval (cm)	Zone* (base)	Species event	Depth (mbsf)	Age (Ma)
306-U1312A-				
1H-CC	NN21	FO *Emiliania huxleyi*	14.25	0.25
2H-CC	NN20	LO *Pseudoemiliania lacunosa*	14.25	0.41
3H-CC	NN19	LO *Fragilariopsis reinholdii*	23.75	0.50
3H-CC		LO large *Gephyrocapsa* spp.	23.75	1.21
3H-CC		LO *Helicosphaera sellii*	23.75	1.27
3H-CC		FO large *Gephyrocapsa* spp.	33.25	1.45
4H-CC		FO *Gephyrocapsa caribbeanica*	39.40	1.73
4H-CC	NN18	FO *Globorotalia truncatulinoides*/*Globorotalia inflata*	42.75	2.08
5H-2, 130–131		LO *Discoaster brouweri*	39.40	1.97
5H-5, 125–126	NN17	LO *Discoaster pentaradiatus*	43.025	2.38
5H-5, 125–126	NN16	LO *Discoaster surculus*	43.025	2.54
5H-CC		LO *Globorotalia puncticulata*/*Neogloboquadrina atlantica*	42.75	2.41
6H-CC		LO *Thalassiosira convexa*	52.25	2.40
6H-CC		LO *Discoaster tamalis*	52.25	2.74
6H-CC		Disappearance *Globorotalia hirsuta*	52.25	3.18
10H-CC		Reappearance *Globorotalia puncticulata*	99.75	3.31
12H-CC	NN15	Disappearance *Globorotalia puncticulata*	109.25	3.57
12H-CC		LO *Reticulofenestra pseudoumbilicus*	109.25	3.85
13H-CC	NN12/NN13/ NN14	LcO *Globorotalia margaritae*	118.75	3.98
13H-CC		LO *Amaurolithus primus*	118.75	4.56
14H-CC		FaO *Globorotalia puncticulata*	137.75	4.52
18H-CC	NN11D	LO *Discoaster quinqueramus*	166.25	5.54
17H-CC	NN11C	FaO *Globorotalia margaritae*	166.25	6.00
18H-CC		LO *Amaurolithus amplificus*	166.25	6.00
17H-CC		Coiling change *Neogloboquadrina pachyderma* (s/d)	166.25	6.30
18H-CC	NN11B	FO *Amaurolithus amplificus*	175.75	6.84
18H-CC	NN11A	FcO gr. *Globorotalia miotumida*	175.75	7.24
18H-CC		FO *Amaurolithus primus*	175.75	7.39
19H-CC		LO *Globorotalia menardii* 4	175.75	7.51
19H-CC	NN10B	FO *Discoaster berggrenii*	185.25	8.28
20H-CC		Coiling change *Neogloboquadrina pachyderma* (d/s)	185.25	7.80
20H-CC		FO *Discoaster loeblichii*	194.75	8.43
21H-CC	NN10A	LO *Globorotalia lenguaensis*	194.75	8.99
21H-CC		FO *Minylitha convallis*	204.25	9.43
22H-CC	NN9	LO *Discoaster hamatus*	204.25	9.64
24H-CC	NN8	FO *Discoaster hamatus*	232.75	10.48
25H-CC	NN7	LO *Coccolithus miopelagicus*	232.75	10.95

Notes: Dark blue = nannofossils, pink = foraminifers, light blue = diatoms. For first occurrences (FO), depth is plotted as the midpoint between the depth at which the species was first observed and the depth of the sample below. For last occurrences (LO), depth is plotted as the midpoint between the depth at which the species was last observed and the depth of the sample above. LcO = last common occurrence, FaO = first abundant occurrence, FcO = first common occurrence. d = dextral, s = sinistral. * = from Martini (1971).

Table T6. Calcareous nannofossil, planktonic and benthic foraminifer, diatom, and radiolarian biostratigraphic events, Hole U1312B.

Core, section	Zone* (base)	Species event	Depth* (mbsf)	Age (Ma)
306-U1312B-				
1H-CC	NN21	FO *Emiliania huxleyi*	8.65	0.25
2H-CC	NN20	LO *Pseudoemiliania lacunosa*	8.65	0.41
3H-CC		LO *Fragilariopsis reinholdii*	18.15	0.50
2H-CC	NN19	FO *Gephyrocapsa parallela*	18.15	0.95
4H-CC		LO *Helicosphaera sellii*	27.65	1.27
4H-CC	NN18	FO *Gephyrocapsa caribbeanica*	37.15	1.73
4H-CC		FO *Globorotalia inflata*	37.15	2.08
4H-CC	NN17	LO *Discoaster brouweri*	27.65	1.97
4H-CC	NN16	LO *Discoaster pentaradiatus*	27.65	2.38
4H-CC		FO *Cycladophora davisiana*	37.15	2.59
5H-CC		LO *Discoaster surculus*	37.15	2.54
5H-CC		LO *Globorotalia puncticulata*	37.15	2.41
5H-CC		LO *Discoaster tamalis*	37.15	2.74
7H-CC		LO *Sphaeroidinellopsis seminulina*	56.15	3.19
8H-CC	NN15	Reappearance *Globorotalia puncticulata*	84.65	3.31
12H-CC		Disappearance *Globorotalia puncticulata*	103.65	3.57
13H-CC	NN12/NN13/ NN14	LO *Reticulofenestra pseudoumbilicus*	113.15	3.85
13H-CC		LcO *Globorotalia margaritae*	113.15	3.98
14H-CC		FaO *Globorotalia puncticulata/Globorotalia crassaformis*	132.15	4.52
15H-CC		LO *Amaurolithus primus*	132.15	4.56
19H-CC	NN11D	LO *Discoaster quinqueramus*	170.15	5.54
18H-CC		FaO *Globorotalia margaritae*	170.15	6.00
19H-CC	NN11C	Coiling change *Neogloboquadrina pachyderma* (s/d)	170.15	6.30
19H-CC	NN11A	FO *Amaurolithus primus*	179.65	7.39
20H-CC		FcO gr. *Globorotalia miotumida*	179.65	7.24
20H-CC	NN10B	LO *Globorotalia menardii* 4	179.65	7.51
20H-CC		Coiling change *Neogloboquadrina pachyderma* (d/s)	179.65	7.80
20H-CC		FO *Discoaster berggrenii*	189.15	8.28
20H-CC		FO *Discoaster loeblichii*	189.15	8.43
22H-CC	NN10A	LO *Globorotalia lenguaensis*	198.65	8.99
21H-CC		FO *Minylitha convallis*	198.65	9.43
22H-CC	NN9	LO *Discoaster hamatus*	198.65	9.64
24H-CC	NN8	FO *Discoaster hamatus*	227.15	10.48
25H-CC		FcO *Neogloboquadrina pachyderma* morphotype *acostaensis*	227.15	10.50
25H-CC	NN7	LO *Coccolithus miopelagicus*	227.15	10.95

Notes: Dark blue = nannofossils, pink = foraminifers, light blue = diatoms, orange = radiolarians. For first occurrences (FO), depth is plotted as the midpoint between the depth at which the species was first observed and the depth of the sample below. For last occurrences (LO), depth is plotted as the midpoint between the depth at which the species was last observed and the depth of the sample above. FaO = first abundant occurrence, FcO = first common occurrence, LcO = last common occurrence. d = dextral, s = sinistral. * = from Martini (1971).

Table T7. Distribution of calcareous nannofossils, Hole U1312A. (Continued on next page.)

Core, section, interval (cm)	Martini (1971) Zone (base)	Age (Ma)	Abundance	Preservation	*Amaurolithus amplificus*	*Amaurolithus delicatus*	*Amaurolithus primus*	*Amaurolithus tricorniculatus*	*Braarudosphaera discula*	*Calcidiscus leptoporus*	*Calcidiscus macintyrei*	*Calcidiscus tropicus*	*Calciosolenia fossilis*	*Ceratolithus cristatus*	*Ceratolithus rugosus*	*Ceratolithus* spp.	*Coccolithus braarudii*	*Coccolithus miopelagicus*	*Coccolithus pelagicus*	*Cryptococcolithus mediaperforatus*	*Cyclicargolithus floridanus*	*Discoaster asymmetricus*	*Discoaster bellus*	*Discoaster berggrenii*	*Discoaster brouweri*	*Discoaster* cf. *exilis*	*Discoaster hamatus*	*Discoaster loeblichii*	*Discoaster neohamatus*	*Discoaster neorectus*	*Discoaster pentaradiatus*	*Discoaster quinqueramus*	*Discoaster surculus*	*Discoaster tamalis*	*Discoaster triradiatus*	*Discoaster variabilis*	*Discoaster variabilis* (3, 5, or 7 ray)	*Ellipsolithus macellus*	*Emiliania huxleyi*	*Gephyrocapsa aperta*	*Gephyrocapsa caribbeanica*	*Gephyrocapsa oceanica*	*Gephyrocapsa parallela*
306-U1312A-																																									
1H-CC	NN21	0.41	V	G															R																		R		R		
2H-CC			V	G															R																			p	C			
3H-CC	NN19		V	G																																			p			
4H-CC		1.97	V	G–M							F	F					R		C																			F	R		
5H-2, 130–131	NN18	2.54	V	G						C	C	F					p		C						F									R			A				
5H-5, 125–126			V	G						F	F	F	R				F		C						F					F		R			R			A				
5H-CC			V	G–M						F	F	F							C						F					R		F						A				
6H-CC			V	G–M					R	p	F	C							C						R					F		F	R					C				
7H-CC	NN16		V	G–M						F	F	C							C						F					F		F	R	R								
8H-CC			V	G–M						p	C	F							C						F							p		R								
9H-CC			V	G–M						C	F	C				R	F		A						F					F		F	R	R	p							
10H-CC			V	G–M						C	C	p		R					C			R			F					F		C	R	R								
11H-CC		3.85	V	G–M						F	C	F	p		R				C			F			F					F		F	C	F	R							
12H-CC	NN15	4.56	V	G–M		?				C	C	C			R				F			F			F					R		F	R	R	R							
13H-CC			V	G–M		R	R			C	C	C							C			F			F					C		C			F							
14H-CC	NN12/NN13/ NN14		V	G–M			F			C	F	F		R					A						R					C					C							
15H-CC			V	G–M			F		R	F	C								C						F					F		R			F							
16H-CC			V	G–M			F			F	F								C						F					C					F							
17H-CC			V	G–M		R	R			C	C								C						F					C		F		R	C	F						
18H-CC	NN11C	6.00 6.84	V	G–M	R	F	F			F	F								C					F	R					R	R	R			F	R						
19H-3, 81–82			V	M				?		C	C	C							A	p		?		F	C			R	F	R	F			R	A	F					
19H-5, 2–3	NN11B		V	M						C	F	C							A	F				F	F			F	F		F	R		R	C	F					
19H-6, 99–100			V	G–M						C	F	F						*	A	F	*			F	F			F	p		F			p	C	F					
19H-CC	NN11A	7.39	V	M						C	R								A			R		F	F			C		F	F				C	F					
20H-CC	NN10B	8.2	V	G–M						C	C	F							A	F			R	F	F			F	R			R			C	F					
21H-CC	NN10A	8.79	V	M						F	C	C							A				R	C	C							R		R	C	R					
22H-CC		9.64	V	M						F	F	C							A	F			p	p	p		F		p													
23H-CC	NN9		V	M							F	C							C	R					F		R		F						C	R					
24H-CC		10.95	V	M						R	F	C							C	R				F	F	p	R		F						C	R					
25H-CC	NN7		V	M							C	C						R	C				R	F	F										C	R	*					

Notes: Abundance: V = very abundant, A = abundant, C = common, F = few, R = rare, p = present, ? = questionable, * = reworked. Preservation: G = good, M = moderate. See "Calcareous nannofossils" in the "Site U1312–U1315 methods" chapter. FO = first occurrence, LO = last occurrence.

Table T7 (continued).

Core, section, interval (cm)	Martini (1971) Zone (base)	Age (Ma)	Abundance	Preservation	Large *Gephyrocapsa* spp.	*Helicosphaera carteri*	*Helicosphaera granulata*	*Helicosphaera inversa*	*Helicosphaera sellii*	*Lithostromation perdurum*	*Minylitha convallis*	*Pontosphaera* spp.	*Pseudoemiliania lacunosa*	*Reticulofenestra asanoi*	*Reticulofenestra pseudoumbilicus*	*Reticulofenestra pseudoumbilicus* (5–7 µm)	*Reticulofenestra productella*	*Reticulofenestra rotaria*	*Reticulofenestra* spp. (<3 µm)	*Reticulofenestra* spp. (3–5 µm)	*Rhabdosphaera clavigera*	*Scyphosphaera* spp.	*Sphenolithus abies*	*Syracosphaera* spp.	*Thoracosphaera* spp.	*Triquetrohabdulus rugosus*	*Umbilicosphaera rotula*	*Umbilicosphaera sibogae*	Event
306-U1312A-																													
1H-CC	NN21	0.41	V	G		R		F									A				R								FO *E. huxleyi*
2H-CC			V	G		C						C	A	F														C	LO *P. lacunosa*
3H-CC	NN19		V	G	F				F				A																Large *Gephyrocapsa* spp., LO *H. sellii*
4H-CC		1.97	V	G–M		p			F			F	A								F							p	FO *G. caribbeanica*
5H-2, 130–131	NN18	2.54	V	G		C			F			F	A								F	R		C	R				LO *D. brouweri*
5H-5, 125–126			V	G		F			F	R		F	A						A	F	F			C					LO *D. pentaradiatus, D. surculus*
5H-CC			V	G–M		C			F			F	C					p	A					F	R				
6H-CC			V	G–M		F			R			F	F			C			A									p	LO *D. tamalis*
7H-CC	NN16		V	G–M		F			F			F	C		*	C			A	A	F	F	*						
8H-CC			V	G–M		F			p			F	C			p				A	p								
9H-CC			V	G–M		C			F			F	F		*	F			A	A	C	F	*		R			F	
10H-CC			V	G–M					F	R		C							A	A	p	F			R			p	
11H-CC		3.85	V	G–M		F			R			F	F			C			A	A		C	*						
12H-CC	NN15	4.56	V	G–M		C			F	R		F	F		C	F			A	A		F	F	C				F	LO *R. pseudoumbilicus*
13H-CC			V	G–M		F				R		p			A	p			A	A		F	C		R			F	LO *A. primus*
14H-CC	NN12/NN13/ NN14		V	G–M		F									A				A	A			F						
15H-CC			V	G–M		F			R						C	C			A	C		C	F						
16H-CC			V	G–M		R			R						C	F			A	A			C						
17H-CC			V	G–M		F									C				A	A			C						
18H-CC	NN11C	6.00 6.84	V	G–M		R									C	F			C	A			C			R			LO *D. quinqueramus, A. amplificus*; FO *A. primus*
19H-3, 81–82			V	M			R								C	A			A	A			C				p		
19H-5, 2–3	NN11B		V	M			F				p				C	C			A	A			F				p		
19H-6, 99–100			V	G–M							C				C	C			A	C			F		R		R		
19H-CC	NN11A	7.39	V	M		F	R				F					A			A	F			F						FO *D. berggrenii*
20H-CC	NN10B	8.2	V	G–M		F	F				C				F	A		R		A			C				F		FO *D. loeblichii*
21H-CC	NN10A	8.79	V	M		R	R				C				A	A		R		F			C				F		FO *M. convallis*
22H-CC		9.64	V	M			F		R		?				C	A		F		F			C				p		LO *D. hamatus*
23H-CC	NN9		V	M		F	R								A	A				F			A		R		F		
24H-CC			V	M		F	F								A	A				F			A				p		FO *D. neohamatus, D. hamatus*
25H-CC	NN7	10.95	V	M			R								A	A				F			C		R		R		LO *C. miopelagicus*

Table T8. Distribution of calcareous nannofossils, Hole U1312B. (Continued on next page.)

Core, section	Martini (1971) Zone (base)	Age (Ma)	Abundance	Preservation	*Amaurolithus delicatus*	*Amaurolithus ninae*	*Amaurolithus primus*	*Amaurolithus tricorniculatus*	*Calcidiscus leptoporus*	*Calcidiscus macintyrei*	*Calcidiscus tropicus*	*Catinaster calyculus*	*Ceratolithus cristatus*	*Ceratolithus* spp.	*Coccolithus braarudii*	*Coccolithus miopelagicus*	*Coccolithus pelagicus*	*Cryptococcolithus mediaperforatus*	*Discoaster asymmetricus*	*Discoaster bellus*	*Discoaster berggrenii*	*Discoaster brouweri*	*Discoaster* cf. *exilis*	*Discoaster hamatus*	*Discoaster loeblichii*	*Discoaster neohamatus*	*Discoaster pentaradiatus*	*Discoaster quinqueramus*	*Discoaster surculus*	*Discoaster tamalis*	*Discoaster triradiatus*	*Discoaster variabilis*	*Discoaster variabilis* (3, 5, or 7 ray)	*Emiliania huxleyi*	*Gephyrocapsa aperta*	*Gephyrocapsa caribbeanica*	*Gephyrocapsa oceanica*	*Gephyrocapsa parallela*	Large *Gephyrocapsa* spp.	*Helicosphaera carteri*	*Helicosphaera granulata*	*Helicosphaera inversa*	*Helicosphaera sellii*	*Minylitha convallis*
306-1312B-																																											
1H-CC	NN21	0.41	V	G					A						C		F																A										
2H-CC	NN19		A	G					C						F		C																A										
3H-CC		2.38	V	G–M					C								C																											
4H-CC	NN17	2.74	V	G–M					C	F							C					R				R					R				R	R			F		R		
5H-CC	NN16		V	G–M					C	F							C					R				F		F	R		R							F		R		
6H-CC			V	G–M					F	F							C					R				F					R							F		R		
7H-CC			V	G–M					C	F							C					R				R		R	R		R							R		R		
8H-CC			V	G–M					C	C							C					F				F		R	R		C							C		F		
9H-CC			V	G–M					C	C							A		R			F				F					F							F		R		
10H-CC			V	G–M					C	C							C		R			R				F		R	R		F							F		R		
11H-CC			V	G–M					C	R							C		R			F				F			F		F							F		F		
12H-CC			V	G–M					C	F							F		F			F				F			F		F							C		R		
13H-CC	NN15	3.85	V	G–M					A	F				p			C					F				C					F							C				
14H-CC			V	G–M					C	F			R				C					F				C					R							C				
15H-CC		4.56	V	G–M			F		C	R							C					F				R					F							F				
16H-CC	NN12/NN13/ NN14		V	G–M			F	F	C	F			R				C					R				F					F							F				
17H-CC			V	G–M	R				C	F	C						C		F			F				C				R	C	R					R	F				
18H-CC			V	M	F	R	F		F	F	C			?			C					F				F	?			R	C	R					F	F				
19H-CC	NN11D	5.54	V	G–M			F		C	F	C						C	F			F	F				F	F	R			C	R						F				
20H-CC	NN11A	7.39	V	G–M					C		C						A	C			F	F			F	F					R	C	R					R	F			C	
21H-CC	NN10A	8.28	V	G–M					C		C						C	C		R		F				F					R	C	R						F			C	
22H-CC	NN9	9.64	V	G–M					F	C	C						A	C				F				p					F	C	R						F				
23H-CC			V	G–M						C	A	R					C	F				F				R						C	F										
24H-1, top			V	G–M					F	C	A	?					A					R	R	R								C						R					
24H-CC		10.95	V	G–M					F	C	C	R					A	C				F	F	R								C	R						F				
25H-CC	NN7		V	G–M					F	C	C					R	A					R	F									C	R						F				

Notes: Abundance: V = very abundant, A = abundant, C = common, F = few, R = rare, p = present, ? = questionable, * = reworked. Preservation: G = good, M = moderate. See **"Calcareous nannofossils"** in the "Site U1312–U1315 methods" chapter. FO = first occurrence, LO = last occurrence.

Table T8 (continued).

Core, section	Martini (1971) Zone (base)	Age (Ma)	Abundance	Preservation	*Pontosphaera* spp.	*Pseudoemiliania lacunosa*	*Pyrocyclus* spp.	*Reticulofenestra asanoi*	*Reticulofenestra productella*	*Reticulofenestra pseudoumbilicus*	*Reticulofenestra pseudoumbilicus* (5–7 µm)	*Reticulofenestra rotaria*	*Reticulofenestra* spp. (<3 µm)	*Reticulofenestra* spp. (3–5 µm)	*Reticulofenestra umbilicus*	*Rhabdosphaera clavigera*	*Scyphosphaera* spp.	*Sphenolithus abies*	*Syracosphaera* spp.	*Thoracosphaera* spp.	*Triquetrorhabdulus rugosus*	*Umbilicosphaera rotula*	*Umbilicosphaera sibogae*	Event
306-1312B-																								
1H-CC	NN21	0.41	V	G	R											C			C	R			p	FO *E. huxleyi*
2H-CC	NN19		A	G	F	A		F					C			F			F	R			R	LO *P. lacunosa*, FO *G. parallela*
3H-CC		2.38	V	G–M	R			R	C				C											
4H-CC	NN17	2.74	V	G–M	F	F			C				C			R	F		R					FO *H. sellii, G. caribbeanica;* LO *D. brouweri, D. pentaradiatus*
5H-CC			V	G–M		F			C	*			A											LO *D. surculus, D. tamalis*
6H-CC			V	G–M		F			F	*			A			R								
7H-CC			V	G–M	R	R							A			R								
8H-CC	NN16		V	G–M							R		A	A		R	F							
9H-CC			V	G–M	R								A	A		R	F							
10H-CC			V	G–M							R		A	A		R	C							
11H-CC			V	G–M	R						C		A	A		R	C							
12H-CC		3.85	V	G–M							R		A	A		R	C							
13H-CC	NN15		V	G–M						C	R		A	A		R	C							LO *R. pseudoumbilicus*
14H-CC		4.56	V	G–M	R					A	C		A			R	F							
15H-CC			V	G–M						C	C		A				F							LO *A. primus*
16H-CC	NN12/NN13/ NN14		V	G–M						C	C		A	A		R	F							
17H-CC			V	G–M	R		F			A	A		A	A			F	C		R		F		
18H-CC			V	M			F			C	A		A	A			R	C		R		F		
19H-CC	NN11D	5.54	V	G–M						C	A		A	A				C				F		LO *D. quinqueramus*, FO *A. primus*
20H-CC	NN11A	7.39	V	G–M						R	C			A				F		R		F		FO *D. berggrenii, D. loeblichii*
21H-CC	NN10A	8.28	V	G–M	R		p			A	C		C					C				C		FO *M. convallis*
22H-CC	NN9	9.64	V	G–M			C			A	A			C				A			R	F		LO *D. hamatus*
23H-CC			V	G–M			F			A	A	F	F	F				A		F		F		LO *C. calyculus*
24H-1, top			V	G–M	R					A	A		F											
24H-CC		10.95	V	G–M	R		C			A	A		F					A				F		FO *D. neohamatus, D. hamatus, C. calyculus*
25H-CC	NN7		V	G–M			F			A	A			C	*			C		R		F		LO *C. miopelagicus*

Table T9. Distribution of planktonic foraminifers, Hole U1312A. (Continued on next page.)

Core, section	Abundance	Preservation	Fill level in PF vial before splitting (mm)	*Globigerinella aequilateralis*	*Globigerinella bulloides*	*Globigerinoides conglobatus*	*Globigerina falconensis*	*Globigerinella calida*	*Globigerina apertura/decoraperta*	*Globigerina nepenthes*	*Globigerinita glutinata*	*Pulleniatina obliquiloculata*	*Neogloboquadrina pachyderma* (d)	*Neogloboquadrina pachyderma* (s)	*Neogloboquadrina humerosa*	*Neogloboquadrina dutertrei*	*Neogloboquadrina atlantica* (s)	*Neogloboquadrina atlantica* (d)	*Neogloboquadrina continuosa*	*Turborotalita quinqueloba*	*Globigerinoides ruber* white/pink	*Globigerinoides trilobus* group	*Globigerinoides obliquus extremus*	*Orbulina universa*	*Globorotalia scitula* (s)	*Globorotalia scitula* (d)	*Globorotalia hirsuta*	*Globorotalia inflata*	*Globorotalia crassaformis*	*Globorotalia crassula*	*Globorotalia menardii* group (d)	*Globorotalia menardii* group (s)	*Globorotalia truncatulinoides* (s)	*Globorotalia truncatulinoides* (d)	*Globorotalia puncticulata*	*Globorotalia margaritae*	*Globorotalia conomiozea/miotumida* group	*Sphaeroidinellopsis seminulina*
306-U1312A-																																						
1H-2	D	M	10	R	D						C		A	F		F				C	F			C			R	A	R			C	C				
1H-CC	D	G	26	C	C		F				A	F	A								C/R	R		R		C		A	A			A	C					
2H-CC	D	M	39	A	C						F		A	A						C	R			C		C		A	F		F		F	F				
3H-CC	D	G	35	A	C	R					C		A	C						F	F	R				C		A	R				R	R				
4H-CC	D	M	44	A	R						F		A							C	C			A		A		A	A				R					
5H-CC	D	G	25	F	A						C		C				R	C		C	C	F	R			C			D					F				
6H-CC	D	G	25	A	A						A		A							F	C	F	F	A		C	R		A	R				C				
7H-CC	D		25	F	A	R					R		C				R			F	R		F	C		C	R		A	R				C				
8H-CC	D		32	C	A			R			F		A								F		R	C		F	R		A	R				C				
9H-CC	D		23	C	A			R			F		A							R	R	R	F	F		F	R		C	R				C				
10H-CC	D		20	R	A			R	R		R		A							F	R	R		F		F	R		A	R				A				
11H-CC	D	G	15	C	A		R		F		C		A				R			F	C	F	R	F		C	F		C	F								R
12H-CC	D	G	21	F	A						F		A							F		C	R	F		F	A		F	A				A				R
13H-CC	D	G	23	R	D		R	R	F		F	A	R							R	R	F	R			R								F	A			R
14H-CC	D	G	16		A				C		R		A	R						R	R		F	R	R	F	R			R				F	A			R
15H-CC	D	G	13	R	A				F		C		A									R		F		C									A			
16H-CC	D	G	13		C	R			F		F		A	R						R			C	F		F									A			
17H-CC	D	M	18		A				C	R	F		C	R						R		R		R		C									C			
18H-CC	D	P	3		C				A	F			R	C												R										C	C	
19H-CC	D	M	9		A				F	F	F		C	R	F							R	F	C		R					A						F
20H-CC	D	G	29		A	R			F				C	C	C							F	F	F	C	F					A							
21H-CC	D	G	24	R	A				C	F	C		F	F		R					C	R	F	R	A	R				R	A						F
22H-CC	D	G	15		A						C		A	R					R				R	F	C	R					C							
23H-CC	D		14		A						C		D	R	R				R	R	C		R		R	F					C							
24H-CC	D	M	12	R	F					A	F		A	R			R		F			R			F	F					C							
25H-CC	D	M	9						R	C	C		C	C				A	R						R	R					C							

Notes: Abundance: D = dominant, A = abundant, C = common, F = few, R = rare. Preservation: G = good, M = moderate, P = poor. See **"Foraminifers"** in the "Site U1312–U1315 methods" chapter. PF = planktonic foraminifers. d = dextral, s = sinistral. P in ostracodes column = presence of valves. IRD = ice-rafted debris, FO = first occurrence, FaO = first abundant occurrence, LO = last occurrence, LcO = last common occurrence.

Table T9 (continued).

Core, section	Abundance	Preservation	Fill level in PF vial before splitting (mm)	*Globoquadrina dehiscens*	*Globoquadrina altispira*	*Globorotalia lenguaensis*	*Globigerinoides bulloideus*	*Catapsydrax parvulus*	Ostracodes	Other species and observations	Stratigraphic event
306-U1312A-											
1H-2S	D	M	10						P	IRD; *Globigerinoides tenellus*	
1H-CC	D	G	26						P	Some IRD; *Globigerina rubescens, Globorotalia tumida*	
2H-CC	D	M	39						P	Some IRD	
3H-CC	D	G	35						P		
4H-CC	D	M	44						P		FO *G. truncatulinoides/G. inflata (*2.08 Ma)
5H-CC	D	G	25						P		LO *G. punticulata/N. atlantica* (2.41 Ma)
6H-CC	D	G	25						P	*Globigerina umbilicata*	Disappearance *G. hirsuta* (3.18 Ma)
7H-CC	D		25						P		
8H-CC	D		32						P		
9H-CC	D		23						P		
10H-CC	D		20						P		Reappearance *G. puncticulata (*3.31 Ma)
11H-CC	D	G	15						P		?LO *S. seminulina* (3.19 Ma)
12H-CC	D	G	21						P	*G. miocenica, G. menardii*	Disappearance *G. puncticulata* (3.57 Ma)
13H-CC	D	G	23						P		LcO *G. margaritae (*3.98 Ma)
14H-CC	D	G	16						P		FaO *G. puncticulata* (4.52 Ma)
15H-CC	D	G	13						P		
16H-CC	D	G	13						P	*N. pachyderma* 37d/3s	
17H-CC	D	M	18						P	*G. margaritae primitiva*	FaO *G. margaritae* (6.0 Ma)
18H-CC	D	P	3							*N. pachyderma* 4d/23s. *G. miotumida, G. apertura, Sphaeroidinellopsis* encrusted	s/d coiling *N. pachyderma* (6.3 Ma), FcO *G. miotumida* group (7.24 Ma)
19H-CC	D	M	9					R		*N. pachyderma* 0d/18s	LcO *G. menardii* 4 (7.51 Ma)
20H-CC	D	G	29						P	*N. pachyderma* 12d/13s	d/s *N. pachyderma* (7.8 Ma)
21H-CC	D	G	24	C		R	F		P	*N. pachyderma* 13d/12s	LO *G. lenguaensis (*8.99 Ma)
22H-CC	D	G	15	R					P	*N. pachyderma* 40d/5s	
23H-CC	D		14			F	R	R	P	*N. pachyderma* 33d/1s	
24H-CC	D	M	12		R	R	R		P	nearly completely d coiling *Neogloboquadrina*	FO *N. pachyderma* (*acostaensis* morphotype) (10.5 Ma)
25H-CC	D	M	9	A	A					d/s ± equal, no *N. acostaensis*	Younger than 11.2 Ma (= LO *N. mayeri*) and 11.6 Ma (= FO *G. nepenthes*)

Table T10. Distribution of planktonic foraminifers, Hole U1312B. (Continued on next page.)

Core, section	Abundance	Preservation	Fill level in PF vial before splitting (mm)	*Globigerinella aequilateralis*	*Globigerina bulloides*	*Globigerinoides conglobatus*	*Globigerina falconensis*	*Globigerinella calida*	*Globigerina apertura/decoraperta*	*Globigerina nepenthes*	*Globigerinita glutinata*	*Pulleniatina obliquiloculata*	*Neogloboquadrina pachyderma* (d)	*Neogloboquadrina pachyderma* (s)	*Neogloboquadrina humerosa*	*Neogloboquadrina dutertrei*	*Neogloboquadrina atlantica* (s)	*Neogloboquadrina atlantica* (d)	*Neogloboquadrina continuosa*	*Turborotalita quinqueloba*	*Globigerinoides ruber* white/pink	*Globigerinoides trilobus* group	*Globigerinoides obliquus extremus*	*Orbulina universa*	*Globorotalia scitula* (s)	*Globorotalia scitula* (d)	*Globorotalia hirsuta*	*Globorotalia inflata*	*Globorotalia crassaformis*	*Globorotalia crassula*	*Globorotalia menardii* group (d)	*Globorotalia menardii* group (s)	*Globorotalia truncatulinoides* (s)	*Globorotalia truncatulinoides* (d)	*Globorotalia puncticulata*	*Globorotalia margaritae*	*Globorotalia conomiozea/miotumida* group	*Sphaeroidinellopsis seminulina*
306-U1312B-																																						
1H, top	D	G		R	A	R	F	R			F		A	R		R				C	C/R	R		R	C	C	R	A			R		F	F				
1H-CC	D	G	43	R	A		R				F		A	R		R				A	F			R		C		A	R		R		R	F				
2H-CC	D	G	42		A						C		A	F						A	R					F		A	F					F				
3H-CC	D	G	39	R	A						C		A							F	C					C	F	A	C				R	C				
4H-CC	D	G	8	C	A						C		A	F						F	F			F	R	F		A	R									
5H-CC	D	G	25	F	A		R				C		A	R		R				C				F		C	R		F						R			
6H-CC	D	G	25	R	A						C		A	R						C	F			C		F			A	R					R			
7H-CC	D	G	26	F	A	R					F		A	R			R			C	F	F		F		F			A						C			R
8H-CC	D	G	21	F	A		C	R	F		A		F	R						A	R		R	F		F			C						A			
9H-CC	D	G	26	F	A				R		C		A	R			R			C	R		R	F		F			A									
10H-CC	D	G	20	R	A		F	R	R		C		C							C				R		R			A	R					A			
11H-CC	D	G	18	A	A	R	F				R		A	F						F	C	F		C		F												R
12H-CC	D	G	11		A		F		R		C		C							C	R	R		R		A			A						C			C
13H-CC	D	G	23	R	A				C		A		C							F	F	R	R	R		F			C						A	F		
14H-CC	D	G	22	R	A			R	F		C		C							C					F	R			A						A	C		R
15H-CC	D	G	18		A	R		R	A		F		A							R			F	C	R	A										C		
16H-CC	D	G	13	R	A	R			F	R	R		A	F	R		F						C	F	C										R	F	F	
17H-CC	D	M	15		A	R	R		F	R	F		A	R				A		R			C	F	C											C	R	
18H-CC	D	M	9		A		R		R	R	R		A	A			F	F		R			F		F											F		
19H-CC	D	P	5		F				R	F	R		C	A									F	C													A	F
20H-CC	D	M	28		A				F	F	R		A	A	R					R				R	F	F						A						
21H-CC	D	G	26		F				F	F	R		C	C	F						F	F	C	C	F	R					R	C						R
22H-CC	D	G	20		C					R			A	R					F		R	F			C	F						C						F
23H-CC	D	P	4		F				F	R			A						F						F							C						F
24H-CC	D	P	10		F					F	A		A	R								F			F	F						R						F
25H-CC	D	P	8		C				C		A		C	R				A	F					R	R	F						A						A

Notes: Abundance: D = dominant, A = abundant, C = common, F = few, R = rare. Preservation: G = good, M = moderate, P = poor. See **"Foraminifers"** in the "Site U1312–U1315 methods" chapter. PF = planktonic foraminifers. d = dextral, s = sinistral. P in ostracodes column = presence of valves. IRD = ice-rafted debris, FO = first occurrence, FaO = first abundant occurrence, LO = last occurrence, LcO = last common occurrence.

Table T10 (continued).

Core, section	Abundance	Preservation	Fill level in PF vial before splitting (mm)	*Globoquadrina dehiscens*	*Globoquadrina altispira*	*Globorotalia lenguaensis*	*Globigerinoides bulloideus*	*Catapsydrax parvulus*	*Ostracodes*	Other species and observations	Stratigraphic event
306-U1312B-											
1H, top	D	G							P	Only fraction >150 µm available	
1H-CC	D	G	43						P	IRD	
2H-CC	D	G	42							IRD	
3H-CC	D	G	39						P		FO *G. truncatulinoides*
4H-CC	D	G	8						P		FO *G. inflata* (2.09 Ma)
5H-CC	D	G	25						P		LO *G. puncticulata* (2.41 Ma)
6H-CC	D	G	25								
7H-CC	D	G	26								LO *S. seminulina* (3.19 Ma)
8H-CC	D	G	21								Reappearance *G. puncticulata* (3.31 Ma)
9H-CC	D	G	26						P		
10H-CC	D	G	20						P		
11H-CC	D	G	18								
12H-CC	D	G	11		R						Disappearance *G. puncticulata* (3.57 Ma)
13H-CC	D	G	23								LcO *G. margaritae* (3.98 Ma)
14H-CC	D	G	22								FaO *G. puncticulata/G. crassaformis* (4.52 Ma)
15H-CC	D	G	18								
16H-CC	D	G	13						P	*Sphaeroidinellopsis subdehiscens, Globigerinoides obliquus obliquus* F, *N. pachyderma* 20d/10s	
17H-CC	D	M	15					R	P	Big, heavily encrusted *N. pachyderma*	
18H-CC	D	M	9							*N. pachyderma* 13d/28s; *N. acostaensis* (d)	FaO *G. margaritae* (6.0 Ma)
19H-CC	D	P	5							*N. pachyderma* 2d/40s; *N. acostaensis* (d + s)	s/d coiling *N. pachyderma* (6.3 Ma); FcO group *G. miotumida* (7.24 Ma)
20H-CC	D	M	28			R		R	P	*N. pachyderma* 10d/32s; *N. acostaensis* (d)	LcO *G. menardii* (4 7.51 Ma)
21H-CC	D	G	26	C	R			R		*N. pachyderma* 13d/22s	d/s *N. pachyderma* (7.8 Ma)
22H-CC	D	G	20	F	F	F				*N. pachyderma* 30d/2s	LO *G. lenguaensis* (8.99 Ma)
23H-CC	D	P	4	F						No *Neogloboquadrina* sp. (s)	
24H-CC	D	P	10	F		F			P	*N. pachyderma* 38d/2s; few lithic grains	FO *N. pachyderma* (*acostaensis* morphotype) (10.5 Ma)
25H-CC	D	P	8							*Globoquadrina* spp. common	Younger than 11.2 Ma (= LO *N. mayeri*) and 11.6 Ma (= FO *G. nepenthes*)

Table T11. Distribution of benthic foraminifers, Hole U1312A.

Core, section	Agglutinated species				Calcareous species																																															
	Eggerelloides bradyi	*Martinottiella comminis*	*Sigmoilopsis schlumbergeri*	*Siphotextularia* sp.	*Astrononion stelligerum*	*Burseolina minuta*	*Cibicidoides kullenbergi*	*Cibicidoides* sp.	*Cibicidoides wuellerstorfi*	*Elphidium* sp.	*Ehrenbergina* sp.	*Epistominella exigua*	*Fissurina* spp.	*Globocassidulina crassa*	*Globocassidulina subglobosa*	*Gyroidina altiformis*	*Gyroidina orbicularis*	*Gyroidina* sp.	*Hoeglundina elegans*	*Islandiella* sp.	*Lagena* spp.	*Laticarinina halophora*	*Nodosaria* spp.	*Melonis barleeanus*	*Melonis pacificus*	*Melonis pompilioides*	*Nodosaria* sp.	*Nonion* sp.	*Nuttalides umboniferus*	*Oolina* sp.	*Oridorsalis umbonatus*	*Pleurostomella alternans*	*Pleurostomella rapa*	*Pullenia bulloides*	*Pullenia quinqueloba*	*Pyrgo lucernula*	*Pyrgo murrhyna*	*Pyrgo* sp.	*Quinqueloculina lamarckiana*	*Quinqueloculina seminula*	*Quinqueloculina* spp.	*Stainforthia* sp.	*Uvigerina interrupta*	*Uvigerina peregrina*	*Uvigerina proboscidea*	*Uvigerina segundoensis*	*Uvigerina* sp.	*Sphaeroidina bulloides*	*Spiroloculina* sp.	*Stilostomella lepidula*	*Stilostomella* sp.	*Triloculina tricarinata*
306-U1312A-																																																				
1H-CC	P		R						A			R	P			P	P	P									P		R		A								C	R	P		P		P							
2H-CC	F						F		F			R	P			P					P		P	A							C			C			A		F					R	R							
3H-CC				F			R		F			R									F			F			P				A			F					P	P												
4H-CC	F				P		C		C				P		F		P									C					C			C	C				P	P										P		P
5H-CC	F								C			F	P		C						P					F			F		C								P													
6H-CC							F		C			F	F		C	P													F		A						F		P	P				F								
7H-CC	F	P	P	P	F		F		F				P		C	F							P			C			F		C	F		C			P													P		
8H-CC	F				C		F		A			F			A	C	F									F					C			F			P															
9H-CC	P				C		F		F						F							R		P		R			F		C			C																		
10H-CC	P								F						F											R					C			C			P		P	R					P							
11H-CC	P				F		P						F		R							P		P					P		A													P	P							
12H-CC	P				F		R		F		P		F		F								R	R					F		C			F		F	P															
13H-CC				P	C		F		F		R		F		F	P							R			F			C		C			F	R										P							
14H-CC	P				R		F		F				P					R													A			R						P									P			
15H-CC					R				R		R				F		R	R			R	P							R		F			F	P					P				R								
16H-CC	P				F		R		R			P	R		R	P	R						R						C								P			P						R				P		
17H-CC					R		F		F		R	P	R		F	R	R						P						C		C											P			C	P			R			
18H-CC					C		C		F				R		R	F													F		F	C		F																		
19H-CC				P	A				C				R				F					R	R						C		F			C	R															P	P	
20H-CC		P		P	A		R		P				R					P			P								R		A		P	F	F					P						P				P	P	
21H-CC					A		R		C				P		R		R					P		R					R	P	F			R	F											P				P	P	
22H-CC	P				C		F		C			C	P		F							P	P								C			C	R															P	P	
23H-CC				P	C		R		C			R	R		C	P		P			P		R				R				C			R												R				P		
24H-CC		P			A							R	R			R						R									C	P		A	R											P				P		
25H-CC	F				P		F		A			R	R		F	R		F				P	R								F			F	F																	

Notes: A = abundant, C = common, F = few, R = rare, P = present. See "Foraminifers" in the "Site U1312–U1315 methods" chapter.

Table T12. Distribution of benthic foraminifers, Hole U1312B.

	Agglutinated species				Calcareous species																					
Core, section	*Eggerelloides bradyi*	*Martinottiella comminis*	*Sigmoilopsis schlumbergeri*	*Siphotextularia* sp.	*Astrononion stelligerum*	*Burseolina minuta*	*Cibicidoides kullenbergi*	*Cibicidoides* sp.	*Cibicidoides wuellerstorfi*	*Elphidium* sp.	*Ehrenbergina* sp.	*Epistominella exigua*	*Fissurina* spp.	*Globocassidulina crassa*	*Globocassidulina subglobosa*	*Gyroidina altiformis*	*Gyroidina orbicularis*	*Gyroidina* sp.	*Hoeglundina elegans*	*Islandiella* sp.	*Lagena* spp.	*Laticarinina halophora*	*Nodosaria* spp.	*Melonis barleeanus*	*Melonis pacificus*	*Melonis pompiloides*
306-U1312B-																										
1H-CC												P												F		F
2H-CC									F			A	P											C		
3H-CC	R			R					C			P			R	R								P		
4H-CC									C								P						P			P
5H-CC	P			R	F							F		P									P			C
6H-CC	F				F								P	F									P			
7H-CC	P				C			P	P		P				C											
8H-CC	P				P				P			P	R		C	R		P			P		P			
9H-CC					F				F						C								F			F
10H-CC	P			P	C		F		F			F	P		C	F					P	R				
11H-CC	R		R		F		F		C		P	F	F		C	R						R				F
12H-CC	R		P		F		F		R				R		C	R					P					
13H-CC				P	C		P		F		P		R		C								P			
14H-CC	R				F		F		F		VA	P			F							P				
15H-CC	P			P	F		R		P						F			P								F
16H-CC				P	C							C														
17H-CC	R						F					R	R		F	R	R	P				P				P
18H-CC					R		R				P	P				P		F				P				
19H-CC					R		F		F			R	P		F	P										
20H-CC				P	A								R		F	R	P	R					P			R
21H-CC					D		P		R				P		F											
22H-CC					A				F	P			P		F						P					
23H-CC	R				A		R		F						F											
24H-CC	R				A		R		F						F	R		R								
25H-CC	R	P		P	A		R		R			P			C	R	P	R				P	P			R

	Calcareous species (continued)																									
Core, section	*Nodosaria* sp.	*Nonion* sp.	*Nuttallides umboniferus*	*Oolina* sp.	*Oridorsalis umbonatus*	*Pleurostomella alternans*	*Pleurostomella rapa*	*Pullenia bulloides*	*Pullenia quinqueloba*	*Pyrgo lucernula*	*Pyrgo murrhyna*	*Pyrgo* sp.	*Quinqueloculina lamarckiana*	*Quinqueloculina seminula*	*Quinqueloculina* spp.	*Stainforthia* sp.	*Uvigerina interrupta*	*Uvigerina peregrina*	*Uvigerina proboscidea*	*Uvigerina segundoensis*	*Uvigerina* sp.	*Sphaeroidina bulloides*	*Spiroloculina* sp.	*Stilostomella lepidula*	*Stilostomella* sp.	*Troloculina tricarinata*
306-U1312B-																										
1H-CC		P			R			R			R		P	R					D			P	P			R
2H-CC					F			A			F					P										
3H-CC					A			P					C	R												P
4H-CC					C					R	P			P					R	A						
5H-CC			F		A			F		P	P		P													
6H-CC			F		F			F																		
7H-CC			F		C			R		R			R					P				P		P		
8H-CC					A			F																		
9H-CC	P				F																	P				
10H-CC			F		F			F			R			P												
11H-CC			F		C					R								P					P	P	P	
12H-CC			F		C									P										P		
13H-CC			R	P	F		P																			
14H-CC			F		C			R												P				P		
15H-CC					R			R											R	P					P	
16H-CC			F		R			R																P	P	
17H-CC					F			C		P	P			R				R								
18H-CC			F		C			F						R				A								
19H-CC			R		F			A															P	P	P	
20H-CC			F		F	R		C	F																	
21H-CC					P			F	R															P	P	
22H-CC			P					R	F								P									
23H-CC			R		R			R	R																P	
24H-CC					C																					
25H-CC			P		R			R												P					P	

Notes: D = dominant, VA = very abundant, A = abundant, C = common, F = few, R = rare, P = present. See **"Foraminifers"** in the "Site U1312–U1315 methods" chapter.

Table T13. Distribution of diatoms, Hole U1312A.

Core, section	Abundance: Processed	Abundance: Raw	Preservation	Transects	*Actinocyclus ingens*	*Actinocyclus marginatus*	*Alveus marinus*	*Alveus marinus* fragments	*Chaetoceros* resting spores	*Coscinodiscus nodulifera*	*Coscinodiscus radiatus*	*Denticula* spp.	*Ethmodiscus* spp. fragments	*Fragilariopsis doliolus* fragments	*Fragilariopsis fossilis*	*Fragilariopsis* aff. *pseudocylindra*	*Fragilariopsis reinholdii*	*Fragilariopsis reinholdii* fragments	*Hemidiscus cuneiformis*	*Nitzschia panduriformis*	*Paralia sulcata*	*Proboscia alata*	*Raphoneis* spp.	*Rhizosolenia* spp.	*Rhizosolenia bergonii*	*Rhizosolenia hebetata* sp.	*Stephanopyxis grunowii*	*Synedra* spp.	*Thalassionema nitzschioides nitzschioides*	*Thalassionema nitzschioides lanceolata*	*Thalassiosira* spp.	*Thalassiosira convexa*	*Thalassiosira eccentrica*	*Thalassiosira leptopus*	*Thalassiosira oestrupii venrickae*	*Thalassiosira oestrupii oestrupii*	*Thalassiosira trifulta*	*Thalassiothrix* spp.	Total diatoms (processed)	Silicoflagellates	Zone	Event
306-U1312A-																																									
1H-2	F	T	M–P	1				6	1		4			2							1								1				1				6	21		*F. doliolus*	
1H-CC	T	t	VP	6							2									1				1						4							8	1		
2H-CC	T	t	P	5					7										1	2			1							2							13			
3H-CC	C	T	M–P	1	1	1		8			2					1	3	4	3		2	1					1			1		6		13		6	2	55	6	*A. marinus*	LO *F. reinholdii* (0.50 Ma)
4H-CC	C	T	M–P	1			1	11							3		5		11	1					2		2	2	1			1	1	3	18	3	2	67	3		
5H-CC	T	t	P	1				1			1																		2							1	5			
6H-CC	C	T	M–P	1				7	3	12	1		1		1		1		7						1			1			3	2	2		1		1	44	4	*T. convexa/jouseae*	LO *T. convexa* (2.40 Ma)
7H-CC	B			1																																	0			
8H-CC	R	t	P	1			6		1			1							3										2				1			2	1	17			
9H-CC	B			1																																	0			
10H-CC	T	t	P	1					1																						1						2			
11H-CC	T	t	P	1						1													1														2			
12H-CC	B			1																																	0			
13H-CC	B			1																																	0			
14H-CC	B			1																																	0			
15H-CC	B	t		1																																	0			
16H-CC	B			1																																	0			
17H-CC	t		VP	1																											1						1			
18H-CC	B			1																																	0			
19H-CC	B			1																																	0			
20H-CC	B			1																																	0			
21H-CC	B			1																																	0			
22H-CC	B			1																																	0			
23H-CC	B			1																																	0			
24H-CC	B			1																																				
25H-CC	B			1																																				

Notes: Abundance: C = common, F = few, R = rare, T = trace, t = single occurrence or fragment, B = barren. Preservation: G = good, M = Moderate, P = poor, VP = very poor. See **"Diatoms"** in the "Site U1312–U1315 methods" chapter. LO = last occurrence.

Table T14. Distribution of diatoms, Hole U1312B.

Core, section	Abundance		Preservation	Transects	*Actinocyclus curvatulus*	*Actinocyclus ingens*	*Actinocyclus marginatus*	*Alveus marinus*	*Alveus marinus* fragments	*Chaetoceros* resting spores	*Coscinodiscus nodulifera*	*Coscinodiscus radiatus*	*Fragilariopsis* spp.	*Fragilariopsis doliolus*	*Fragilariopsis doliolus* fragments	*Fragilariopsis fossilis*	*Fragilariopsis reinholdii*	*Fragilariopsis reinholdii* fragments	*Hemidiscus cuneiformis*	*Neodenticula seminae*	*Nitzschia bicapitata*	*Nitzschia panduriformis*	*Nitzschia sicula*	*Paralia sulcata*	*Rhizosolenia bergonii*	*Rhizosolenia hebetata* sp.	*Roperia tesselata*	*Stephanopyxis turris*	*Thalassionema nitzschioides nitzschioides*	*Thalassionema nitzschioides lanceolata*	*Thalassionema nitzschioides parva*	*Thalassiosira* spp.	*Thalassiosira convexa*	*Thalassiosira eccentrica*	*Thalassiosira fenilineata*	*Thalassiosira leptopus*	*Thalassiosira nordenskjoeldii*	*Thalassiosira oestrupii venrickae*	*Thalassiosira oestrupii oestrupii*	*Thalassiothrix* spp.	Total diatoms (processed)	Silicoflagellates	Event
306-U1312B-	Processed	Raw																																						
1H-CC	A	T	M–P	1	5	1	3		1	11	2	5		55	5				1									10	2		1		11	2	5	1		6	9	136	8	
2H-CC	T	t	P	5		1				4		1	1					1		1				2	2	3	1	1			3					2		1	24	3	
3H-CC	A	T	M–P	1	1	3	16		2	5	2	2		5		18	25	9	7		5	1	1			5	10		8		1	2		11	5	2	1	6	6	13	172	17	LO *F. reinholdii* (0.50 Ma)
4H-CC	R	t	M–P	1		1	3	1						1		2	2		1													1				1	1		14		
5H-CC	T	t	P	1			2			1																													3		
6H-CC	F	t	P	1	1		6							3	1				2													2						5	20	1	
7H-CC	T	t	P	1												1												1										1	3		FO *F. doliolus* (1.90 Ma)
8H-CC	R	t	M	1			1	1			2	3				1			1													1		2				6	18		
9H-CC	C	T	M	1	5		4					1				4	2		2					1	4			4				5			1			11	44	16	
10H-CC	T	t	P–D	1													1														3	1						5		LO *T. convexa* (2.40 Ma)
11H-CC	T	t	P–D	1		1				1																												2		
12H-CC	T	t	P–D	1																											2						1	3		
13H-CC	B			1																																				
14H-CC	B			1																																				
15H-CC	B			1																																				
16H-CC	B			1																																				
17H-CC	B			1																																				
18H-CC	B			1																																				
19H-CC	B			1																																				
20H-CC	B			1																																				
21H-CC	B			1																																				
22H-CC	T	t	P–D	1																											2						1	3		
23H-CC	B			1																																				
24H-1	F		M–P	8			6	1		3	2		1				2	3							1			2			2		3		1			4	31	1	Mid–late Miocene silicoflagellates
24H-CC	B			1																																				
25H-CC	B			1																																				

Notes: Abundance: A = abundant, C = common, F = few, R = rare, T = trace, t = single occurrence or fragment. B = barren. Preservation: M = Moderate, P = poor, D = dissolved. See **"Diatoms"** in the "Site U1312–U1315 methods" chapter. FO = first occurrence, LO = last occurrence.

Table T15. Distribution of radiolarians, Hole U1312A.

Core, section	Abundance	Preservation	Ice-rafted debris	Tephra grains
306-U1312A-				
1H-CC	T	P	F	F
2H-CC	T	P	C	F
3H-CC	T	P		
4H-CC	T	P		
5H-CC	T	P		
6H-CC	T	P		
7H-CC	T	P		
8H-CC	T	P		T
9H-CC	T	P		C
10H-CC	B		T	T
11H-CC	B			
12H-CC	B		T	
13H-CC	B		T	
14H-CC	B			
15H-CC	Ta	P		
16H-CC	B			
17H-CC	B			
18H-CC	B			
19H-CC	B			
20H-CC	B			
21H-CC	B			
22H-CC	B			
23H-CC	T	P		
24H-CC	B			
25H-CC	B			

Notes: Abundance: C = common, F = few, T = trace, B = barren, a = potential reworking. Preservation: P = poor. See **"Radiolarians"** in the "Site U1312–U1315 methods" chapter.

Table T16. Distribution of radiolarians, Hole U1312B. (Continued on next page.)

Core, section	Abundance	Preservation	Ice-rafted debris	Tephra grains	*Acanthocyrtis anthemis*	*Acrosphaera lappacea*	*Acrosphaera spinosa*	*Actinomma antarctica*	*Actinomma boreale*	*Actinomma haysi*	*Actinomma leptoderma*	*Actinomma popofskii* (?)	*Actinomma sol*	*Amphirhopalum ypsilon*	*Androcyclas gamphonycha*	*Anomalocantha dentata*	*Anthocyrtidium ophirense*	*Axoprunum stauraxonum*	*Botryostrobus aquilonaris*	*Bortyostrobus auritus/australis* group	*Carpocanarium papillosum*	*Carpocanistrum* spp.	*Collosphaera murrayana*	*Cornutella profunda*	*Cycladophora bicornis*	*Cycladophora d. davisiana*	*Cycladophora d. cornutoides*	*Dictyocorone profunda*	*Dictyocorone euclidis*	*Dictyophimus crisiae*	*Didymocyrtis tetrathalamus*	*Druppatractus* group C	*Euchitonia furcata/elegans* group	*Eucyrtidium acuminatum*	*Eucyrtidium calvertense*	*Eucyrtidium hexagonatum?*	*Eucyrtidium teuscheri*	*Heliodiscus asteriscus*	*Hexacontium hostile*	*Hexacontium enthacanthum*	*Hexacontium pachydermum*	*Hexapyle* spp.	*Lamprocyclas maritalis*	*Larcopyle butschlii*	*Larcospira minor*	*Lirella melo (Phaeodaria)*	*Lithelius nautiloides*	*Litharachnium tentorium*	*Lithocampe* sp.
306-U1312B-																																															
1H-CC	F	P		F	+		+	+	+		+	+						+		+	+	+		+	+	+		+	+				+	+	+	+		+		+	+		+		+	+
2H-CC	T	P	C	T																						+																					
3H-CC	C	G		T	+	+	+	+	+	+	+	+	+	+	+	+	+	+	+	+	+	+	+	+	+	+	+	+	+	+	+	+	+	+	+	+	+	+	+	+	+	+	+	+	+	+
4H-CC	F	P		C	+				+		+	+		+			+			+	+	+		+	+	+	+		+		+			+	+	+									
5H-CC	B																																														
6H-CC	C	M		A			+		+		+			+	+			+		+	+	+		+			+		+			+		+	+					+					
7H-CC	R	P	T															+																													
8H-CC	F	P		C														+																													
9H-CC	T	P		T																																										
10H-CC	F	P		T								+						+																													
11H-CC	T	P		T																																										
12H-CC	T	P		T																																										
13H-CC	B																																														
14H-CC	B																																														
15H-CC	B																																														
16H-CC	B																																														
17H-CC	B																																														
18H-CC	B																																														
19H-CC	B																																														
20H-CC	B																																														
21H-CC	B																																														
22H-CC	B																																														
23H-CC	T	P	T																																												
24H-CC	B																																														
25H-CC	B																																														

Notes: Abundance: A = abundant, C = common, F = few, T = trace, R = rare, B = barren. Preservation: G = good, M = moderate, P = poor. See **"Radiolarians"** in the "Site U1312–U1315 methods" chapter.

Core, section	Abundance	Preservation	Ice-rafted debris	Tephra grains	*Lithomelissa* "gigantic"	*Octopyle stenozona*	*Periphyramis circumtexta*	*Pterocanium praetextum*	*Pterocanium trilobum*	*Sphaeropyle langii*	*Sphaeropyle robusta*	*Spongocore puella*	*Spongopyle osculosa*	*Spongotrochus glacialis*	*Stylatractus universus*	*Styloclamydium venustum*	*Stylodictya validispina?*	*Tetrapyle octacantha*	*Thecosphaera dedoensis*	*Theocorythium trachelium*
306-U1312B-																				
1H-CC	F	P		F	+		+					+	+	+			+	+	+	+
2H-CC	T	P	C	T													+			
3H-CC	C	G		T		+	+	+	+	+	+	+	+	+	+	+	+	+	+	+
4H-CC	F	P		C		+	+	+	+	+					+	+	+	+		+
5H-CC	B																			
6H-CC	C	M		A		+	+	+	+	+		+	+	+	+	+	+	+	+	+
7H-CC	R	P	T																	
8H-CC	F	P		C													+	+		
9H-CC	T	P		T													+			
10H-CC	F	P		T								+						+		
11H-CC	T	P		T																
12H-CC	T	P		T																
13H-CC	B																			
14H-CC	B																			
15H-CC	B																			
16H-CC	B																			
17H-CC	B																			
18H-CC	B																			
19H-CC	B																			
20H-CC	B																			
21H-CC	B																			
22H-CC	B																			
23H-CC	T	P	T																	
24H-CC	B																			
25H-CC	B																			

Table T16 (continued).

Table T17. Position of paleomagnetic transitions, Holes U1312A and U1312B.

Polarity chron boundary	Name	Age (Ma)	Hole U1312A		Hole U1312B	
			Depth (mbsf)	Relative uncertainty (m)	Depth (mbsf)	Relative uncertainty (m)
C1n (b)	Brunhes/Matuyama	0.78	18.4	0.15	16.95	0.1
C1r.1n (t)	Jaramillo (t)	0.99			20.9	0.15
C1r.1n (b)	Jaramillo (b)	1.07			24.8	0.1
C2n (t)	*Olduvai (t)*	1.77			*42.05*	*0.15*
C2n (b)	*Olduvai (b)*	1.95			*42.5*	0.2
C2An.1n (t)	Matuyama/Gauss	2.58			51.6	0.15
C2An.3n (b)	*Gauss/Gilbert*	*3.58*			*72.2*	*0.55*
C5n.1n (t)		*9.74*	*207.6*	*0.15*	*204.7*	*0.6*
C5n.2n (b)		*10.95*	*236.65*	*0.15*		

Notes: Interpretations in italics correspond to uncertain ties to the reference geomagnetic polarity timescale. t = top, b = bottom.

Table T18. Disturbed intervals, Holes U1312A and U1312B.

Core, section, interval (cm)	Type of disturbance
306-U1312A-	
1H-1, 0–150	Flow-in
1H-2, 0–150	Flow-in
1H-3, 0–150	Flow-in
1H-4, 0–150	Flow-in
1H-5, 0–140	Flow-in
2H-1, 0–150	Flow-in
2H-2, 0–150	Flow-in
2H-3, 0–150	Mildly deformed
2H-4, 0–150	Mildly deformed
3H-1, 0–150	Flow-in
3H-2, 0–150	Flow-in
3H-3, 0–150	Flow-in
3H-4, 0–150	Flow-in
3H-5, 0–150	Flow-in
3H-6, 0–100	Flow-in
4H-1, 0–120	Top of core
5H-1, 0–150	Flow-in
5H-2, 0–150	Flow-in
5H-3, 0–150	Flow-in
5H-4, 0–150	Flow-in
6H-1, 0–150	Top of core
6H-2, 0–150	Mildly deformed
6H-3, 0–150	Mildly deformed
7H-1, 0–20	Top of core
7H-2, 62–150	Flow-in
7H-3, 0–100	Flow-in
7H-4, 0–150	Mildly deformed
7H-5, 0–150	Mildly deformed
7H-6, 0–150	Mildly deformed
7H-7, 0–150	Mildly deformed
8H-1, 0–150	Mildly deformed
8H-2, 0–150	Mildly deformed
8H-3, 0–150	Mildly deformed
8H-4, 0–150	Mildly deformed
8H-5, 0–150	Mildly deformed
10H-1, 0–150	Top of core
11H-1, 0–150	Top of core
12H-1, 0–45	Top of core
13H-1, 0–150	Mildly deformed
13H-3, 110–150	Turbidite
13H-4, 0–40	Turbidite
14H-2, 46–50	Void
14H-5, 0–150	Mildly deformed
14H-6, 0–150	Mildly deformed
14H-7, 0–150	Mildly deformed
15H-1, 0–20	Top of core
16H-1, 0–15	Top of core
16H-7, 0–50	Large pyrite nodule
18H-4, 0–150	Mildly deformed
19H-3, 46–60	Disturbed
21H-1, 30–38	Void
21H-1, 87–92	Void
21H-6, 58–62	Void
22H-1, 31–35	Void
306-U1312B-	
3H-1, 0–30	Top of core
4H-1, 0–20	Top of core
5H-1, 0–70	Top of core
7H-1, 0–20	Top of core
8H-1, 0–10	Top of core
8H-1, 10–104	Mildly deformed
8H-1, 104–150	Flow-in
8H-2, 0–150	Flow-in
8H-3, 0–150	Flow-in
8H-4, 0–150	Flow-in
8H-5, 0–150	Flow-in
8H-6, 0–150	Flow-in
8H-7, 0–150	Flow-in
9H-2, 135–150	Disturbed
9H-3, 0–10	Disturbed
13H-4, 122–150	Turbidite
13H-5, 0–4	Turbidite
15H-1, 0–60	Top of core
16H-1, 0–25	Top of core
17H-1, 0–10	Top of core
17H-6, 0–150	Mildly deformed
18H-1, 0–130	Void + soupy
18H-2, 0–5	Disturbed
19H-1, 0–150	Disturbed
19H-2, 0–150	Disturbed
19H-3, 0–150	Mildly deformed
20H-1, 0–150	Disturbed
20H-2, 0–150	Disturbed
20H-3, 0–20	Disturbed
20H-3, 110–150	Disturbed
20H-4, 0–150	Mildly deformed
21H-1, 0–65	Top of core
22H-1, 0–150	Top of core
23H-1, 0–20	Top of core
24H-1, 0–150	Top of core
24H-2, 80–82	Void

Notes: The top ~20 cm of all cores should be avoided. When the interval listed is 0–150 cm, the entire section is included even if the true section length is <150 cm. For correlation purposes, we retained the turbite zone and mildly deformed intervals. These intervals, however, may be too deformed for other types of studies.

Table T19. Shipboard composite depths, Holes U1312A and U1312B.

Core	Top depth (mbsf)	Top depth (mcd)	Offset
306-U1312A-			
1H	0.00	3.23	3.23
2H	9.50	8.04	–1.46
3H	19.00	17.65	–1.35
4H	28.50	28.80	0.30
5H	38.00	36.70	–1.30
6H	47.50	48.10	0.60
7H	57.00	57.74	0.74
8H	66.50	68.00	1.50
9H	76.00	80.90	4.90
10H	85.50	90.85	5.35
11H	95.00	100.11	5.11
12H	104.50	110.86	6.36
13H	114.00	119.99	5.99
14H	123.50	132.54	9.04
15H	133.00	142.98	9.98
16H	142.50	159.18	16.68
17H	152.00	168.43	16.43
18H	161.50	180.23	18.73
19H	171.00	190.48	19.48
20H	180.50	199.98	19.48
21H	190.00	209.48	19.48
22H	199.50	218.98	19.48
23H	209.00	228.48	19.48
24H	218.50	237.98	19.48
25H	228.00	247.48	19.48
306-U1312B-			
1H	0.00	0.00	0.00
2H	3.90	3.90	0.00
3H	13.40	13.40	0.00
4H	22.90	22.90	0.00
5H	32.40	32.05	–0.35
6H	41.90	41.90	0.00
7H	51.40	51.40	0.00
8H	60.90	64.10	3.20
9H	70.40	74.55	4.15
10H	79.90	86.05	6.15
11H	89.40	95.45	6.05
12H	98.90	106.61	7.71
13H	108.40	118.54	10.14
14H	117.90	127.89	9.99
15H	127.40	137.33	9.93
16H	136.90	149.33	12.43
17H	146.40	159.08	12.68
18H	155.90	167.23	11.33
19H	165.40	174.13	8.73
20H	174.90	183.73	8.83
21H	184.40	193.18	8.78
22H	193.90	202.18	8.28
23H	203.40	211.68	8.28
24H	212.90	232.03	19.13
25H	222.40	248.13	25.73

Table T20. Splice tie points, Site U1312.

Core, section, interval (cm)	Depth (mbsf)	Depth (mcd)		Core, section, interval (cm)	Depth (mbsf)	Depth (mcd)
306-				306-		
1312B-1H-3, 62.0	3.62	3.62	Append to	1312B-2H-1, 0.0	3.90	3.90
1312B-2H-7, 70.0	13.60	13.60	Append to	1312B-3H-1, 0.0	13.40	13.40
1312B-3H-7, 60.0	23.00	23.00	Append to	1312B-4H-1, 0.0	22.90	22.90
1312B-4H-6, 106.0	31.46	31.46	Tie to	1312A-4H-2, 116.0	31.16	31.46
1312A-4H-5, 58.0	35.08	35.38	Tie to	1312B-5H-3, 32.5	35.73	35.38
1312B-5H-7, 70.0	42.10	41.75	Append to	1312B-6H-1, 0.0	41.90	41.90
1312B-6H-6, 130.0	50.70	50.70	Tie to	1312A-6H-2, 110.0	50.10	50.70
1312A-6H-5, 130.0	54.80	55.40	Tie to	1312B-7H-3, 100.0	55.40	55.40
1312B-7H-6, 64.0	59.54	59.54	Tie to	1312A-7H-2, 30.0	58.80	59.54
1312A-7H-7, 72.0	66.72	67.46	Append to	1312A-8H-1, 0.0	66.50	68.00
1312A-8H-6, 110.0	75.10	76.60	Tie to	1312B-9H-2, 55.0	72.45	76.60
1312B-9H-6, 135.0	79.25	83.40	Tie to	1312A-9H-2, 100.0	78.50	83.40
1312A-9H-5, 145.0	83.45	88.35	Tie to	1312B-10H-2, 80.0	82.20	88.35
1312B-10H-6, 25.0	87.65	93.80	Tie to	1312A-10H-2, 145.0	88.45	93.80
1312A-10H-6, 55.0	93.55	98.90	Tie to	1312B-11H-3, 45.0	92.85	98.90
1312B-11H-6, 85.0	97.75	103.80	Tie to	1312A-11H-3, 68.5	98.69	103.80
1312A-11H-6, 20.0	102.70	107.81	Tie to	1312B-12H-1, 120.0	100.10	107.81
1312B-12H-6, 40.0	105.90	113.61	Tie to	1312A-12H-2, 125.0	107.25	113.61
1312A-12H-6, 115.0	113.15	119.51	Tie to	1312B-13H-1, 95.5	109.37	119.51
1312B-13H-7, 55.0	117.95	128.09	Tie to	1312B-14H-1, 20.0	118.10	128.09
1312B-14H-6, 10.0	125.50	135.49	Tie to	1312A-14H-2, 145.0	126.45	135.49
1312A-14H-6, 5.0	131.05	140.09	Tie to	1312B-15H-2, 124.0	130.16	140.09
1312B-15H-6, 45.0	135.35	145.28	Tie to	1312A-15H-2, 77.5	135.30	145.28
1312A-15H-6, 55.0	141.05	151.03	Tie to	1312B-16H-2, 20.0	138.60	151.03
1312B-16H-7, 37.5	146.27	158.71				

Table T21. Lithologic features and magnetic reversal boundaries used for correlating Holes U1312A and U1312B.

Feature description	Hole U1312A Core, section, interval (cm)	Hole U1312A Depth (mbsf)	Hole U1312B Core, section, interval (cm)	Hole U1312B Depth (mbsf)	MIS
Dark/light contact	1H-1, 133	1.33	2H-1, 133	5.23	5/6
Dark band (~2 cm thick) above light unit			2H-2, 99	6.39	8/9
Diffuse dark/light contact			2H-3, 114	8.04	9/10
Gray/white contact			2H-4, 130	9.7	10/11
Diffuse light/dark contact with another gray/brownish gray contact below	2H-5, 132	16.82	3H-1, 47	13.87	13/14
Dark/light contact	2H-6, 21	17.21	3H-2, 25	15.15	14/15
Light/dark contact	2H-6, 33	17.33	3H-2, 70	15.6	15/16
Brunhes/Matuyama	2H-6, 140	18.4	3H-3, 55	16.96	19.3
Top Jaramillo			3H-6, 15	21.05	28
Base Jaramillo			4H-2, 45	24.85	31
Thin turbidite	4H-3, 88	32.38	5H-1, 87	33.26	
Top of foraminifer turbidite	13H-3, 110	118.1	13H-4, 122	114.12	
Base of foraminifer turbidite	13H-4, 38	118.5	13H-5, 4	114.44	

Notes: Contacts are described as young/old (e.g., dark/light is a darker layer overlying a lighter layer). MIS = marine isotope stage in which the lithologic feature or magnetic reversals occur.

Table T22. Interstitial water geochemical data, Hole U1312A.

Core, section, interval (cm)	Depth (mbsf)	Core quality	SO_4^{2-} (mM)	Cl^- (mM)	pH	Alkalinity (mM)	Salinity (g/kg)	Cations (mM)				Trace elements (µM)							
								Na^+	K^+	Mg^{2+}	Ca^{2+}	B	Ba^{2+}	Ba^{2+}*	Fe^{2+}	Li^+	Mn^{2+}	H_4SiO_4	Sr^{2+}
306-U1312A-																			
1H-4, 145–150	6.0	x	23.18	575.68	7.41	3.29	34	453.5	10.0	46.5	9.9	459.8	57.8	0.28	0.0	21.8	13.3	447.5	133.6
2H-4, 145–150	15.5	(x)	6.07	569.79	7.01	3.33	34	442.7	9.0	47.1	10.1	419.7	57.8	0.24	16.1	15.8	7.8	487.4	201.4
3H-4, 145–150	25.0	x	22.98	563.58	7.29	3.48	34	428.8	8.3	43.8	8.2	468.9	57.8	0.28	17.8	12.7	4.7	467.2	288.5
4H-4, 145–150	34.5		26.71	569.79	7.31	3.73	35	445.6	9.4	43.9	10.0	412.0	57.8	0.26	9.6	9.0	3.4	536.6	367.8
5H-4, 145–150	44.0	x	25.81	565.21	7.31	3.89	34	452.0	9.4	45.9	10.3	443.6	57.9	0.32	6.3	7.7	3.2	561.1	427.4
6H-4, 145–150	53.5		25.80	562.60	7.30	4.06	34	441.7	9.6	44.5	11.1	416.3	57.9	0.39	3.3	5.6	3.1	640.9	487.2
9H-4, 145–150	82.0		25.54	563.25	7.29	4.77	34	432.0	8.4	41.2	9.6	431.1	58.2	0.69	9.0	2.9	3.1	582.0	704.9
12H-4, 145–150	110.5		23.24	553.11	7.26	3.96	33	454.3	9.0	44.0	11.4	460.4	57.9	0.39	2.4	6.2	2.9	425.3	769.9

Notes: x = flow-in, (x) = mildly deformed (see Table **T18**). * = see text.

Table T23. Headspace gases, Hole U1312A.

Core, section, interval (cm)	Depth (mbsf)	C_1 (ppmv)
306-1312A-		
1H-5, 0.0–5.0	6.00	2.4
2H-5, 0.0–5.0	15.50	3.1
3H-5, 0.0–5.0	25.00	3.1
4H-5, 0.0–5.0	34.50	3.7
5H-5, 0.0–5.0	44.00	3.2
6H-5, 0.0–5.0	53.50	3.1
7H-5, 0.0–5.0	63.00	3.8
8H-5, 0.0–5.0	72.50	2.9
9H-5, 0.0–5.0	82.00	2.9
10H-5, 0.0–5.0	91.50	3.6
11H-5, 0.0–5.0	101.00	2.7
12H-5, 0.0–5.0	110.50	2.8
13H-5, 0.0–5.0	120.00	3.0
14H-5, 0.0–5.0	129.50	0.0
15H-5, 0.0–5.0	139.00	1.9
16H-5, 0.0–5.0	148.50	2.0
17H-5, 0.0–5.0	158.00	2.1
18H-5, 0.0–5.0	167.50	2.3
19H-5, 0.0–5.0	177.00	2.3
20H-5, 0.0–5.0	186.50	2.2
21H-5, 0.0–5.0	196.00	2.0
22H-5, 0.0–5.0	205.50	2.0
23H-5, 0.0–5.0	215.00	1.7
24H-5, 0.0–5.0	224.50	1.9
25H-5, 0.0–5.0	234.00	2.1

Note: No other gases than C_1 detected.

Table T24. Bulk sedimentary C and N, Hole U1312A.

Core, section, interval (cm)	Depth (mbsf)	Carbon (wt%)				Total nitrogen (wt%)
		Inorganic	$CaCO_3$	Total	Organic	
306-U1312A-						
1H-1, 90–91	0.90	10.45	87.05	10.69	0.24	0.14
1H-4, 145–150	*5.95*	*9.94*	*82.81*	*10.27*	*0.33*	*0.17*
1H-6, 90–91	8.40	11.43	95.19	11.12	0.00	0.11
2H-3, 91–92	13.41	11.31	94.21	11.72	0.41	0.12
2H-4, 145–150	*15.45*	*7.98*	*66.48*	*8.86*	*0.87*	*0.11*
2H-6, 33–34	17.33	7.07	58.88	7.40	0.34	0.15
3H-4, 57–58	24.07	11.19	93.21	11.22	0.03	0.11
3H-4, 145–150	*24.95*	*8.05*	*67.05*	*8.16*	*0.11*	*0.11*
3H-6, 127–128	27.77	8.22	68.44	8.41	0.19	0.12
4H-2, 82–83	30.82	9.64	80.29	10.03	0.39	0.13
4H-4, 88–89	33.88	11.26	93.81	11.43	0.17	0.10
4H-4, 145–150	*34.45*	*9.64*	*80.34*	*10.58*	*0.94*	*0.10*
5H-1, 22–23	38.22	7.99	66.54	8.11	0.13	0.11
5H-4, 145–150	*43.95*	*9.94*	*82.78*	*10.69*	*0.75*	*0.08*
5H-6, 84–85	46.34	10.25	85.38	10.35	0.10	0.11
6H-1, 86–87	48.36	10.43	86.88	10.29	0.00	0.10
6H-4, 145–150	*53.45*	*10.55*	*87.92*	*11.02*	*0.47*	*0.12*
6H-7, 69–70	57.19	11.26	93.78	11.41	0.15	0.10
7H-1, 69–70	57.69	11.23	93.54	11.17	0.00	0.11
7H-5, 105–106	64.05	11.15	92.86	11.31	0.16	0.10
8H-1, 105–106	67.55	11.52	95.95	11.46	0.00	0.11
8H-7, 51–52	76.01	11.41	95.05	11.28	0.00	0.10
9H-1, 77–77	76.77	10.59	88.20	10.91	0.33	0.10
9H-4, 145–150	*81.95*	*9.86*	*82.16*	*10.23*	*0.37*	*0.11*
9H-7, 59–60	85.59	11.34	94.44	11.15	0.00	0.09
10H-1, 40–41	85.90	11.13	92.68	11.03	0.00	0.10
10H-7, 10–11	94.60	10.84	90.30	10.75	0.00	0.09
11H-1, 77–78	95.77	11.55	96.21	11.39	0.00	0.12
11H-7, 13–14	104.13	11.55	96.21	11.50	0.00	0.11
12H-2, 78–79	106.78	11.40	94.96	11.48	0.08	0.09
12H-4, 145–150	*110.45*	*9.78*	*81.45*	*9.94*	*0.16*	*0.12*
12H-6, 78–79	112.78	11.44	95.30	11.46	0.02	0.09
13H-2, 78– 79	116.28	11.50	95.80	11.40	0.00	0.08
13H-6, 102–103	122.52	11.51	95.88	11.32	0.00	0.08
14H-1, 79–80	124.29	11.47	95.55	11.54	0.07	0.08
14H-5, 79– 80	130.29	11.55	96.21	11.56	0.01	0.09
15H-1, 38–39	133.38	11.01	91.71	11.06	0.05	0.09
15H-6, 80–81	141.30	11.58	96.46	11.47	0.00	0.10
16H-2, 78–79	144.78	11.55	96.21	11.62	0.07	0.09
16H-5, 69–70	149.19	11.69	97.38	11.78	0.09	0.08
17H-1, 70–71	152.70	11.56	96.29	11.59	0.03	0.08
17H-5, 74–75	158.74	11.72	97.63	11.63	0.00	0.10
18H-1, 117–118	162.67	11.47	95.55	11.46	0.00	0.10
18H-5, 78–79	168.28	11.60	96.63	11.61	0.01	0.07
19H-1, 39–40	171.39	11.68	97.29	11.57	0.00	0.07
19H-7, 40–41	180.40	11.52	95.96	11.23	0.00	0.08
20H-1, 29–30	180.79	11.41	95.05	11.08	0.00	0.09
20H-6, 70–71	188.70	11.31	94.21	11.13	0.00	0.10
21H-1, 44–45	190.44	11.43	95.21	10.96	0.00	0.08
21H-7, 50–51	199.50	11.46	95.46	11.26	0.00	0.08
22H-1, 60–61	200.10	11.44	95.30	11.04	0.00	0.12
22H-7, 40–41	208.90	11.20	93.30	11.27	0.07	0.10
23H-1, 20–21	209.20	11.80	98.29	11.39	0.00	0.08
23H-7, 22–23	218.22	11.54	96.13	11.33	0.00	0.10
24H-1, 40–41	218.90	11.48	95.63	11.29	0.00	0.09
24H-7, 50–51	228.00	11.26	93.80	11.17	0.00	0.10
25H-1, 69–70	228.69	11.04	91.96	11.05	0.01	0.11
25H-6, 69–70	236.19	11.38	94.80	11.29	0.00	0.11

Note: Italics = values originating from interstitial water squeeze cake samples.